Microenvironments to regulate cellular behavior for neural development and regeneration

Dissertation

zur Erlangung des Grades

des Doktors der Naturwissenschaften

der Naturwissenschaftlich-Technischen Fakultät
der Universität des Saarlandes

von

Shifang Zhao

Saarbrücken
2018

Tag des Kolloquiums: **20. August 2018**

Dekan:	Prof. Dr. Guido Kickelbick
Berichterstatter:	Prof. Dr. Aránzazu del Campo
	Prof. Dr. Benedikt Berninger
Vorsitz:	Prof. Dr. Gregor Jung
Akad. Mitarbeiter:	Dr. Gergely Kali

Microenvironments to regulate cellular behavior for neural development and regeneration

Shifang Zhao

geb. in Changzhi, China

Dissertation

Max Planck Institute for Polymer Research, Mainz, Germany
INM – Leibniz Institute for New Materials, Saarbrücken, Germany

Saarbrücken, May 2018

定风波·莫听穿林打叶声

宋. 苏轼

莫听穿林打叶声，何妨吟啸且徐行。竹杖芒鞋轻胜马，谁怕？一蓑烟雨任平生。

料峭春风吹酒醒，微冷，山头斜照却相迎。回首向来萧瑟处，归去，也无风雨也无晴。

Acknowledgments

Without proper signal and support from extracellular microenvironment, it is hard for new born neurons to find their destination and fulfill their function. A similar case, without an interesting and comforting environment, it will become an impossible mission to carry out the work in this thesis. It is a great pleasure to thank the institutes, founding and many people who create this wonderful environment. The work in this thesis would be impossible without having support from Max Planck Institute for Polymer Research (Mainz), Institute of New Material (Saarbrücken), Saarland University and China Scholarship Council (CSC).

First, I would like to thank my supervisor Prof. Dr. Aránzazu del Campo for giving me the opportunity to complete my PhD in her group. I highly appreciate that she supports me to attend conferences and courses. I learned a lot during my stay, especially cell biological training. I still remember how embarrassed I was after our first discussion. Due to my poor English, we have to communicate each other by drawing. Thank you Arancha for all the personal support, your patience, your wisdom and many things I learn from you.

I am thankful to Prof. Dr. Benedikt Berninger, Institute of Physiological Chemistry JGU, Mainz, for helpfully providing us with the facilities about neural cultures at his laboratories. I am thankful to him for the discussion, suggestions and supporting.

I am thankful to my scientific supervisor Prof. Dr. David Scheschkewitz, Saarland University, Saarbrücken for his valuable advice and feedback during research work.

I would like to show my gratitude to Dr. Marcelo Salierno, for his training, guidance and support during this research work. Thanks to him for all the discussion and suggestion.

I am thankful to Prof. Dr. Adolfo Cavalié, for teaching and training me how to dissect cortex of mouse embryo. And Thanks to Dr. Konstantin Lepikhov for helping me to euthanize the mouse. Thanks a lot for your time and patience. Without your help, I won't access to the primary neuron and finish my project after shifting to Saarbrücken.

Many thanks to colleague and my friend Wenqiang Fan for helping me with the primary neurons cell culture and time-lapse experiment. I still remember that we work together until the midnight. Without your help, I couldn't finish this thesis.

I would like to thank Dr. Roshna Vakkeel for collaboration and preparing Novc-CytoD compound and for discussions and advice.

Special thanks to Prof. Dr. Franziska Lautenschläger. I highly acknowledge the discussion and suggestion. Dr. Emmanuel Terriac is acknowledged for his help for microscopy and data quantification.

I am thankful to Dr. Shrikrishnan Sankaran for his kind cooperation and preparing bacterial based living biomaterial. I highly acknowledge to him for all the discussions, understanding and helping.

I would like to thank Dr. Aleeza Farrukh for preparing photoactivable IKVAV and PAAm hydrogels, and her help with chemical coupling experiments. I am thankful to her for the discussion about science and life.

It is a pleasure for me to thank all the people of my current and former group for their help, without them this thesis would have not been completed:

I am thankful to Dr. Tilman Sauter, Dr. Quanchao Zhang and Dr. Fusheng Yan for their kind support when I first time arrived in Germany.

Dr. Longjian Xue is acknowledged for his valuable guidance about microcontact printing experiments. Special thanks to Noelia Carabelos for her kindly guidance about cell culture experiments and warmly discussion. I also would like to thank Dr. Xuan-Anh Ton, Oya Ustahüseyin and Melanie Wirkner. I acknowledge to Dr. Julieta Paez for interesting discussion.

I am thankful to Dr. Karin Kiefer for guidance about cell culture and toxicity experiment at Institute of New Material, Saarbrücken, and her help with time-lapse experiments. Many thanks to Dr. Thomas Ruckelhausen for his help with microscopy. Special thanks to Jun Feng for kind cooperation and I have lots of fun time with you. I would like to thanks to Dr. Yijun Zheng and Dr. Jiaxi Cui for their kind support to my wife and I during our stay in Saarbrücken.

I would like to thank to Master Nan. The light of your wisdom guides me in the darkness, enables me to overcome all difficulties, and raised me up to be a better man.

At last, I am especially thankful to my amazing family and my wife's family who have been always very supportive. Thank you Xiang for all the understanding, supporting and accompanying throughout these years. Especially, when I feel frustrated, depressed and close to collapse, you always stand behind me. Thank you father, mother and brother for your trust through my whole life. Without your support and encouragement, I would not be able to create the ideas leading me to study abroad for PhD and finally achieve it.

Abstract

Strategies for regeneration after injury or during aging require the development of biomaterials able to reconstruct the essential components and properties of natural extracellular microenvironment. A particular feature in neural regeneration is the oriented disposition of neurons within nerves and cortex. In this thesis, through the spatiotemporal control of the availability of adhesive ligands at the surface of a biomaterial, these biomaterials allow directing the migration of neuron. This Thesis is structured in four parts. The first part presents microcontact printed patterns with adhesive compositions and geometries to allow directional migration and, uniquely, *in vitro* reconstruction of the somal translocation events occurring during cortical layering. In part 2 *in situ* directed neurites extension in defined directions is demonstrated using biomaterials functionalized with photo-activatable peptidomimetics of the laminin. In part 3 spatiotemporal and reversible regulations of actin dynamics in living cells is demonstrated using light-dosed delivery of Cytochalasin D. In the last part, the first demonstration of a light-regulated adhesive interaction between mammalian cells and a bacterial biointerface is provided.

Zusammenfassung

Strategien zur Regeneration nach Verletzungen oder während des Alterns benötigen die Entwicklung von Biomaterialien, die essentielle Komponenten und Eigenschaften der nativen extrazellulären Mikroumgebung rekonstruieren können. Eine besondere Eigenschaft in der Regeneration von Nervengewebe ist die elongierte Morphologie und gerichtete Disposition von Neuronen in Nerven und Kortex. Die räumlich-zeitliche Kontrolle der Verfügbarkeit von Zell-adhesiven Liganden auf der Oberfläche des Biomaterials, wie in dieser These beschrieben,erlaubt es hierbei die Migration von Neuronen steuern. Diese These ist in vier Abschnitte gegliedert. Der erste Teil präsentiert Mikrokontakt gedruckte Muster mit optimisierten, adhesiven Komponenten und Geometrien, um eine gerichtete Migration und *in vitro* erstmalig die Rekonstruktion der somalen Translokation zu gewährleisten, welche während der embryonalen Entwicklung des zerebralen Kortex stattfindet. In Teil 2 wird *in situ* der gerichtete Neuritenauswuchs in definierter Richtung gezeigt. Hierbei werden Biomaterialien verwendet, die mit Photo-aktivierbaren Peptidomimetika des Matrixproteins Laminin funktionalisiert sind. Im Teil 3 wird die räumlich-zeitliche und reversible Regulation der Dynamik des Actinzytoskellettes unter Zugabe von Licht-dosiertem Cytochalasin D gezeigt. Im letzten Teil, wird erstmalig die Licht-regulierte Interaktion zwischen Säugetierzellen und einer bakteriellen Biogrenzfläche demonstriert.

Contents

Motivation and Scope of this Thesis

Strategies for neural regeneration heavily depend on our ability to temporally reconstruct the natural cellular microenvironment of neural cells. A particular feature in nerve tissue is the migration directionality and the oriented disposition of axons along the nerve axis. Therefore, biomaterials for effective nerve regeneration need to contain guiding cues for oriented axonal growth to reconnect the edges of the damaged tissue. Oriented axon extension is also relevant during corticogenesis, where individual neurons polarize and migrate radially across the cortex layers to finally position their body at precise locations (terminal somal translocation). Chemotactic signals and underlying glial and Schwamm cells are believed to provide positional guidance to neurons. Approaches to mimic cortical layer formation in vitro also need to implement the natural guiding cues for layering. These two scenarios have inspired the main work in this Thesis. Herein new approaches to guide adhesion, migration and positioning of neuronal cells have been investigated.

Biomaterials to support neuronal cell adhesion and migration are typically coated with charged polymers able to interact with the negatively charged cell membrane, or with specific cell adhesive molecules able to interact with adhesive receptors at the cell membrane. The introduction of topographical features (i.e. ridges on a 2D surface or aligned fibers in 3D construct) is often used to guide neural polarization and axon extension in vitro and in vivo. An extensive literature in Chapter 1 of this Thesis describes the state-of-the art of this field. In this Thesis neuronal migration and directional neuronal growth and differentiation is achieved solely by spatial control of adhesive molecules, without the need of topographical features. Moreover, in situ

control of neuronal polarization and migration is achieved using photoresponsive approaches. In particular, this Thesis presents:

- Biomaterials with microcontact printed areas with high affinity for neuronal attachment on a low adhesive background. By balancing the contrast between low and high adhesive regions, a compositional region where polarized cells showed the characteristic phenomenon of terminal somal translocation during corticogenesis was identified. Such phenomenon has only been observed randomly in *in vitro* neuronal cultures. Chapter 2 presents generic adhesive cues and model microenvironments that can, for the first time, guide this phenomenon on purpose in *in vitro* cultures. The role of growth cone expansion and spreading area for somal translocation and the involvement of actin fibers and microtubules are presented.
- A light-sensitive biomaterial that can guide directional neurite growth *in situ*. It exploits photoactivatable adhesive peptidomimetics of the matrix protein laminin to control the interaction between integrin at the neuronal cell membrane and the supportive biomaterials. Using a scanning laser, in situ and light-regulated directional control of axon growth is demonstrated by controlling the availability and spatial localization of the adhesive motifs in an artificial matrix. These results are presented in Chapter 3.

Both chapters present new biomaterial designs and extensive biological experiments to prove their biofuctionality and potential interest for studies in neurobiology or for application in regenerative therapies.

In parallel to this work, this Thesis also contains results related to photoregulated cellular processes performed in cooperation with coworkers in del Campos Lab.

- The study of the biological response to a photoactivatable derivative of the drug Cytochalasin D. In particular, the demonstration of *in situ* and spatially confined interference with the actin cytoskeleton of a living cell upon light exposure (Chapter 4).
- The study of the interactions and cellular responses to photoactivated adhesive miniproteins presented at “bacterial biointerface”. This study represents the first example of how optogenetic can be used to regulate biomaterial properties and cellular responses to them (Chapter 5).

Chapter 6- summarizes the important conclusions from the above work and gives a brief outlook for future development.

Chapter 1

1. Background and Introduction

Note: Part of this chapter has been submitted as a review: Biomaterials designed to support growth and function of neuronal cells, Aleeza Farrukh, Shifang Zhao, Aránzazu Del Campo, Frontiers in Materials, section Biomaterials, 2018.

The morphology and spatial organization of neurons in neuronal tissues is critical for their function. During corticogenesis, for example, new born neurons elongate and migrate long distances from their birthplace to their final destination and form a highly organized 6 layered structure. Alterations in this structure leads to severe brain dysfunctions like lissencephaly with cerebellar hypoplasia (LCH). Neurons also grow their axons in a directional way to form nerves. Regeneration of nerve function after trauma involves oriented extension of neurites and formation of functional synapses across the damage site [1, 2]. Regenerative therapies in neuronal tissue need to address the issue of directed neuronal positioning and growth.

The brain itself has very low self-regenerative capacity due to low number of available stem cells. Over the last two decades nerve regeneration therapies based on stem cell transplantation to the injury site have been explored [3-5]. Different biomaterials have been used as carriers for stem cell delivery in order to improve the viability and to support differentiation of implanted cells [6]. However, without spatial

guidance cues for directional neuronal migration and neurite growth, current biomaterials-based regeneration approaches fail to achieve full functional regeneration of neural tissue. This introductory chapter reviews recent biomaterials that provide guidance cues for functional and directional neuronal migration and neurite growth.

1.1 The guiding cues at the natural extracellular microenvironment

For regenerative purposes, biomaterials have to be designed to reproduce the properties of the natural extracellular microenvironment around neuronal cells. This includes the presence of structural and adhesive proteins and growth factors, adequate mechanical properties, defined morphologies to allow basic cellular functions like proliferation or guided differentiation, and also the contact to other neighboring cells (**Figure 1**)[7]. Man-made biomaterials to support cellular function cannot reproduce the whole complexity of the natural microenvironment, and are typically designed to fulfill minimum requirements to support cellular development to an acceptable level of functionality. Biomaterials are modified with adhesive proteins and peptidomimetics, loaded with growth factors, prepared with adjustable mechanical properties depending on the cell type and processed to form fibrous and porous matrices to allow proliferation and migration. Cells are often grown in co-cultures with other cells from their microenvironment that secrete relevant molecules to support their function, or serve as highways for cells to migrate. The following chapters describe different approaches undertaken in this context to promote migration of neuronal cells in particular.

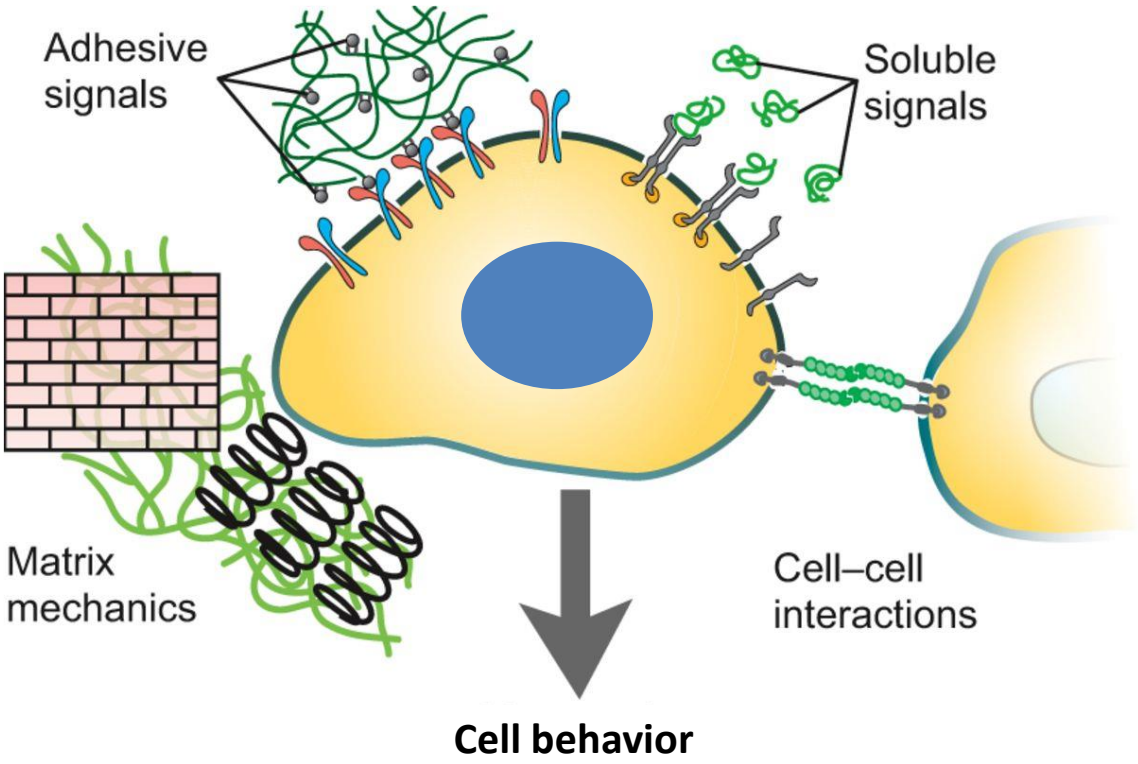

Figure 1 Cell microenvironment features that affect cell behavior. Features of the cell microenvironment play an important role in regulate cellular behavior. These features include adhesive ligands from extracellular matrix (ECM) components such as collagen and fibronectin; soluble factor like growth factors and cytokines; ECM mechanical features including stiffness, viscosity and local tension or compression; and cell–cell interactions. Adapted with permission from respective publisher [8].

1.2 Biomaterial parameters relevant for neuronal migration

Neural migration is influenced by biochemical (adhesive ligands, growth factors), topographical and mechanical factors of the extracellular matrix, and also by

adhesive contacts to neighboring cells. Examples of reported migratory responses of neural cells to these material parameters are detailed bellow.

The influence of adhesive molecules

The binding of ECM ligands with cell surface molecules is the first step for migration. The type and concentration of adhesive ligand on a biomaterial influences migration of neural cells by stabilizing the attachment of the growth cone of neurites. Laminin, for example, has been demonstrated to stimulate and guide migration of olfactory epithelial neurons *in vitro*.[9] Depending on the cell type, different responses to the same adhesive coating can be expected. For example, adult neural stem cells (aNSCs) and astrocytes migrated on Poly(lysine) surfaces and became less migratory on PL/LN mixtures, while neuron preferred to spread and not move on PL [10, 11]. In vivo, laminin-coated scaffolds promote migration of neuroblasts to injured brain tissue, contributing to neuronal regeneration after stroke in mice (**Figure 2**).[12].

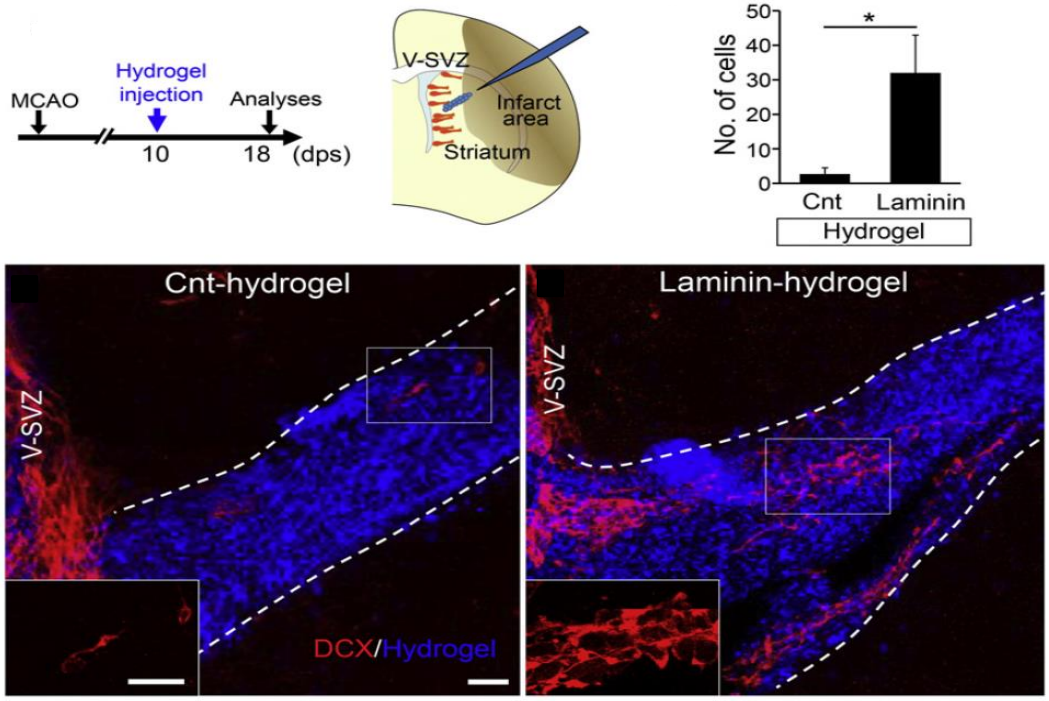

Figure 2: Migration of neuroblasts along a laminin coated 3D hydrogel scaffold toward the injured area in vivo. [12].

The influence of gradients of soluble factors

Gradients of soluble neurotrophic factors and neurotransmitters influence neuronal migration [13]. These molecules can be added to cell cultures, or secreted by other co-cultured cells like astrocytes.[14] Glial and neural migration through hydrogels was demonstrated to be enhanced through delivery of soluble growth factors such as NGF from fibrin in in vitro cultures [15]. In vivo, the delivery of stimulating molecules to the CNS represents a clinical challenge because the blood–brain barrier limits the diffusion of molecules into the brain by traditional oral or intravenous routes. Injectable hydrogels have the capacity to overcome the challenges associated with drug delivery to the CNS [16]. Intraventricular sequential delivery of epidermal growth factor (EGF) and erythropoietin (EPO) into a stroke injured rat brain showed enhanced migration of endogenous NSPCs to the injury site, resulting in neurogenesis and improved functional recovery [17].

The influence of glial cells for neuronal migration

Studies have shown that neuron migration can also be modulated through cell-cell contact, specifically involving glial cells. Recently, it was found that the gap junction proteins connexin 46 and 23 are expressed by radial glia during glial-mediated migration of neurons [18]. These proteins provide adhesive contacts between the radial glia and neurons which stabilize the processes of migrating neurons. Direct cell contact mediated by CAMs, specifically L1-CAM and neural cell adhesion molecule (NCAM), also influence neuronal migration[19]. CAMs generally bind through homophilic and heterophilic interactions (i.e. binding to identical or similar, as well as different CAMs, respectively), and therefore provide structural cell-to-cell, axon-to-cell, or axon-to-axon linkages [20]. Lastly, physical properties of the cell, such as polarity, can influence migration. Thus, the incorporation of these various cues into so called

“living scaffolds” for neural cultures can direct neural cell migration to the appropriate sites to promote regeneration[21].

Living scaffolds not only provide haptotactic, chemotactic, and mechanical cues, but also allow active regulation of signaling molecules (adhesive ligands) or matrix mechanics upon application of external stimuli through the use of genetically engineered cells. Due to the properties of the ECM are heterogeneous and dynamic, the development of tunable and responsible living biomaterials was required.

The influence of biomaterial stiffness in neuronal migration

Biological tissues are mechanically inhomogeneous, for example, stiffness gradients have recently been reported in CNS tissue[22]. During growth and migration, cells are exposed to different mechanical stimuli. The importance of mechanical signaling for cell functioning is becoming increasingly clear. For example, muscle cells, neurons, and many other tissue cells have since been shown to sense substrate stiffness [23-25]. The migration of fibroblasts has been shown to be guided by stiffness gradients in their substrate (‘mechanotaxis’) in vitro[26].

In addition to well-established chemical factors, during brain development neurons can sense and be guided by mechanical interaction between neighbor cells and their microenvironment[27]. For example, mechanical tension along neurites not only been involved in the generation of axons [28], but also been suggested to contribute to the directionality of migrating neurons [29].

The relevance of mechanical signaling in different contexts of cell function is a current vivid area of research, also related to neural tissue. Stiffness gradients have been reported in CNS tissue by atomic force microscopy [22]. A recently research

reported that Xenopus retinal ganglion cell axons grew toward softer part of substrate in vitro. And in vivo, after altered brain stiffness, blocked mechanotransduction pharmacologically and so on, there were aberrant axonal growth and pathfinding errors[30]. Laminin-coated polyacrylamide hydrogel with high stiffness(20 kPa) greatly promoted the migration of Schwann cells progenitors from embryonic dorsal root ganglions (DRGs) compared to low stiffness hydrogel (1 kPa)[31]. There were chemical, adhesive, mechanical, topographical, and electrical types of gradients, which could influence neural directed migration. A systematic review of gradient approaches to neural tissue engineering has investigated the role of combined gradients on the neural directional migration[32].

The influence of topography

During development, migration of neuronal cells often occurs in a directional way. Neurons attach and migrate along fibers of the extracellular matrix or along glial cell tracts [33]. The sensitivity of neurons to topographical features has been exploited in vitro and in vivo [34, 35]. Oligodendrocytes[36] and neurons [37], have been shown to migrate along grooved topographies. The average migration speed of cells was higher on microgrooved substrates than on flat surfaces[38]. In 3D environments, DRG cells exhibited unidirectional migration into micro-channels of the PEGylated fibrinogen hydrogel[39].

1.3 Biomaterial designs to support directional neurite extension

In order to achieve successful regeneration of neural tissue, sprouting axons from the proximal stump of one neuron need to grow and establish a new connection with the

distal stump of the next neuron [40]. Following injury in central neural system (CNS), the remaining functional neurons will try to grow processes and reestablish connections with neighboring partners, but they often meet an impenetrable scar tissue composed of myelin, cellular debris and other cells (astrocytes, oligodendrocytes, microglia) at the injury site. The scar tissue blocks existing neurons from reaching their synaptic target and hinder the regeneration process.[41] In order to achieve successful regeneration of neural tissue, the axon of neuron need to grow in right direction and establish a new connection with target neuron [40]. Guidance in neurite growth plays a vital role in nerve repair. Many approaches to support nerve regeneration, therefore, have focused on the development of biomaterials that provide guidance cues for directional neurite growth.

1.3.1 Neural growth on patterns of cell adhesive ligands

Successful nerve regeneration requires tissue-engineered scaffolds that provide not only mechanical support for growing neurites and prevention from ingrowth of fibrous scar tissue, but also biological signals to direct the axonal growth cone. And biological ligand, which are derived from ECM proteins that are involved in specific interactions with neural cells, have been incorporated to produce biomimetic scaffolds[42]. Among numerous ECM proteins identified to be expressed during development of neurons, an initial attempt to generate biomimetic scaffold has focused on using laminin, an active promoter of neural cell attachment, differentiation, migration and neurite outgrowth. The RGD containing peptide in laminin was biologically active to promote neuron adhesion and neurite outgrowth. In addition, the penta-peptide IKVAV is recognized by a 110-kDa receptor[43], and YIGSR binds to a 67 kDa receptor [44] (see table 1).

Table 1

Synthetic sequences	Origin	Function	References
IKVAV YIGSR	Laminin Laminin B1	Neurite extension Neuron adhesion	[45]
RNIAEIIKDI	Laminin B2	Neurite extension	[42]
KHIFSDDSSE	Neural cell adhesion molecules	Astrocyte adhesion	[46]
ASKKPKRNIKA	Neural cell adhesion molecules	Neurite outgrow	[47]
SIDRVEPYSSTAQ (FRM)	Neural cell adhesion molecules	Proliferation and migration	[48]
CDPGYIGSR (p31)	Laminin	Neuron adhesion	
RNIAEIIKDI (p21)	Laminin	Neurite extension	[49]
silk-like polymer having FN fragments(SLPF)	Fibronectin	Neuron adhesion	
AcN–RADARADARADARADA–CONH2 (RADA-16)	NA	Neurite outgrow Synapse formation	[50]
N-Ac-HAVDIGGGC-OH(HAV)	N-cadherin	Neurite extension	[51]

Patterns of adhesive ligands (full proteins or peptidomimetics) on nonadhesive backgrounds (typically PEG) can be used to selectively promote neuronal attachment and guided outgrowth on the adhesive regions of the pattern [11, 52, 53]. Recent studies demonstrate that responsive biomaterials can be used to in situ guide axonal growth. Using photoactivatable adhesive ligands, light-guided outgrowth of neurites

on substrates has been recently demonstrated [54]. In vivo, poly(vinyl chloride) (PVC) channels filled with different adhesive matrices (a YIGSR peptide containing agarose gel, a plain gel, and PBS solution) have been applied to fill a 4mm segment of dissected dorsal root. A significant increase of myelinated axons was shown in the peptide modified agarose gel [55].

Growth factor Gradient

In addition to promoting cell growth, the presentation of neurotrophic factors in a gradient distribution within scaffold has also been studied for guidance of regenerating neurons. Several in vitro studies have demonstrated that neuronal cells are guided by immobilized gradients of nerve growth factors or neurotrophic factors on scaffolds[56, 57]. The presence of laminin and NGF gradients in agarose scaffolds has also shown better functional recovery of long peripheral nerve gaps than uniform concentration scaffolds[56].

1.3.2 Topographical cues for guiding neurite extension

The topography of the neuronal microenvironment, including fibrillar extracellular matrix proteins and elongated glial cells, plays a major role for the directional growth of neurites. In the biomaterials field nerve guidance channels, surface topographies and 3D fibrillar meshwork have been used as supportive scaffolds for directional neural regeneration.

1.3.2.1 Nerve guidance channels (NGCs) for peripheral nerve Regeneration

Nerve guidance channels (NGCs) are tubular constructs with a hollow lumen through which the neuron axon should grow. This geometry has several advantages for

spatial guidance of peripheral nerve regeneration: protection of the regenerating nerve against compression by the surrounding tissue, isolation of the regenerating axons from surrounding tissue, and longitudinal directional guidance of the regenerating neurites towards target tissue. Hollow nerve conduits have been widely used in research and clinical applications (**Figure 3**). Porous and not porous NGCs providing longitudinally oriented grooves in their lumen surface, [58] and eventually functionalized with cell adhesive ligands (e.g. laminin-derived peptides YIGSR and IKVAV [59] or controlled released growth factor (neurotrophic factors [60] promote directional axon growth in vivo in small animals test. However, in some cases dispersion of the regenerating axons through the comparatively large lumen of the NGCs leads to inappropriate target reinnervation or polyinnervation of different targets by the axonal branches of the same neuron. Single hollow lumen NGCs are thus only recommended for small lesions (<30 mm) in the sensory nerves[61]. In vitro neuronal, Schwann and dorsal root ganglion culture were used to test the NGCs and in vivo a thy-1-YFP-H mouse common fibular nerve injury model or a nerve gap in the rat sciatic nerve were normally used. Generally, typical NGCs dimensions for experimental use in small animals are inner diameters of 1–2 mm and lengths of several millimeters, depending on the experimental gap.

Considerable effort has been focused on the development of more effective NGCs, in which a microstructured lumen of the NGC provides higher directionality. Structured lumens including multichannels, porous matrices or oriented fibrous conduits have been proposed (Fig. 8). Multichannel NGCs mimic the natural compartment structure of nerves [62, 63]. They reduce axon dispersion and offer higher surface area for functionalization and cell adhesion and migration as compared to single lumen NGCs. The disadvantages of the multichannel NGC design are reduced permeability and

mechanical flexibility. In fact, multichannel NGCs did not lead to significant functional improvement in the repair of a 1-cm nerve gap in the rat sciatic nerve compared to single lumen nerve tubes [64]. NGCs might also incorporate fillers to form an internal porous or aligned 3D matrix. Fillers may include longitudinally aligned fibers, porous sponges or gels. Fillers can also be functionalized with specific peptides/proteins or growth factors, as described in recent reviews [60, 65]. Filling of the lumen of silicon NGCs with longitudinally oriented polyamide filaments lead to improved nerve regeneration by bridging a 15-mm sciatic nerve gap in rats [66].

An alternative strategy to guide neurites growth within the luminal cavity of the NGC involves the use of electrospun tube walls (**Figure 3**). The use of tubes with walls consisting of oriented fibers has a number of advantages over the filled lumen strategy. (i) The materials are highly flexible and porous, well adapted for use within biological systems; (ii) nano- and micro-scale fibers have a high surface area-to-volume ratio increasing the area available for protein absorption, neural cells migration and regeneration of axons; (iii) fibers that can be preferentially aligned resulting in increased promotion of guided axonal growth.[67]

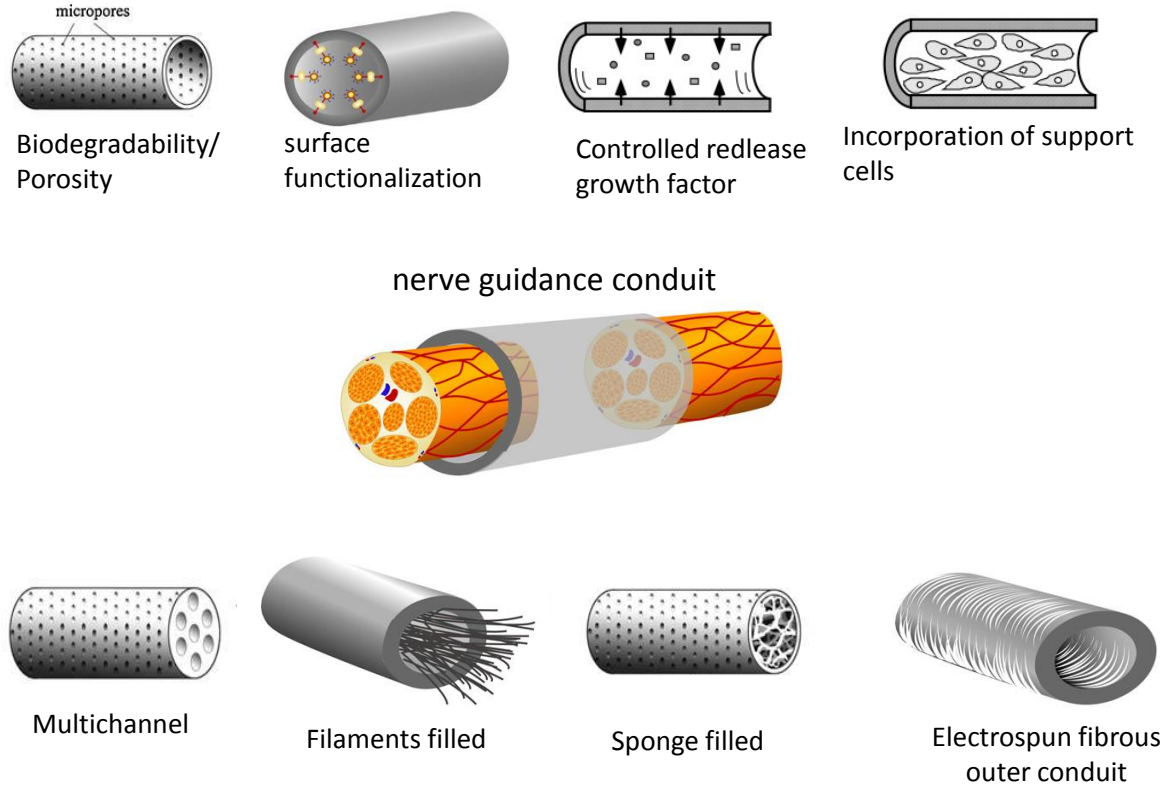

Figure 3 Different designs of nerve guidance conduits (NGCs). The basic design parameters include: a biodegradable and porous channel wall, a biofunctionalized wall surface including adhesive and growth factors, intraluminal structures to mimic the structure of nerve fascicles, intraluminal guidance structures (filaments, sponge or hydrogel-like) or wall microstructures to support cell migration and axonal growth. Support cells can also be incorporated to the NGC. Adapted with permission from reference[67] and [41].

1.3.2.2 Scaffolds for guided central nerve regeneration

Although regeneration of the mammalian CNS was thought to be impossible, studies have shown that axonal growth after spinal cord injury can occur when neurons are provided with the suitable substrata that support directional growth [68, 69]. Natural, ECM-derived biomaterials and also synthetic polymers processed in different ways to

generate microtopographies have been used as matrices for supporting spinal nerve regeneration.

The relationship between microscale topography and neuronal development has been recently investigated in vitro in a high-throughput screening assay[70]. Primary neurons were presented to patterned substrates with a large library of topographical features including isotropic (e.g. dots, grids, squares) and anisotropic pattern designs (e.g. gratings) with lateral width between 5 and 15 µm and 1 µm depth. Anisotropic topographies enhanced axonal and in some cases dendritic extension *vs.* isotropic ones. However, dendritic branching occurred preferentially on planar substrates. The depth of the topographical features also influences the growth of processes. Murine neural progenitor cells (mNPCs) sensed the depth of micro-gratings and neurite elongation, alignment and neuronal differentiation increased with grating depth [71].

In vivo studies using poly(2-hydroxyethyl methacrylate-co methylmethacrylate) hydrogel channels demonstrated improved tissue regeneration of transected rat spinal cords[72]. The hydrogel guidance channels were designed to match the dimensions and modulus of the rat spinal cord: the outside diameter of the channels was approximately 4.2 mm, the inside diameter was 3.6 mm, giving a wall thickness of 0.3 mm and the length was 6mm. By inserting the transected cord stumps into the hydrogel nerve guidance channels, alignment of the cord stumps and cells were able to migrate along them. Axonal regeneration was enabled and scar formation did not occur to a significant extent.

1.3.2.3 Guided neurite extension on 3D fibrillar meshworks

Fibrillar 3D matrices can serve as substrates for neuronal growth. The fibrils provide spatial guidance to the extension of processes, while retaining an open matrix structure to be repopulated by the growing cells. [73, 74]. This is of particular interest in the development of biomaterial-based scaffolds intended to promote the repair of highly organized nerve tissues, such as the retina or white matter tracts of the spinal cord.

Protein based and synthetic polymer fibers have been used to form fibrillar matrices and guide axonal growth. Fibers can be processed by different technologies, like electrospinning, bioprinting or self-assembly. Among these methods, electrospinning offers an uncomplicated and low-cost method for processing, applicable to different kinds of materials. Electrospun membranes with randomly or aligned fibers can be produced, and neuronal growth along the fibers has been demonstrated [75]. Neural progenitor cells and dorsal root ganglia cells grew preferentially along aligned poly(lactate) electrospun scaffolds with fiber diameters between 150 to 3000 nm independently of the adhesive coating [76, 77]. Neural stem cells (NSCs) elongated and outgrew neurites along aligned fiber scaffolds without adhesive coating[77], as shown in **Figure 4A**. Authors could not establish a significant effect of the fiber diameter (between 300 and 1500 nm) on the cell orientation. NSC differentiation rate was found to be higher on PLLA nanofibers (diameter 300nm) than that of micro fibers (diameter 1500nm), independently of alignment. Aligned nanofibers significantly improved neurite outgrowth compared to random ones. On thicker fibers and fibers coated with adhesive factors, however, different tendencies were observed. Fibers of 35µm coated with PL and LN promoted directional neurite outgrowth and promoted greater oriented process growth than large-caliber fibers (500µm) [78, 79].

Many studies have demonstrated that the aligned nanofibers, pattern nanofibers (half random and half aligned) and also cross-patterned nanofiber can guide the neurites to extend along the nanostructure (**Figure 4B**). However, the contact cues provided by the nanofibers can be far more complicated than just guiding the neurites to extend along them. Xie et al. demonstrated that the neurites could not only project along the nanofibers, but also be directed to grow along a direction perpendicular to the aligned nanofibers. The neurites Dorsal root ganglia (DRG) grew perpendicularly to the alignment direction of electrospun poly-(ε-caprolactone) (PCL) fibers (**Figure 4c**). The growing direction of neurite on fibers was dependent on the adhesive interaction between neurites and nanofibers and on the dimensions and separation between fibers. A strong interaction lead to parallel growth of neurites along the fibers (e.g. low density fiber and fiber with Laminin coating), while a weak interaction (i.e. fibers without adhesive proteins) lead to perpendicular growth. [80] High density meshworks lead also to perpendicular growth.

In vivo, aligned oriented fibers elicit regeneration, while randomly distributed fibers do not, demonstrating how topographical cues can influence endogenous nerve repair mechanisms in the absence of exogenous growth promoting proteins[81]. Using electrospinning method, poly(acrylonitrile-co-methylacrylate) (PAN-MA) fibrillar constructs (19 mm long and 1.5 mm inner diameter) were produced. Axons regenerated across a 17 mm nerve gap, re-innervated muscles, and reformed neuromuscular junctions. Electrophysiological and behavioral analyses revealed that aligned but not randomly oriented constructs facilitated both sensory and motor nerve regeneration, improving significantly functional outcomes.

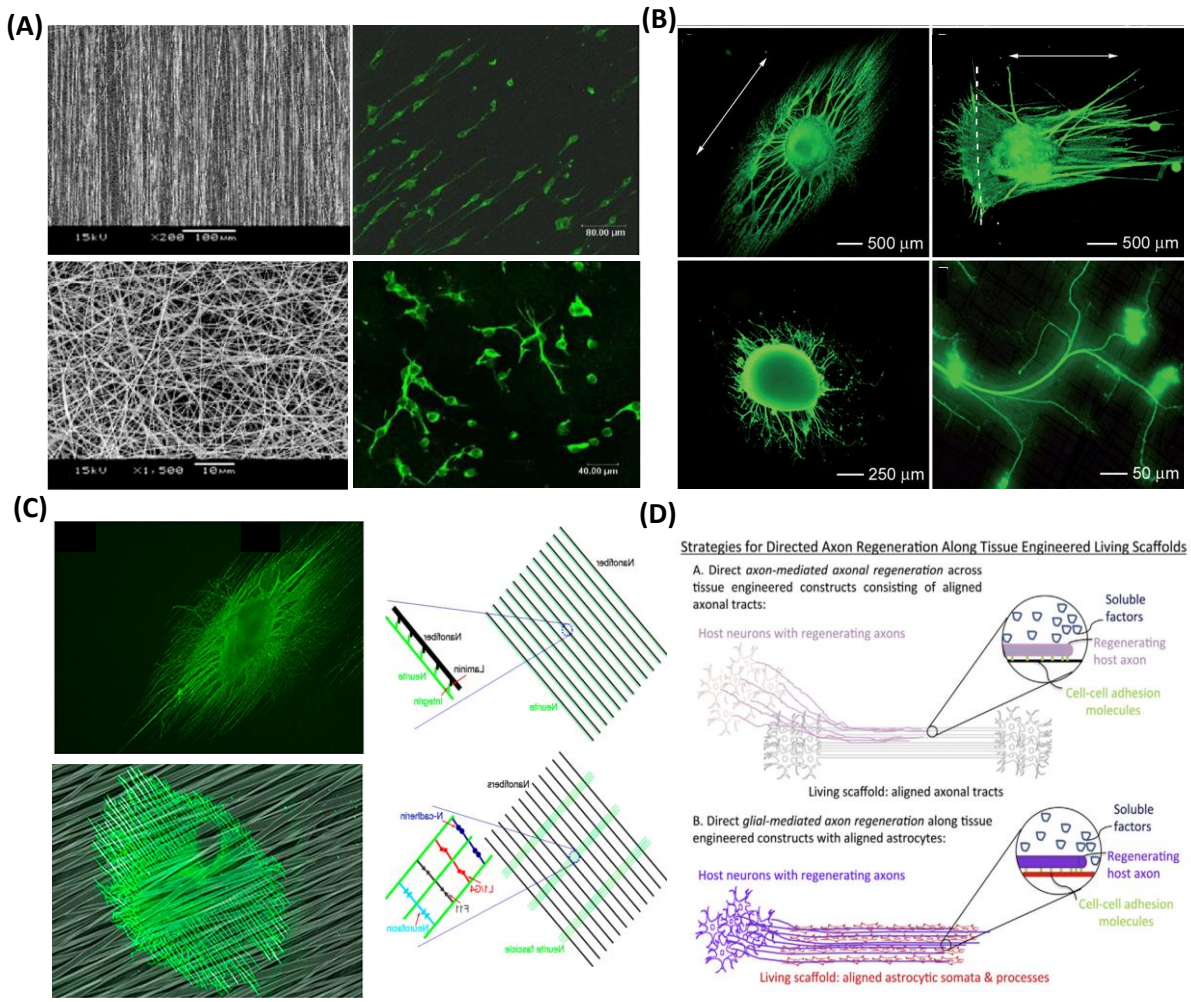

Figure 4: (A) Neural stem cells cultured on random and aligned fibers[77]. (B) dorsal root ganglia cultured on patterned poly-caprolactone nanofibers: aligned fiber, random and aligned fiber combination, and grid pattern fibers[82]. (C) Neurites of dorsal root ganglia oriented along the nanofibers previously coated with laminin and perpendicularly to the nanofibers without adhesive coating [80]. (D) Structural and soluble cues directing axonal outgrowth along “living scaffolds” [21].

Fibers have been also integrated within hydrogel materials to provide hybrid three-dimensional construct for neuronal guidance within a growth promoting environment [83, 84]. Studies showed that magnetic collagen fibers in collagen gels, aligned using magnetic fields, provide an improved template for neurite extension compared

to randomly oriented collagen fibers [85, 86]. Natural protein based hydrogels also provide adhesive factors to support attachment and neurite grown. Yao et al. developed a hierarchically aligned fibrillar fibrin hydrogel (AFG) with low rigidity and aligned topography to mimics both the soft and oriented features of nerve tissue. They found that the AFG exhibit co-effects on promoting the neurogenic differentiation of human umbilical cord mesenchymal stem cells (hUMSCs) in comparison to random fibrin hydrogel (RFG) and tissue culture plate (TCP). Also, AFG induces dorsal root ganglion (DRG) neurons to rapidly project numerous long neurite outgrowths longitudinally along the AFG fibers[87]. Recently, Rose et al developed a hydrogel that can be injected and form an anisotropic matrix using rod-shaped, magnetoceptive microgel doped with superparamagnetic iron oxide nanoparticles [88]. Firstly, the microgels are dispersed in a biocompatible gel precursor. Then after injection of gel, the microgels become orientated by external magnetic fields and are fixed inside the matrix hydrogel. The macroscopic unidirectional orientation created by the anisometric microgels, is strongly sensed by the neural cells resulting in parallel neurite extension.

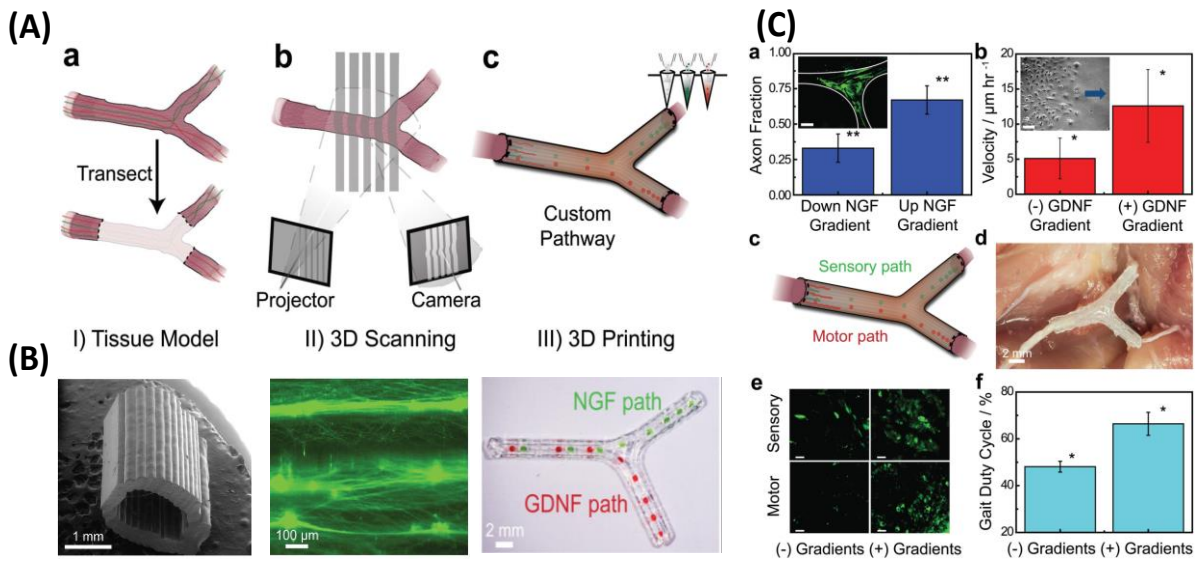

Figure 5 (A) Nerve regeneration pathways enabled by 3D scanning and printing. (B) The 3D printing process provided the ability to introduce advantageous physical and biochemical cues in the form of microgrooves and multicomponent diffusive biomolecular gradients (nerve growth factor, NGF, and glial cell line-derived neurotrophic factor, GDNF – in the sensory and motor paths, respectively). (C) In vitro and in vivo characterization of regeneration with 3D printed nerve pathways. In vitro, effect of the NGF gradient on the guidance of the primary embryonic sensory neurons' neurite network growth, and effect of the GDNF gradient on the migration velocity of Schwann cells were tested. In vivo, implanted nerve guide showing bifurcation into sensory and motor nerve paths was implanted into rat hind limbs with a 10 mm complex nerve gap injury. Histology of regenerated nerve and the functional return in regenerated rat hind limbs were compared between with or without biomolecular gradients [89].

Recently, Johnson et al. have developed a novel 3D printing approach for manufacturing of a custom nerve repair technology which is personalized to anatomical geometries, and augmented with physical (microgrooves) and

biochemical cues (multicomponent diffusive biomolecular gradients) to promote the regeneration of multiple nerve pathways[89]. The custom scaffolds are prepared via a 3D printing using 3D models, which are reverse engineered from patient anatomies by 3D scanning. The bifurcating pathways (sensory and motor path) are augmented with microgrooves and path-specific biochemical cues for the regeneration of complex mixed nerve injuries (**Figure 5**). This 3D printed scaffold provides axonal guidance in vitro and achieved successful regeneration of bifurcated injuries across a 10 mm complex nerve gap in rats in vivo. Synthetic hydrogels formed by self-assembling peptide-amphiphiles show also a nanofibrillar structure that has been used in nerve regeneration. Encapsulated neural progenitor cells were observed to differentiate into neurons and extensive neurite outgrowth within nanofibrillar hydrogels [90].

1.3.3 Guided neurite growth by rigidity patterns

The rigidity of the biomaterial contributes to the oriented growth of neurites in spiral ganglion neurons (SGN) on micropatterns. Alignment was significantly enhanced when the material stiffness increased from 649 ± 35 MPa to 1901 ± 97 MPa [91]. Increasing substrate stiffness of a laminin-coated polyacrylamide hydrogel also promoted directional neurite outgrowth from embryonic dorsal root ganglions (DRGs)[31]. The neurite in low stiffness substrate (1 kPa) show relax and less aligned morphology, whereas the neurite display stretch, more aligned morphology in high stiffness(20 kPa). Interestingly, the opposite observation was made in 3D cultures. A hyaluronic acid (HA) hydrogel with tunable Young’s Modulus between 400 and 800 Pa was used to culture hippocampal neural progenitor cells (HNPCs) [92]. Neurites of HNPCs grew into the soft HA hydrogel at increased outgrowth and density. The growth of neurites (in quantity and length) from dorsal root ganglia was

also promoted in softer (0.5 kPa) elastin-like hydrogels [93]. Authors hypothesize that on 2D environments the stiffer substrates provide more stable anchoring to facilitate the outgrowth of neurite. In contrast, stiffer 3D matrices (i.e. higher crosslinking degree) hinder the outgrowth of neurites due to the small pore sizes.

1.3.4 Directed growth on “living scaffolds”

During neural morphogenesis and development, directed axon growth and cell migration typically occurs along pathways formed by other cells. This concept has long been appreciated in developmental neurobiology as crucial to the proper formation of the nervous system, including necessary axonal connectivity and localization of cellular constituents. This idea has also been embraced by the tissue regeneration community and lead to the concept of “living scaffolds” for regeneration. These are tissue engineered constructs containing supporting guiding material and cells from the neural environment, typically glial cells and astrocytes. These follow the haptotactic cues of the scaffold and arrange in oriented dispositions. These cells secrete neural growth factor, and combine haptotactic and chemotactic signals to neuronal cells to grow along them. (**Figure 4 D**)[21]

In vitro, Winter et.al. have developed a living scaffold that structurally mimicked the glial tube. It consisted of aligned astrocytes that guided the migration of neuronal progenitor cells and facilitated directed axonal regeneration for central nervous system repair. The networks of longitudinally aligned astrocytes on patterned hydrogels, supported seeded neurons to extend neurites along the aligned astrocytes bundles[94]. In a different approach, collagen sheets supported alignment of astrocytes in the presence of transforming growth factor.[95]. The collagen sheets were then rolled to create cylindrical constructs. Dissociated DRG neurons and astrocytes were seeded together on the scaffolds. Neurites preferentially grew along

the aligned astrocytes. Higher order structures can be formed by first culturing and aligning support cells on microgrooves, followed by seeding of neurons.[38]. Micropatterned Poly(lactic acid) substrates containing grooves selectively coated with laminin were used to culture rat Schwann cells to support neurites outgrowth[96]. Neurons cultured on those substrates displayed accelerated outgrowth of nerve fibers and 98% alignment of neurites along the microgrooves. In a different study, micropatterned Schwann cells controlled by micropatterned polymer substrates(stripe pattern coated with Laminin) were used to direct neuronal regeneration [97, 98].

In vivo, living scaffolds consisting of neurons and stretch-grown axonal tracts were grown to 10 mm in length, encapsulated in collagenous matrices, and transplanted to repair equally sized lateral hemisection spinal cord lesions in rats for spinal cord repair.[99]. At one-month post-surgery, the constructs had integrated with the host by extending axons into the spinal cord. Similar constructs containing “stretch-grown” axonal tracts were also used for peripheral nerve repair.[95]

1.3.5 Guiding neurite extension by light and photoactivatable biomaterials

Light has emerged as an advantageous stimulus in this context. It allows non-invasive, spatiotemporally resolved activation, tunable regulation by varying exposure dose, and multiplexing by using different wavelengths. Weak optical forces have been shown to guide the direction of a growth cone of a nerve cell [100]. A near-IR laser (800 nm) spot placed in front of a nerve’s leading edge enhances the growth of the dendrites following the beam focus. Likewise, it has been shown that an IR laser (1455 nm) triggers the growth of dendrites and axons by as much as 10 μm in 1 min [101]. The mechanism by which neurons follow light stimulus is unclear. One

hypothesis is that gradient forces bias the actin polymerization- driven lamellipodia extension. Another hypothesis is that cellular response follows localized temperature changes during exposure [102]. However, experiments performed at two near-IR wavelengths (780 and 1064 nm) showed equal effectiveness in guiding neuronal growth, suggesting that the possible temperature rise is insufficient to change the rate of actin polymerization[103].

Beside using light to guide neuron directly, light-regulated adhesive ligand availability [104, 105] have been achieved in biomaterials to improve cell attachment through the introduction of synthetic chromophore in the ligand structure. It would be more interesting that using a photoactivated adhesive ligand allow to specially interact with neuron receptors and to guide neurite extension in a more efficient way. This Thesis presents some results in this direction.

Chapter 2

2. Microenvironments to trigger migration and somal translocation in cortical neurons

Note: The content of this chapter was published in: Microenvironments to study migration and somal translocation in cortical neurons. Biomaterials (2017). 156:238-247. Zhao, S., W. Fan, X. Guo, L. Xue, B. Berninger, M.J. Salierno, and A. del Campo.

Migrating post-mitotic neurons of the developing cerebral cortex undergo terminal somal translocation (ST) when they reach their final destination in the cortical plate. This process is crucial for proper cortical layering and its perturbation can lead to brain dysfunction. Here a reductionist biomaterials platform is presented that faithfully supports and controls the distinct phases of terminal ST *in vitro.* The described microenvironments with different adhesive molecules support neuronal attachment, neurite extension, and migration in distinct manners. Efficient ST occurred when the leading process of migratory neurons crossed from low- to high-adhesive areas on a substrate, promoting spreading of the leading growth cone. These results indicate that elementary adhesive cell-substrate interactions strongly influence migratory behavior and the final positioning of neurons during their developmental journey. This *in vitro* model allows advanced experimentation to reveal the microenvironmental requirements underlying cortical layer development and disorders.

2.1 Introduction

During the mammalian corticogenesis, neurons migrate long distances from their birthplace to their final destination [106-108]. New post-mitotic neurons at the ventricular (VZ) and subventricular zones (SVZ) first migrate along radial glial fibers in a mode frequently referred to as “locomotion” [109-111]. When the leading process of the migrating neuron reaches the cortical plate (CP), cells undergo terminal somal translocation (ST). Cells detach from the radial fibers and complete their migration beneath the marginal zone (MZ)[110, 112]. Terminal ST is believed to be used by late-generated neurons to make a final adjustment of their destination, and adopted by early-generated neurons to migrate directly to their final position [113, 114]. This process shows characteristic features: Initially neurons develop a prominent leading process with a growth cone (GC) structure that explores the properties of the surrounding microenvironment. When the GC reaches the final destination, it spreads and anchors within the CP. Finally, the nucleus and surrounding organelles translocate towards the tip of the leading process [110, 112, 114].

Despite extensive studies on the topic, the guidance cues that trigger growth GC spreading and terminal ST that determines the final destination of migrating neurons remain unclear. The expression of particular extracellular molecules was found to play a critical role in directing neuronal migration [113, 115-118]. The most studied one is Reelin, a key regulator in mammalian cortical lamination [119-124] and terminal ST [114, 125, 126]. The interplay between Reelin and the adhesion receptors integrin α5β1, α3β1 and N-cadherin has been documented [120, 127-130]. Control of cellular migration processes through the regulation of membrane adhesive receptors seems logical[106]. Binding of cell adhesive receptors to extracellular

counterparts is fundamental to cellular locomotion, and the spatial distribution of adhesive ligands in the extracellular matrix and/or on neighboring cells can guide migration direction and persistence [131-134]. In this context, spatial localization of extracellular adhesive cues could be an effective regulator of neuronal positioning during corticogenesis.

Reports on neuronal migration in vitro are mostly based on spontaneously occurring neuronal locomotion in cell cultures, with no control on the migration mode [135, 136]. Although recent studies have highlighted the sensitivity of neuronal migration to the properties of the underlying substrate [10, 11], the concrete factors that control, trigger or direct ST to re-locate neuronal cells at predesignated positions *in vivo* or *in vitro* remain unknown. Interesting experimental observations in an older report demonstrated that neuronal migration could be induced on glass substrates patterned with poly(lysine) micropatterns.[137]

In this chapter, the underlying hypothesis is that substrates with spatially confinement regions of different surface properties (“adhesiveness”) could trigger, guide or hinder somal translocation on a biomaterial surface. By using microcontact printed patterns of different adhesive molecules, contrasting adherent regions on the surface were provided to the neurons. In this chapter the influence of the substrates with spatially confinement regions of different surface properties (“adhesiveness”) on cell behavior is presented.

2.2 Results

2.2.1 Protein micropatterns on substrates by multistep microcontact printing

Microcontact printing (μCP) technique was used to pattern different proteins onto a Nexterion coverslip H. See **Fig.1** for a detailed description of the method. The PDMS stamp for printing was fabricated from a SU-8 lithographic template. In order to increase the affinity with proteins water solution, the stamps were treated with oxygen plasma to become more hydrophilic.

The peptide-inked stamps were placed in contact with Nexterion Coverslip H, allowing patterned covalent immobilization of the molecules by covalent reaction of their amine groups with the activated carboxylic acids at the Nexterion surface. After the first printing, a second stamp with a different peptide-inked was placed in a perpendicular way to obtain a cross pattern. Alternatively, a peptide solution was incubated to form line-background pattern. Due to part of activated carboxylic acids at the Nexterion surface have been occupied by the peptide from the first printing, the peptides from second printing will only bind to the rest place of Nexterion coverslip by activated carboxylic acids.

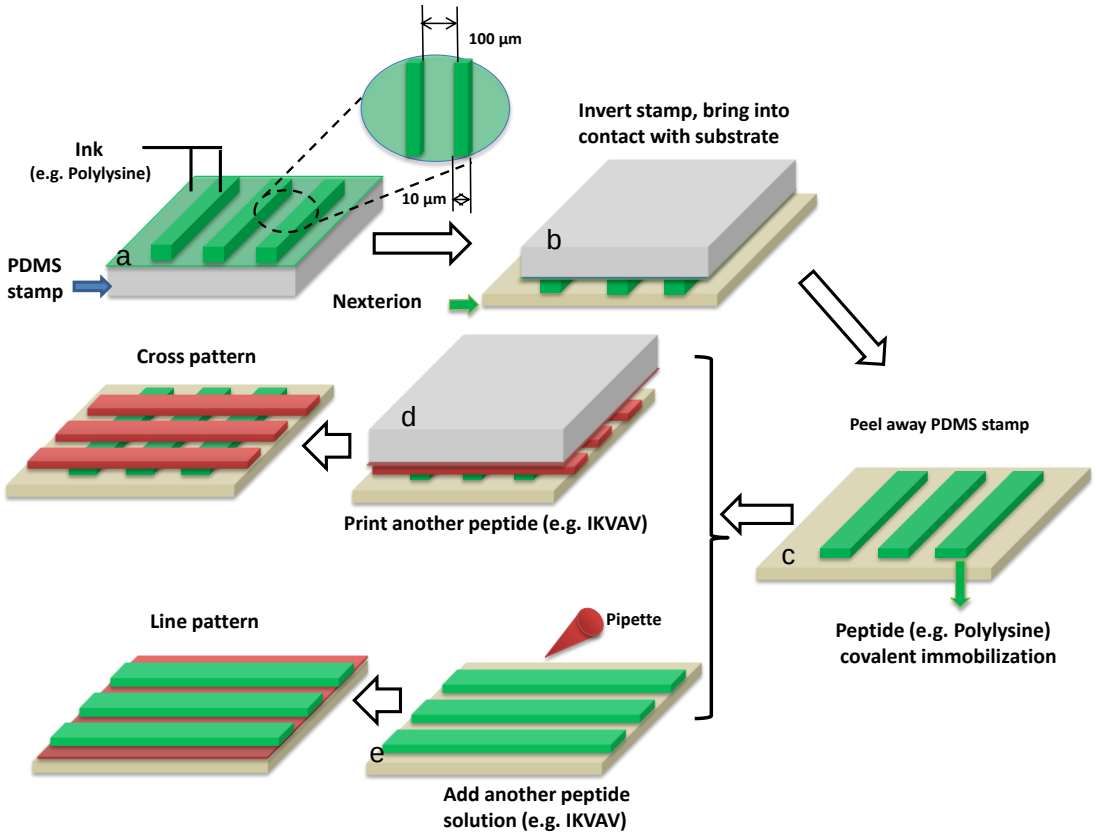

Figure 1: Schematic depicting the steps of microcontact printing process to obtain protein patterns.

(a) The PDMS stamps of 10 microns lines spaced by 100 microns were inked with varying peptide solution: polylysine with FITC (1mg/ml or 0.1 mg/ml in PBS), 19mer-IKVAV (0.1mg/ml in water), RGD (0.1mg/ml in PBS), Fibronectin with Rhodamin (0.1 mg/ml in PBS), Reelin (0.1 mg/ml in PBS).

(b) The peptide-inked (e.g. PL) stamps were placed in contact with activated Nexterion Coverslip H. These coverslips contain a coating layer of cross-linked poly (ethylene glycol) (PEG) functionalized with N-hydroxysuccinimide (NHS) esters, providing a means for peptides covalent immobilization through the amine groups.

(c) After the peeling of PDMS stamp, there is stripe pattern of peptides on the coverslips.

(d) Another peptide inked stamps were brought into contact with Coverslip with the strip orientation perpendicular to that of the previous strips to form cross pattern.

(e) Alternatively, another peptide solution was pipetted directly to Nexterion coverslips to form line-background pattern.

2.2.2 Study of terminal somal translocation *in vitro* as function of adhesive properties of the substrate

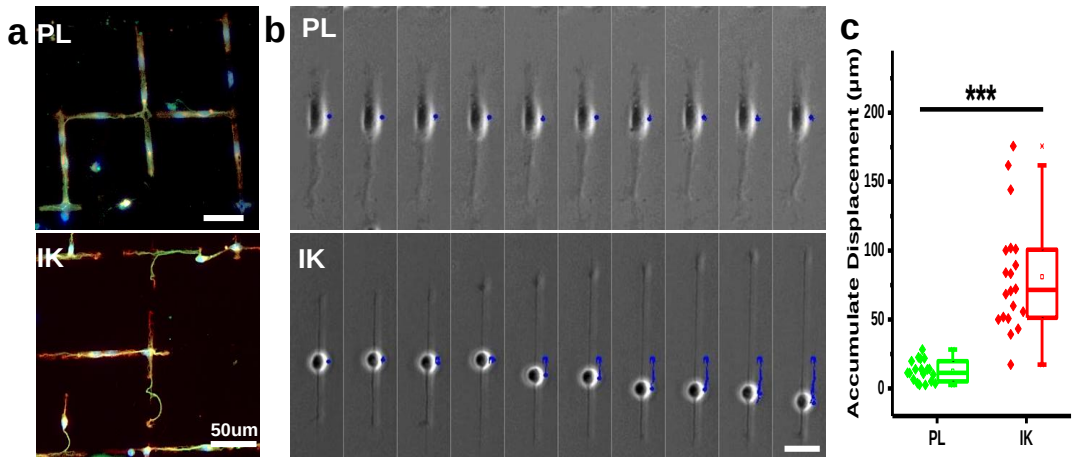

Figure 2: The morphology and behaviors of embryonic cortical early post-mitotic neurons on PL or IK patterns.

(a) Early postmitotic cortical neurons on micro-contact printed PL or IKVAV patterns after 48h culture. (b) Time-lapse Images sequence of a neuron on IK line or PL line. Pictures (from left to right) were taken every 1 hour, showing the displacement of the cells body on the IK line or on the PL line. Blue lines depict the trajectory of the cell body. Scale bar is 20 µm. (c) The accumulate displacement of cell soma in both direction during 10 hours. Neurons show a 6.6 fold increase in the average accumulated displacement on IK patterns VS PL patterns.

I patterned cell adhesive areas onto non-adhesive poly(ethyleneglycol) coatings using the micro-contact printing (µCP) method. I selected Poly (lysine) (PL) and Laminin (LN) as adhesive molecules because they are typically used for neuronal cell cultures [11, 135, 138, 139]. These two molecules have very different physicochemical properties: PL is positively charged at neutral pH and does not have any specific biological function [139, 140]. LN is an extracellular matrix (ECM) protein that specifically interacts with integrin and other cell membrane receptors [141, 142]. I used a 19-mer laminin peptidomimetic (CSRARKQAASIKVAVSADR, abbreviated IK) as alternative to LN to improve the reproducibility of the µCP process. This peptide effectively supported neurite outgrowth in neuronal cell cultures [143]. Early postmitotic cortical neurons were seeded on PEG substrates printed with 10 µm lines of PL or IK. Cells were mainly attached to the printed PL or IK lines and formed patterns reflecting the adhesive contrast of the surface pattern (**Fig. 2a**). On the PL lines, neurons adopted a spreading morphology (cell body area 207 ± 42 μm^2) with wide (7.8 ± 1.4 µm) and short (14.9 ± 4.6µm) neurites (**Fig. 3a-d**). On the IK patterns cells showed less spreading (148 ± 42 μm^2) and extended thin (1.9 ± 1.1 µm) and long (25.9 ± 18.7 µm) neurites (**Fig. 3.b-d**). Cells remained static on the PL lines, but became bipolar and migrated along the IK lines (**Fig. 2b-c**). These results suggest a lower exploratory and migratory activity of the cells on the PL patterns, indicating a stronger attachment.

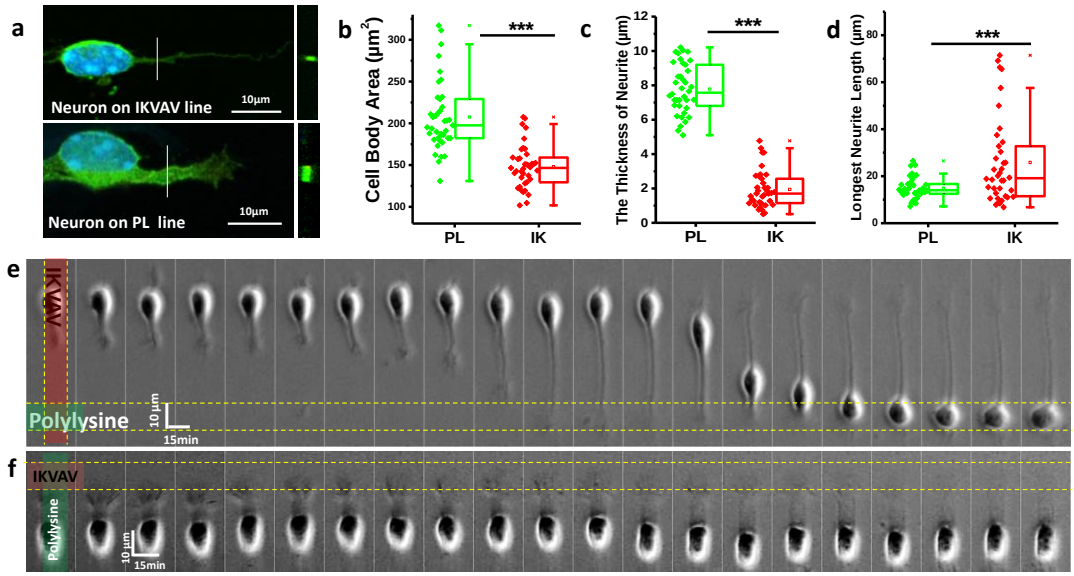

Figure 3: Somal translocation of embryonic cortical early post-mitotic neurons on PL and IK patterns.

(a) Representative image of neurons morphology on PL or IK micro-lines (blue=DAPI, green=SMI, neurofilament marker). Line scan perpendicular the neurite (white line) was performed and images of the yz optical section are shown for better illustration of neurite thickness (right). (b-d) Quantification of the cell body spreading area (b), thickness of neurites (c) and the length of longest neurite (d) on PL or IK lines. (e) Time-lapse Images of a neuron on IK line undergoing somal translocation when the leading process finds the PL intersecting line. Pictures (from left to right) were taken every 15 min. (f) Time-lapse Images of a neuron on PL line. The cell remains static, even when the growth cone touches the IK line. Pictures (from left to right) were taken every 15 min.

When PL and IK were combined in crossed line patterns (PL/IK), single neurons on the IK lines underwent somal translocation events. This occurred when the leading process of a neuron growing along the IK line touched a transversal PL line (**Fig. 3e)**. The GC spread on the intersecting PL line and somal translocation occurred towards

the PL region. As the soma moved forward, the leading process remained anchored to the PL area, while a trailing process appeared and eventually developed into a trailing axon (indicated by neurofilament marker in **Fig. 4a**). After ST, the cell body remained static on the PL line (**Fig. 4b**). This effect was highly reproducible and was not observed for cells attached to the PL lines (**Fig. 3f**). These features resemble those observed during somal translocation *in vivo* [109, 110, 113, 114, 125]. Our results demonstrate that the PL/IK cross pattern is an *in vitro* scenario that replicates the characteristic features of terminal somal translocation observed *in vivo*.

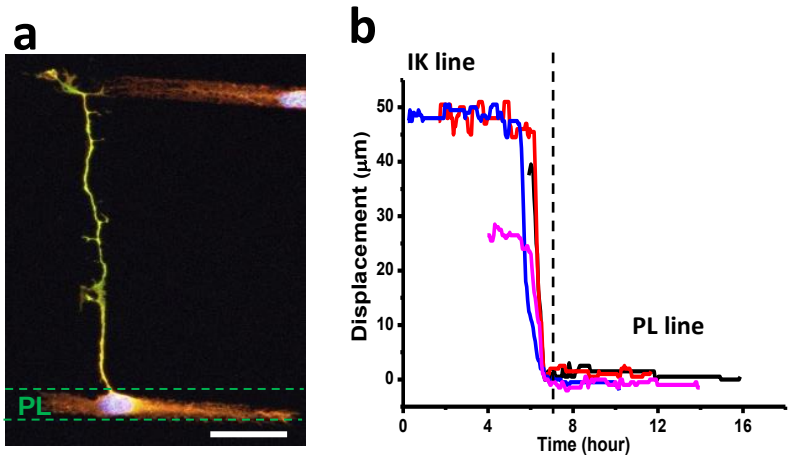

Figure 4: (a) Representative fluorescent image of trailing process after somal translocation (blue=DAPI, red=DCX, Green=neurofilament marker, SMI). Scale bar is 20 µm. (b) The typical changes in the distance of the cell soma on IK lines from the PL lines before/during and after ST, where "after ST" is indicated by the dotted line.

In order to study the influence of the line geometry in terminal ST, neurons were seeded onto substrates homogeneously coated with IK (background) and with 10 µm PL printed lines. Again, single cells on the IK background underwent ST when the leading process touched a PL line (**Fig 5).** Three different phases could be

distinguished during ST: During the first phase (**P_1**) neurons adhering to the IK became multipolar, extending and retracting their neurites and exploring the surrounding area. Eventually the GC of one of these neurites made contact with a PL µ-line triggering the second phase (**P_2**) with two main morphological features. First, the process in contact with the PL line becomes the leading process and the cell morphology changes from multipolar to unipolar or bipolar. Second, the GC of the leading process spreads on the PL µ-line while the leading process becomes straight and thicker. Finally (**P_3**) the soma was displaced towards the PL line. During and after somal translocation, a remnant of the cell body was left behind and often became the trailing axon (Fig. 3a). Notably, the sequence of the morphological alterations was comparable those reported for *in vivo* terminal translocation of early-born pyramidal neurons and other neuronal cell types.[113] These results demonstrate that polarization and somal translocation occurred independently of geometrical guidance (IK microlines), and was only triggered by the adhesiveness contrast between the IK and the PL.

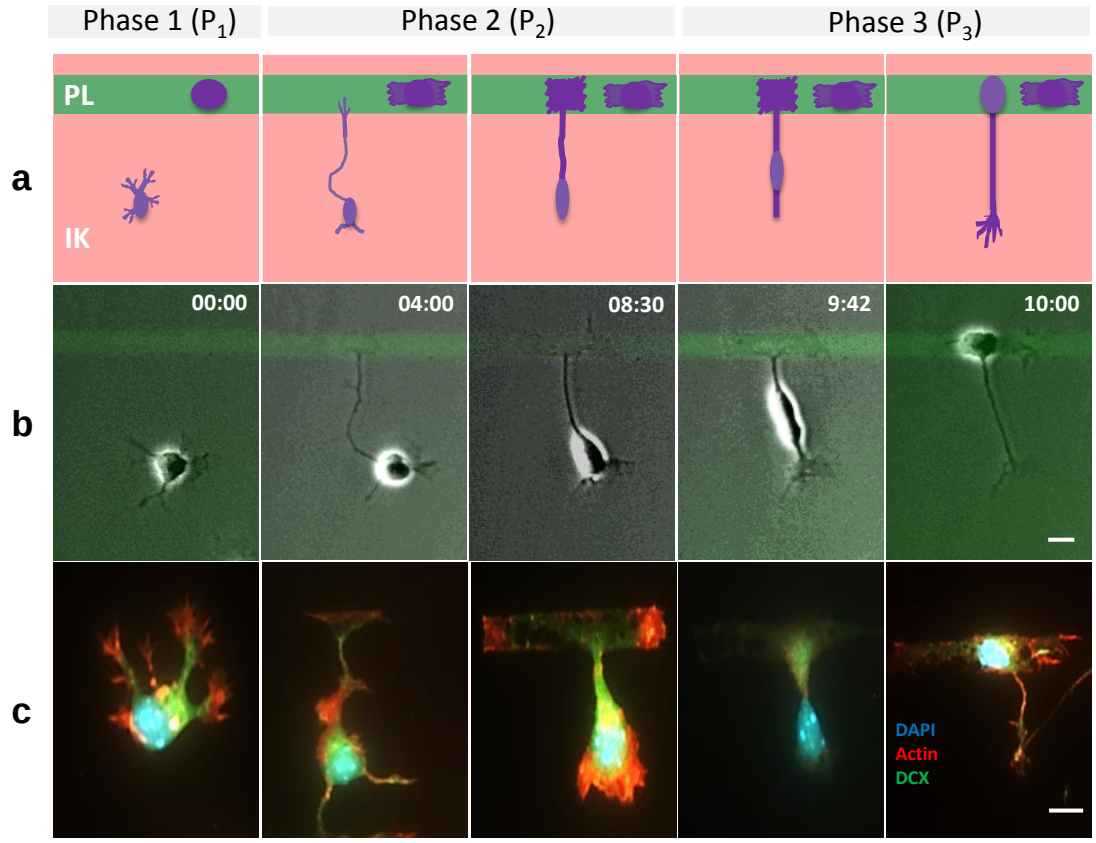

Figure5: Phases of neural somal translocation. (a) Schematic showing the 3 phases: P1- cell attached on IK background outgrow neurites until one the tip of one process reaches the PL line by chance. At that point, the neuron polarizes and this process becomes the leading process. P2- The growth cone of the leading process spreads over the PL line. In parallel, remnant neurites are reabsorbed while the leader process becomes more straight and thicker. P3- Cell body moved towards the PL line, leaving a trailing process behinds. **(b)** Time-lapse images of a cell at the three phases. The different time points are indicated as h: min. Fluorescently labeled PL was used for micropatterning. **(c)** Fluorescent images showing F-actin (red) distribution during the different phases of ST. (blue=DAPI, green=neuronal marker, DCX). Scale bar = 10 µm.

I next asked if the observed behavior was specific for the PL/IK pattern, or if it could be also stimulated by other adhesive molecules. Similar experiments were performed on substrates coated with Collagen IV (COL), Fibronectin (FN) or laminin proteins as background and printed with PL lines (**Fig. 6a and 7a**). Cells on FN and LN coatings showed larger spreading (**Fig. 7c**), shorter neurites (**Fig. 7d**) and preferentially rounded shape (>60%, **Fig. 7e**). IK and COL coatings favored the development of longer neurites (**Fig. 7d, e and Fig.8**). Although ST was observed on all adhesive combinations, the frequency of ST events was significantly higher in cells on IK and COL (52.3% and 53.9%) backgrounds compared to LN (28.9%) or FN (7.2%) (**Fig.7f**). Cells with multipolar and long neurites explored their surrounding more effectively, increasing the probability or reaching the PL µ-lines. For all patterns, GCs were found to spread on the PL lines to cover similar areas (**Fig. 6 b and c**). The time that GCs needed for spreading upon reaching the PL line (T_2) and the speed of somal translocation were similar for all adhesive combinations **(Fig. 6 d and e)**. These results demonstrate that the triggering of ST by adhesive contrast is not specific for PL/IK pattern.

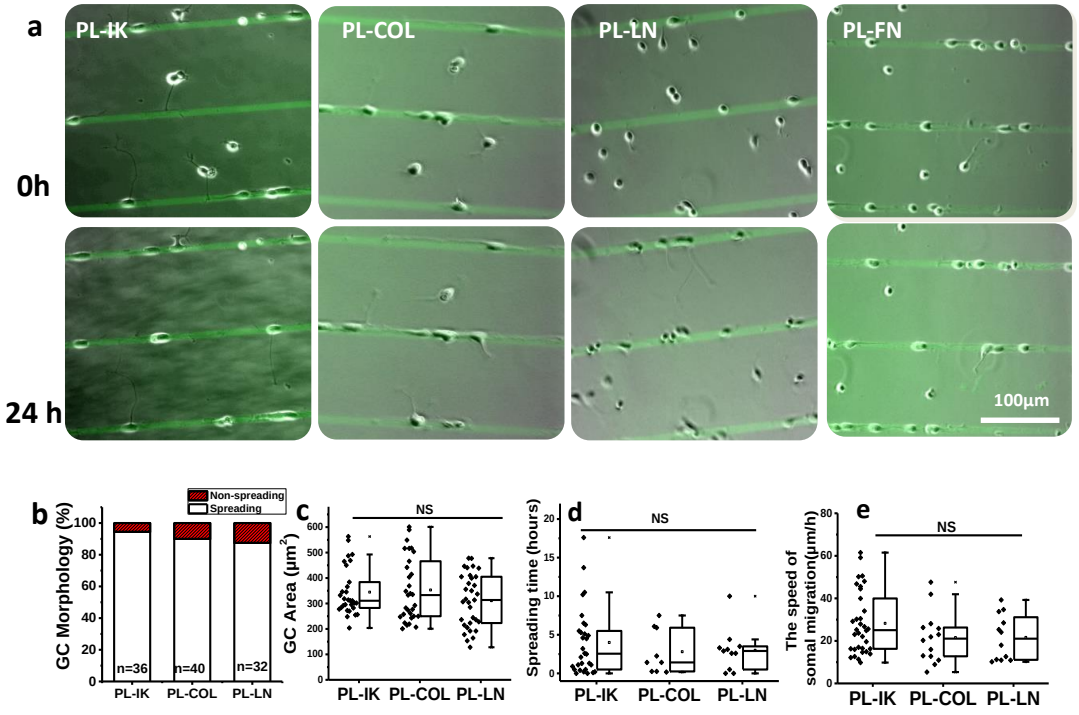

Figure 6: Influence of different background protein in neuronal somal translocation. (a) Time lapse images showing the cell distribution at 0 and 24 h on PL/IK, PL/COL, PL/LN and PL/FN coated substrates, as an indicator of efficiency of somal translocation. Scale bar is 100 µm. (b-e) Quantification of morphological and functional parameters on the different adhesive combinations: (b) morphology of the GC on the PL area, (c) Area of the growth cone, (d) Time required for GC spreading during phase 2 (see Fig.2 and Fig.S12), (e) The speed of somal translocation in µm/h.

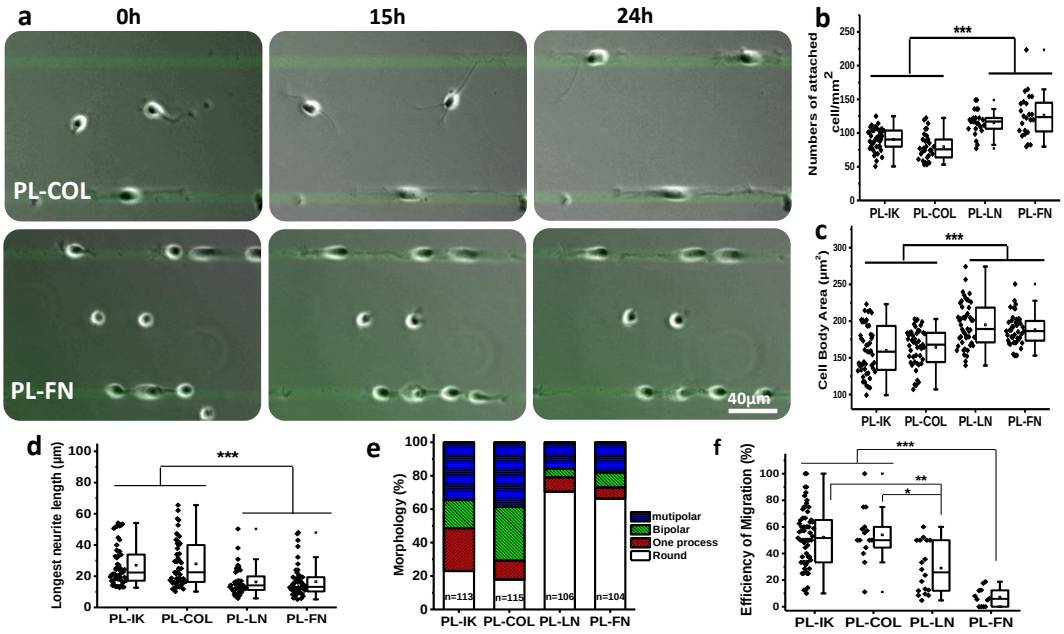

Figure 7: (a) Time lapse images showing the cells at 0 and 24 h of time-lapse on PL/Collagen IV (PL/COL) and PL/Fibronectin (PL/FN) coated substrates. Scale bar is 40 µm. Fluorescently labeled PL was used for micropatterning. See Fig. S3 for other adhesive combinations. **(b-f)** Quantification of morphological parameters on the different adhesive combinations: **(b)** Number of attached cell per mm^2 after cell attachment, **(c)** Area of cell body, **(d)** Length of the longest neurite (*** p <0.001), **(e)** Percentage of cells attached on background proteins that show rounded, one process, bipolar, or multipolar morphology after 12 h (See also Fig.S4). N= number of quantified cells, and **(f)** ST efficiency (*** p <0.001, ** p <0.01; * p <0.05). n= quantified areas (708 ×531 $µm^2$).

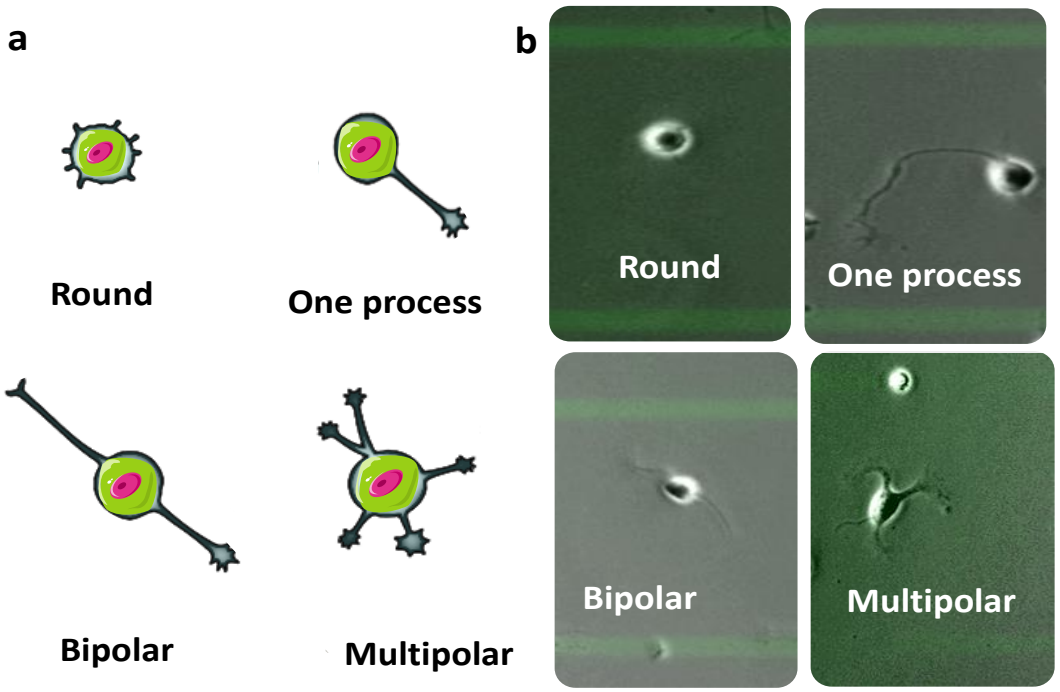

Figure 8: Representative images of early postmitotic cortical neurons with different morphologies: round, extending one single process, with bipolar or multipolar morphology.

I also tested if other adhesive substrates than PL could trigger ST. I printed fibronectin (FN), fibronectin peptidomimetic cyclic(RGDfK) [131, 144], and Reelin protein[125] lines on IK background. Around 95% of the GCs on PL lines showed large spreading areas, whereas less than 51% of GCs spread on FN, RGD or Reelin lines (**Fig 9a, b**). Instead, GCs often showed a branched structure (**Fig 9a**). Somal translocation was observed on all patterns, although the efficiency of somal translocation was significantly higher on PL (52.3%) than on RGD (36.5%), Reelin (29.2%) or FN (24.1%) patterns (**Fig 9c and Fig.10**). In order to demonstrate a possible correlation between GC spreading and ST efficiency, I quantified the percentage of cells that underwent ST from spreading or branched GC morphologies. ST efficiency was >90% when a spreading GC was formed, while it dropped to 40-55% when the GC showed a branched morphology (**Fig. 9 d**). These results highlight a

strong GC-substrate interaction in triggering ST in neurons. The GC spreading time (T_2), and the somal translocation speed (V_3) showed no significant differences among the different protein combinations tested **(Fig. 11)**, indicating that, once activated, the process of somal translocation on the substrates was independent of the type of molecule providing anchoring to the GC and other cell areas.

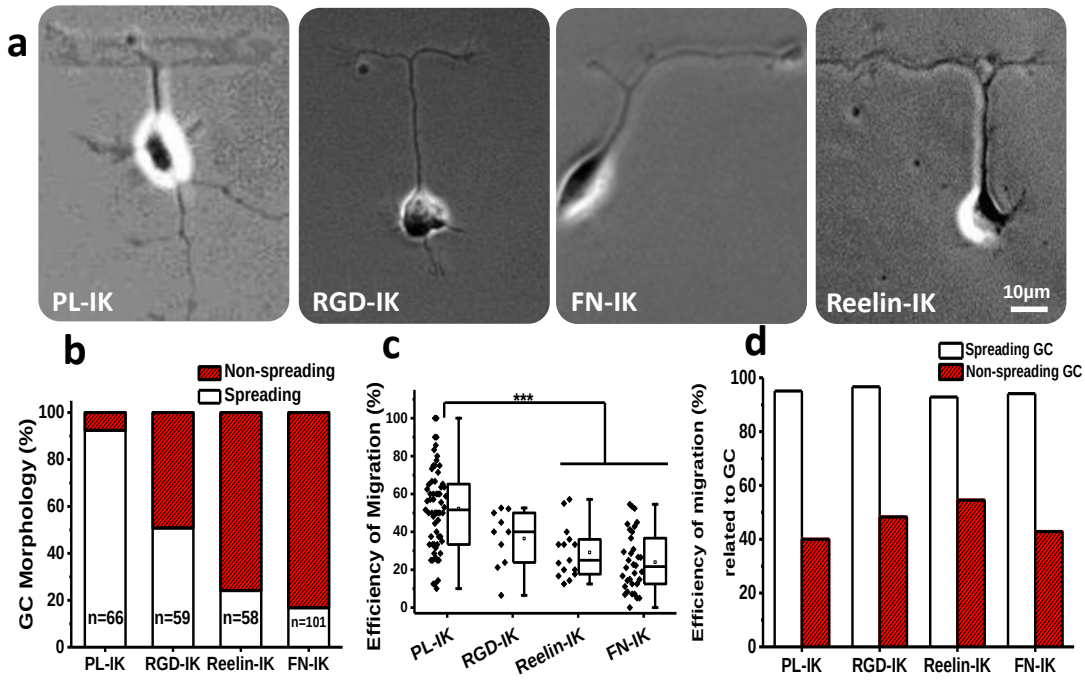

Figure 9: Influence of different adhesive proteins for triggering neural somal translocation. (a) Microscopy images of the morphology (spread or branched) of the growth cone on PL, FN, RGD or Reelin lines on IK background. Scale bar is 10 µm. (b) The abundance of spread or branched morphologies of the GC on the lines with different adhesive molecules. (c) Efficiency of ST on the different adhesive combinations (*** p <0.001). (d) The efficiency of ST for spread or branched GC morphologies (n=61, 5, 30, 29, 14, 44, 17 and 84).

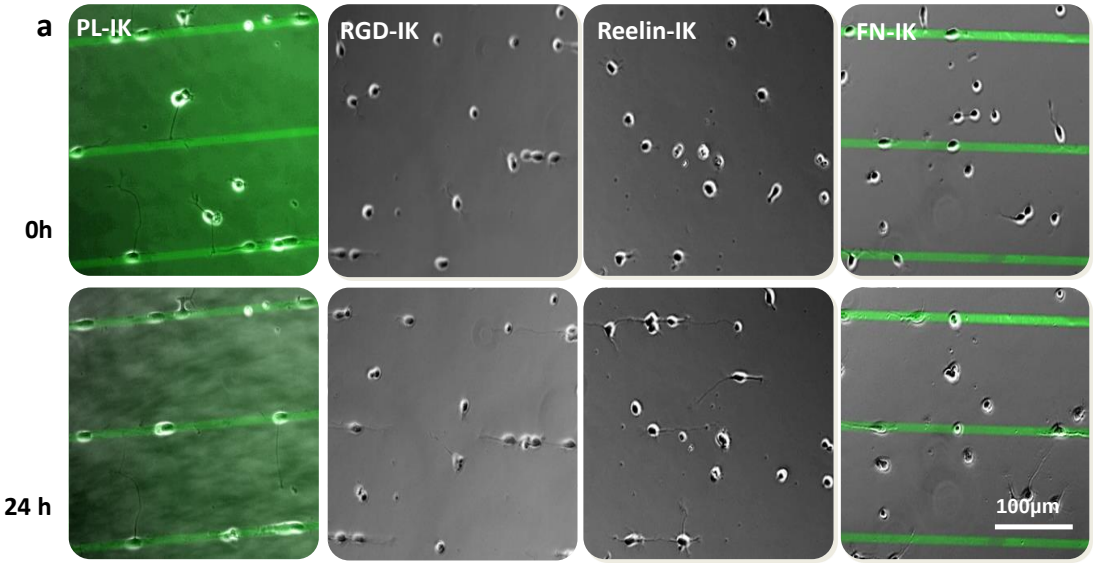

Figure 10: Time lapse images showing the cell distribution at 0 and 24 h on PL/IK, RGD/IK, Reelin/IK and FN/IK coated substrates, as an indicator of efficiency of somal translocation. Scale bar is 100 µm.

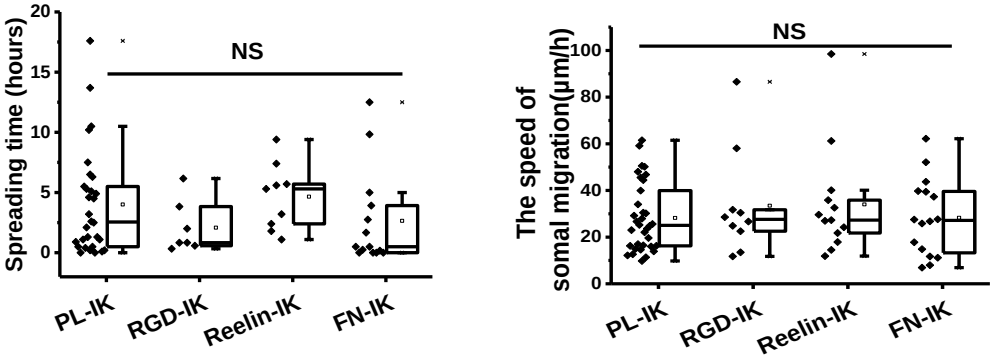

Figure 11: Comparison of GC spreading time and the speed of somal translocation on PL/IK, RGD/IK, Reelin/IK and FN/IK coated substrates.

It should be noted that the concentration of the protein printed on the surface and the PL in our patterns might be different for the different individual combinations. This could also be a reason for the differences in the efficiency of ST among the different proteins, not necessarily the adhesive molecule itself. I asked if adhesive changes caused by different surface density of the same adhesive molecule could also trigger

somal translocation. To address this, I coated background surfaces with different concentrations of PL, and printed microlines with same concentration of PL as well. Contrast profiles and fluorescent images of printed PL line pattern with background coated with different PL concentration were used to proof the contrast of PL density on the same surface (**Fig. 12**).

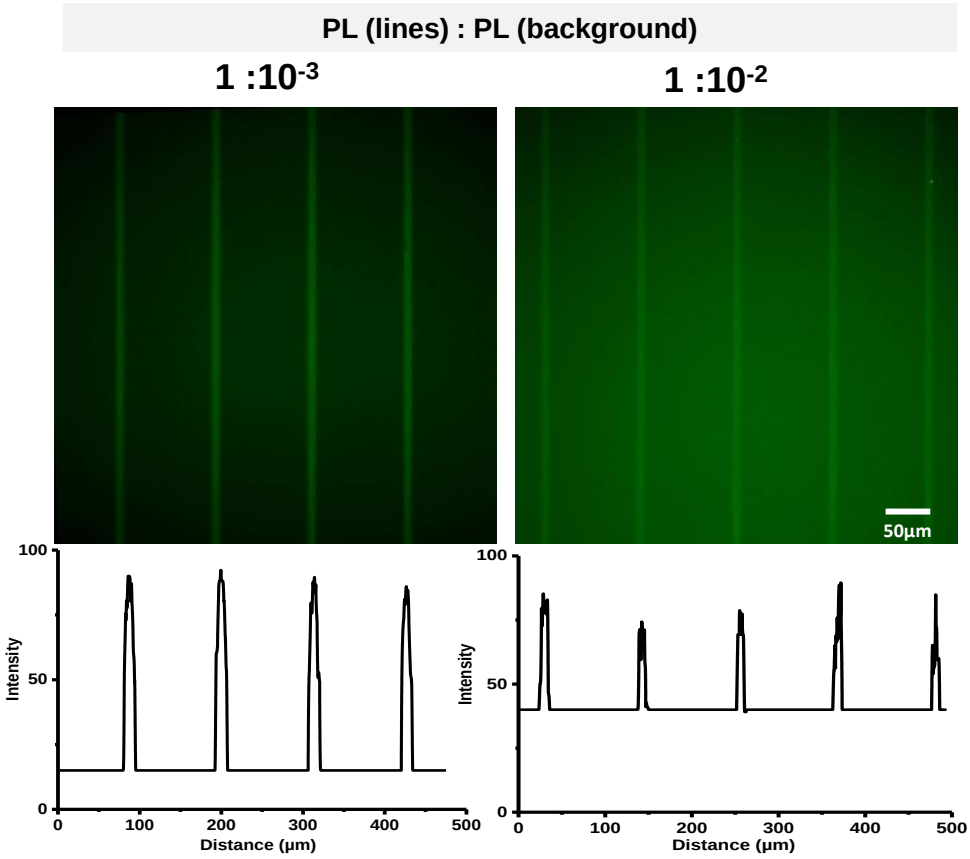

Figure 12: Representative fluorescent images and contrast profiles for PL (lines): PL (background) pattern with 1:10^{-3} and 1:10^{-2}. Green line is PL-FITC, and scale bar is 50µm.

After 24 h most cells on surfaces with 1:10^{-4} and 1:10^{-3} (PL_{lines}:$PL_{background}$, see experimental section for details) patterns underwent ST towards the higher concentrated lines, but little not much ST was observed on substrates with less

pronounced concentration contrasts (**Fig. 13a, b**). Neurons were static on surfaces with PL background concentrations >10^{-2} mg/mL (Fig. 5a). Surfaces with lower PL background concentrations <10^{-3} mg/mL favored exploratory phenotypes (**Fig. 14**) and supported ST efficiently (**Fig. 13c**). These results confirm that ST can be triggered from surfaces where cells remain exploratory and motile to more adhesive areas where GC spreading occurs. Note that in a previous report Hippocampal neurons seeded on glass substrates were found to migrate to PL patterned areas as well [137]. These findings evince that the adhesive properties of the molecular environment may serve as key determinant of neuronal ST and neuronal organization during corticogenesis, challenging the view of specific membrane receptor-ligand molecular interactions as triggers for ST. However, with the current data the role of specific membrane receptor-ligand cannot be completely excluded. Additional work is required to fully discharge specific interactions.

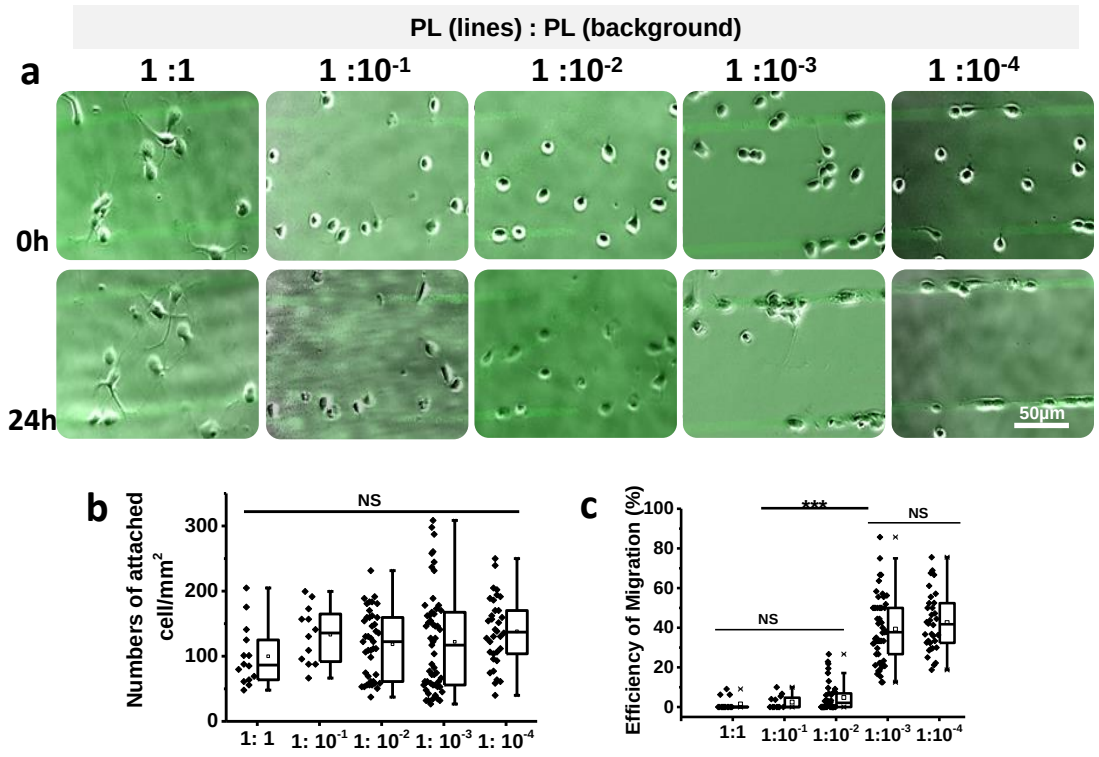

Figure 13 Adhesive contrast triggers somal translocation. (a) The distribution of cells on PL/PL patterns with PL micro-contact printed lines and decreasing PL background concentrations (1:1, 1:10-1, 1:10-2, 1:10-3 and 1:10-4) at 0h and 24h of time-lapse. Scale bar = 50 µm. Fluorescently labeled PL was used for microcontact printing. (b) The number of cell attached per mm2 after cell attachment. (c) The efficiency of somal translocation on the different PL/PL patterns (*** p <0.001, NS = not significance). n= number of quantified area (708 ×531 µm2).

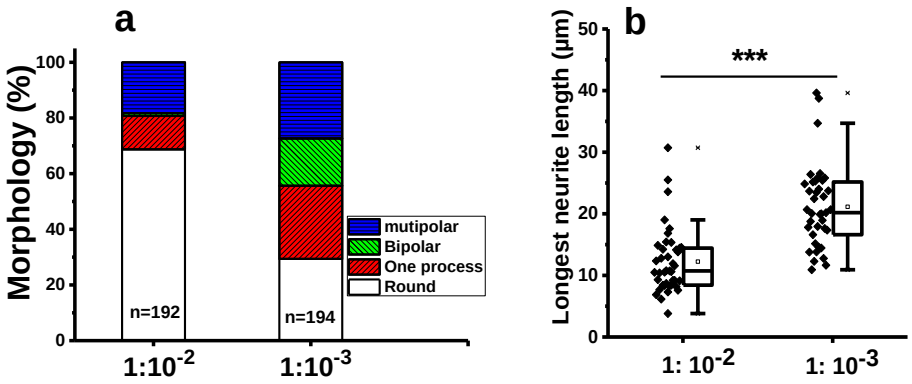

Figure 14: (a) Percentage of cells that show round, one process, bipolar, or multipolar morphology on PL/PL patterns (see Fig 5 in manuscript). N= number of quantified cells. (b) The length of the longest neurite at 12 hours (*** p <0.001).

2.2.3 Spreading of the growth cone determines somal translocation

The central role of the GC during locomotion has been evinced in several reports.[135,136]. In our study, the GC spreading on the PL lines to cover areas of 363 ± 117µm^2, i.e. approximately 5.5 times larger than the area of the GC on the IK coatings (**Fig. 15**).

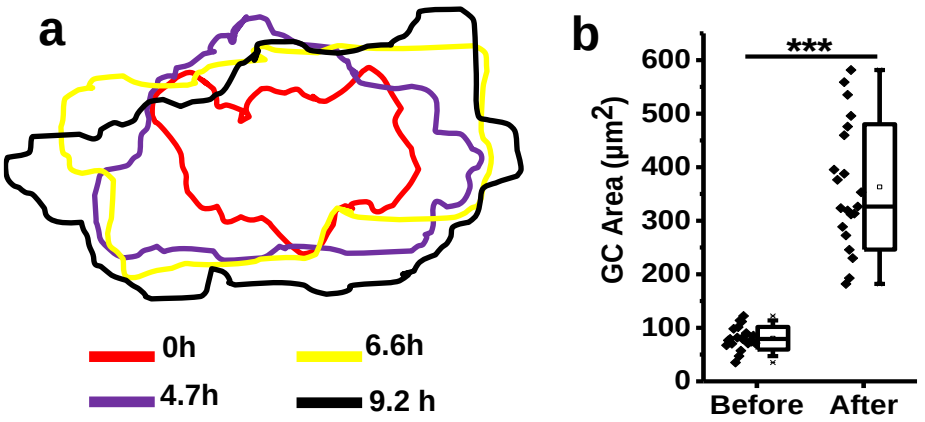

Figure 15: Spreading of the GC on the PL line. (a) Contours of GC traced from the time-lapse and superimposed contours with pseudo-colors. The GC reached the PL line at 4.7h and ST occurred at 6.6h. (b) The average GC area of cells on IK background before and after contacting PL line on PL-IK pattern.

During the spreading of the GC, the leading process stretched to form a straight line between the anchored GC and the soma, independently of the trajectory of the GC during exploration phase (**Fig. 16a,**). The stretching process also became wider before ST. These features support a scenario where anchoring and stabilization of the GC on the PL line enables force generation at the leading process for effective translocation of the soma [122, 135, 136]. I examined if a minimum spreading area is required to mechanically stabilize the GC in order to support ST. IK-coated substrates were printed with PL circles with diameters between 10 µm (78.5 μm^2 area, i.e. the typical size of the GC on IK background) and 20 µm (314 μm^2 area, i.e. the typical size of GC spread on the PL lines) (**Fig.15, Fig. 16b, and Table 1)**. When a GC reached the PL circle, it spread over the whole adhesive area (**Fig. 16c and Fig.17**). On the 10 µm PL circles approximately 40% of the cells retained multipolar morphologies and 56% failed to translocate their soma after GC spreading. On the 20 µm circles more than 90% of cells developed a single process or bipolar morphology

and underwent ST (**Fig. 16d, e**). Intermediate behavior was observed on the 15 µm PL circles. These results indicate that the spreading area of the GC strongly affects the efficiency of ST.

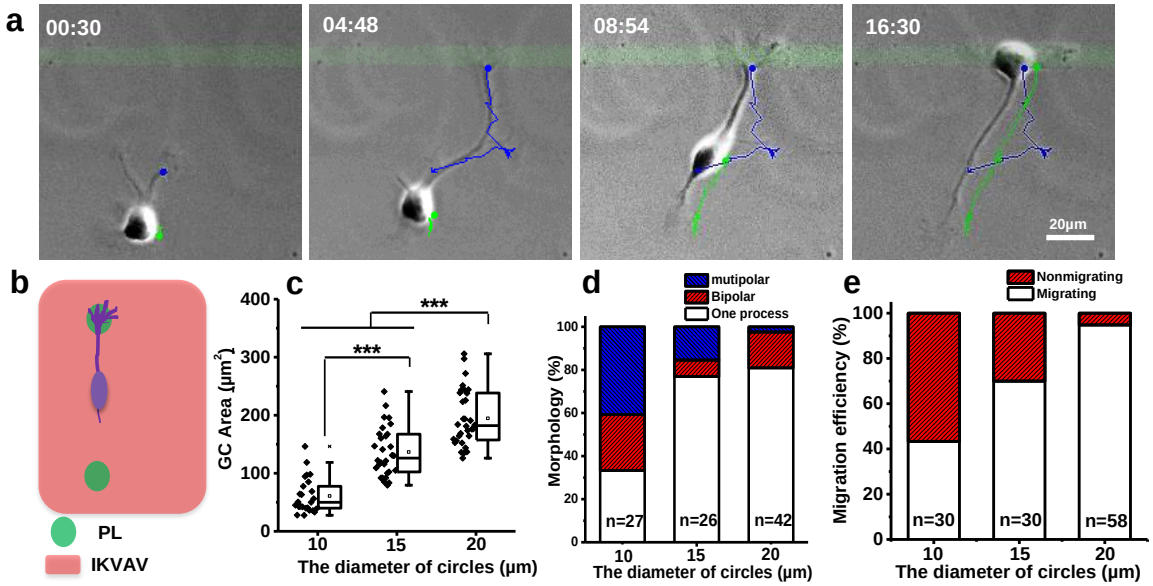

Figure 16: Spreading of the Growth cone on leading process is a crucial step for somal translocation. (a) Snap shot images of a trajectory of a neuron on IK background migrating towards PL line (green fluorescent). Blue and green lines depict the trajectory of the GC and soma respectively. Scale bar corresponds to 20 µm, the different time points are indicated as h:min. (b) Schematic of the PL circle patterns with increasing diameter. (c) Area of the GC on the PL circles of different diameter. (d) The percentage of cells that show one process, bipolar, or multipolar morphology after attachment of their neurites to the PL circles. (e) Efficiency of the somal translocation on the circle patterns of different diameter.

PL –IK Pattern			
Average Growth Cone Area (µm²)	Before contact PL	After contact PL	
	80.5 ± 21.2	363.2 ± 117.1	
Circle pattern substrate			
Diameter of Circle	10 µm	15 µm	20 µm
Circle Area (µm²)	78.5	176.6	314

Table 1 The average area of GC before and after contacting PL and the circle pattern with different diameter and area.

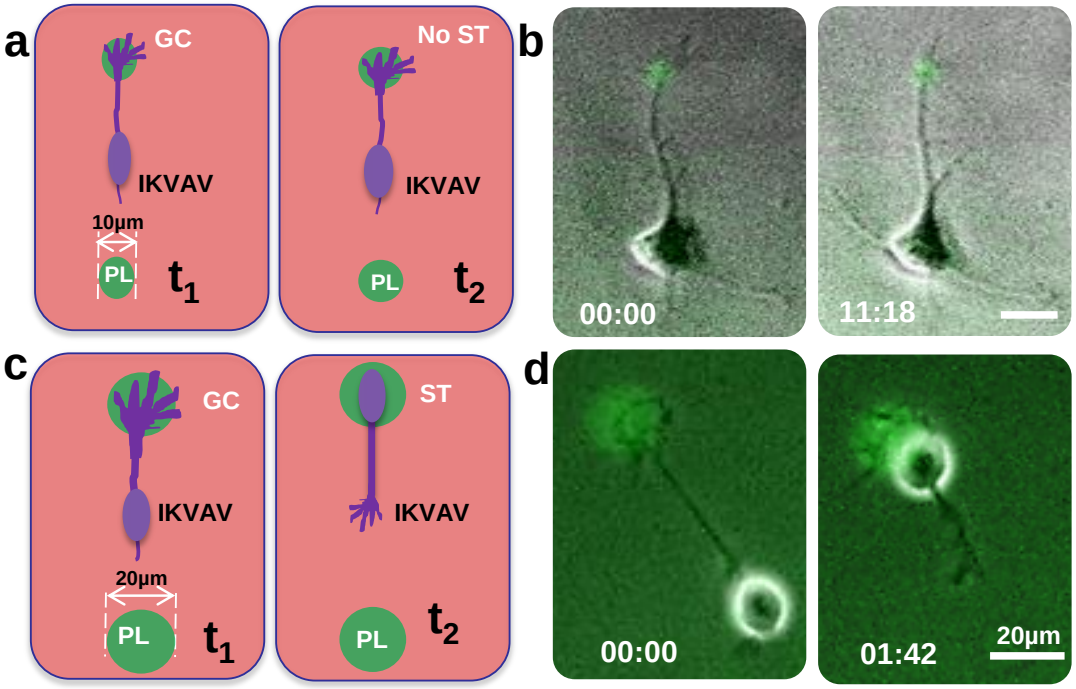

Figure 17: The behavior of neuronal cells when the GC reaches an adhesive 10 µm (a and b) and 20µm circle patterns (c and d) at different time points. The different time points are indicated as h: min. Scale bar is 20 µm.

2.2.4 Actin filaments and microtubules are required for somal translocation

Actin and microtubule scaffolds play a major role in the movement of the soma in granular cells [136]. I scrutinized the involvement of actin fibers, myosin contractility, and microtubular structures in ST on our platform by applying different

pharmacological treatments: Blebbistatin (Blebb), Latrunculin B (LB), Cytochalasin D (Cyto-D), Y27632 (Y27) or Paclitaxel (PTX) (**Fig. 18**). I observed drug treated cells showed higher percentages of round morphologies (21.4% Blebb, 53.8% LB, 36.9% Cyto-D, 62.5% Y27 and 33.3%Paclitaxel). The cell body of drug treated cells occupied larger areas compared to control conditions (**Fig. 18a**). LB- and Y27-treated neurons displayed significantly shorter neurites than the controls (**Fig. 18b**). There was a general reduction in GC spreading among the drug-treated cultures (44.4% Blebb, 31.6% LB, 57.9% Cyto-D and 53.1%Paclitaxel) *vs.* the controls (94.7%), with the exception of Y27 (95.8%) (**Fig. 18d**). In line with this, efficiency of ST was markedly reduced (1.5 to 3.8 fold) after most of the drug treatments (**Fig. 18e**). Our results are in agreement with previous findings showing that both cytoskeletal structures, i.e., actin filaments and microtubules, are needed to mobilize the cell soma [135, 136].

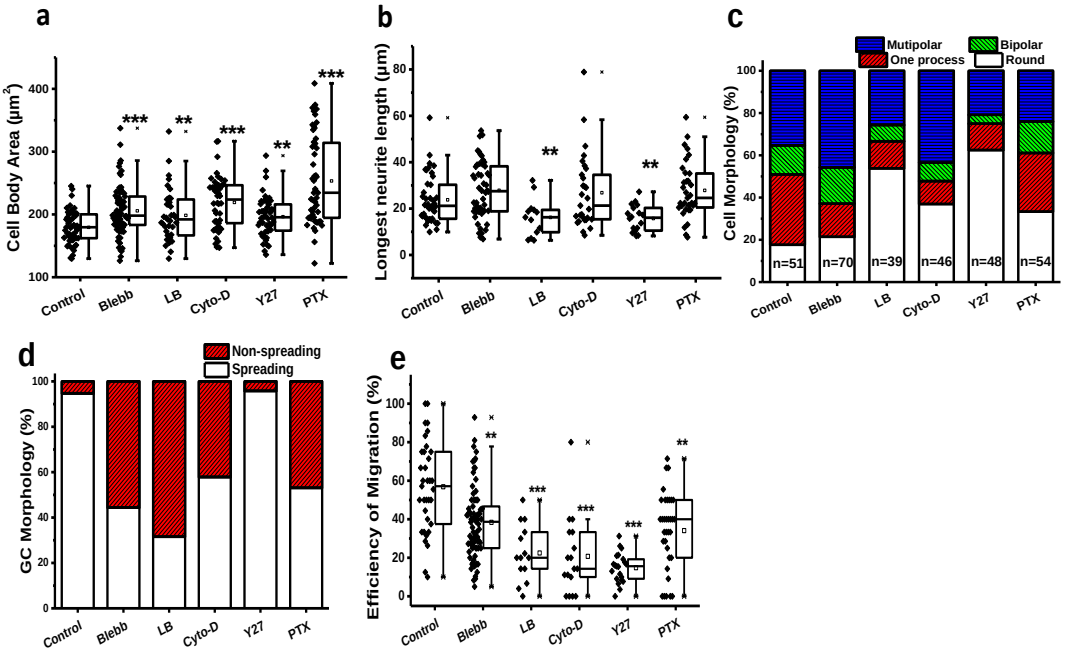

Figure 18 The role of cell cytoskeleton on somal translocation. The figures show a comparative analysis of different parameters of cell morphology measured after

application of the pharmacological treatment: Blebbistatin (Blebb), Latrunculin B (LB), Cytochalasin D (Cyto-D), Y27632 (Y29) or Paclitaxel (PTX). (a) The area of the cell body. (b) The length of the longest neurite of cells. (c) The percentage of cells that show round, one process, bipolar, or multipolar morphology. And n= number of quantified cells, *** p <0.001; ** p <0.01. (d) The morphology of the GC on the PL line (n = 38, 54, 19, 19, 24, and 38 cells). (e) The efficiency of the somal translocation. p<0.001; ** p <0.01.

2.3 Discussion

Micropatterned substrates with adjacent areas of different adhesiveness replicate relevant signals found in the natural microenvironment of the developing cerebral cortex and can support, trigger, and spatially guide neuronal somal translocation. The combination of a low-adhesive background and high-adhesive patches stimulated the expansion of long neurites in the former, and reproducibly promoted GC expansion and ST to the latter in early postmitotic cortical neurons. This novel platform allowed us to successfully reproduce and quantify the morphological features of ST, including neurite formation and reabsorption, growth cone spreading, thickening of the leading process, and translocation dynamics. This is an ideal *in vitro* model to interrogate environmental cues stimulating neuronal migration with the possibility to study cytoskeletal regulation and organization.

I have found a relationship between substrate properties and morphological parameters to describe neuronal behavior on ST-supporting substrates. On low-adhesive coatings neurons showed low spreading of the cell body, dynamic neurite

growth and retraction, and thin processes. On high-adhesive coatings neurons displayed a spreading soma and thicker and wider neuronal processes. When the GC of a neuron on a low-adhesive substrate crossed to a high-adhesive area, it spread and ST was triggered. Our adhesive contrast hypothesis is supported by *in vivo* data. Stabilization of the GC of the leading process in the marginal zone is necessary for neuronal migration *in vivo*, and the different concentrations of FN at these zones could be a relevant triggering signal[120, 128]. The *in vitro* scenario proposed here is chemically simpler, but it agrees with reported migration behavior of cortical neurons when the leading process anchors near the pia during the radial expansion of the developing cortex[106, 114, 145, 146]. Interestingly, Jiang et al. recently demonstrated that the GC of leading process is attached more strongly than the trailing process during ST[136] consistent with distinct degrees of adhesiveness provided *in vivo*.

Adhesion strength strongly modulates cell migration by providing anchorage and allowing force application and transmission[147]. Polarization and migration directionality are relevant and are interconnected factors in neuronal migration, and are highly dependent on the adhesive properties of the environment [148]. In neurons, ligand density seems to affect GC directionality [143]. This is particularly relevant in terminal ST, as it could define the final position of the migrating neuron[106, 113, 114]. Consistent with this data, I demonstrate that the expansion of the GC is associated with the thickening of the leading process as fundamental morphological changes to trigger migratory action. Here I provide a simple experimental microenvironment to study ST under conditions of controlled variable adhesive ligand

types and densities, while simultaneously imaging of the cytoskeletal components during the different phases of ST.

I observed the retraction of minor neurites in multipolar cells in correlation with the spreading and anchoring of the leading GC during ST *in vitro*. Remarkably, neurons that found GC expansion limitations also failed to induce the absorption of the other processes. The permanence of these neurites could become a mechanical obstacle that would thwart the formation of an actin contractile rim at the rear of the soma. It has been shown that the actin contractile center forms after the GC expansion and the actin rim was found to be essential to develop ST forces [136] . In light of the sequence of phases during ST observed in our *in vitro* model, I hypothesize that GC expansion not only enhances anchoring, but ultimately is the up-stream initiator of the remodeling of the cytoskeleton to support the mechanical tension required for dragging the soma.

2.4 Conclusion

Elucidating the mechanical requirements and parameters of the molecular environment that regulate migration is crucial for the understanding of the neuronal positioning occurring in the developing brain. Here I demonstrate how substrates with spatially confinement regions of different surface properties (“adhesiveness”) can trigger, guide or hinder somal translocation on a biomaterial surface. Using microcontact printed patterns of different adhesive molecules, I engineered a platform which allows for *in vitro* triggering and studying terminal ST. The contrasting adherent regions on the substrate can guide and direct ST, and represent a simple yet flexible method to control it by tuning surface interactions. I demonstrate that GC expansion

and spreading area are intimately related to the onset of ST. In addition, the process of nucleokinesis towards the GC requires both actin fibers and microtubules to succeed. This novel platform emerges as a promising tool to study the fundamentals of neuronal migration during development and neuronal disorders with dramatic consequences in cortex development, such as lissencephaly with cerebellar hypoplasia (LCH)(Gupta et al., 2002; Hong et al., 2000).

2.5 Materials and methods

Reagents and Materials

N-hydroxysuccinimide (NHS) functionalized Nexterion coverslip H (Schott, Material code: 1098523), silicon gasket (ibidi GmbH, Material code: 81201), Poly-D-lysine (SERVA Electrophoresis GmbH), RGD (cyclo(Arg-Gly-Asp-D-Phe-Lys), peptides international), Recombinant Mouse Reelin (R&D systems), Fibronectin–FITC Labeled (Cytoskeleton, Inc.), 19mer IKVAV (Alfa Aesar), Y27632 (Miltenyi Biotec GmbH) and Cytochalasin D (Santa Cruz Biotechnology) were purchase from specified companies. Poly-L-lysine–FITC Labeled, Laminin, Collagen IV, Blebbistatin, Latrunculin B and Paclitaxel were purchased from Sigma-Aldrich. All other reagents were obtained from Sigma-Aldrich unless otherwise specified.

PDMS stamps for microcontact printing

The PDMS stamp for printing was fabricated by standard soft lithography techniques [149]. A SU-8 lithographic template was used for double soft molding to obtain PDMS stamps [150, 151]. The SU-8 template was previously functionalized with

(1H,1H,2H,2H-perfluorodecyltrichlorosilane) to avoid mold sticking. PDMS precursor (Dow Corning, Sylgard 184) was mixed with 10:1 ratio of prepolymer:curing agent and degassed for 30 min before poured on the SU-8 template and cured at 90 °C for 1 h. PDMS precursor was poured onto the PDMS soft template and baked at 90 C for 1 h to get the PDMS stamp. Stamps were cut to fit into the wells of the silicon gasket for printing.

Functionalization of substrates by multistep microcontact printing

PDMS stamps were washed with acetone and water by sonication to remove the uncross-linked oligomers and clean the surface. The stamps were treated with oxygen plasma (100W, 0.1mbar) for 30s to become more hydrophilic and inked with various peptide or protein solutions (1mg/ml or 0.1mg/ml PLL-FITC, 1mg/ml PDL, 0.1 mg/ml Fibronectin-FITC, 0.1 mg/ml Reelin and 0.1mg/ml RGD) for 60 min, followed by rinsing with Milli-Q water, and drying with N_2 flow. Only stamps inked with 0.1 mg/mL IK were dried by air drying. The peptide-inked stamps were placed in contact with Nexterion Coverslip H for 60 min. The Nexterion coverslip was divided in 12 wells (0.56 cm^2 per well) by placing a silicone gasket on the top. After the peeling of stamp, a second printing step with a different peptide-inked stamp (0.1 mg/mL IKVAV) was performed to obtain a cross pattern. Alternatively, a peptide solution (0.01 mg/ml IKVAV, 0.01 mg/ml Laminin, 0.01mg/ml collagen IV and 0.01 mg/ml Fibronectin) was incubated Nexterion for 60 min to form line-background pattern. Printing and coupling steps occurred at room temperature and at a relative humidity >80%. Substrates were blocked by immersing in 50mM ethanolamine in PBS for 60 min, rinsed with water 3 times. Before the cell experiment, the substrates were sterilized by incubated in 70% ethanol for 5 min and rinsed with sterile PBS 3 times.

Cell isolation and cell seeding

Cerebral cortex from E14.5 of C57BL/6 mice (Janvier-Labs) was digested in 0.5% trypsin EDTA (GIBCO) for 15 min at 37 C. Then trypsin was inactivated by the plating medium (DMEM, GIBCO) and 10% FBS (Hyclone) and gently triturated with 5-ml disposable pipette to get single cell. After centrifugation at 1000rpm for 5 min cell pellets were resuspended in 1 ml differentiating medium (DMEM-GIBCO and 2% B27-invitrogen) and seeded directly in the 12 wells at a density of 62 500 cells / ml. The cell density was obtained with a TC20™ Automated Cell Counter (Bio-Rad). After the cells attached, the substrates were imaged by time-lapse microscopy for 24 or 48 hours. All animal procedures were carried out in accordance with the Policies on the Use of Animals approved by the Institute of Physiological Chemistry, University Medical Center, Johannes Gutenberg University Mainz.

Time-Lapse microscopy

Video microscopy of neurons was performed with a Cell Observer microscope (Zeiss) at 37°C and 5% CO_2. Phase contrast images were acquired every 6 minutes during 2 days using a 20x phase contrast objective (Zeiss) and an AxioCamHRm camera with self-written VBA module remote controlling Zeiss AxioVision 4.7 software. Single-cell tracking and movies assembling were performed using ImageJ 1.42q (National Institute of Health, MD, USA) software.

Immunostaining and Image acquisition

Cells were fixed with 4% paraformaldehyde for 10 min. After washing with PBS three times, cells were pre-incubated with blocking solution (3 % BSA and 0.2 % Triton X-100 in PBS) at RT for 1 h and then incubated with following primary antibodies overnight at 4 °C: Mouse anti-neuronal filaments (SMI-312, abcam, 1:800 diluted), Guinea Pig anti-DCX (Jackson ImmunoResearch Laboratories, Inc, 1:500). The secondary antibodies (1:1000) were A488-conjugated goat anti-Mouse (Invitrogen) and Cy3-conjugated anti- Guinea Pig (Jackson ImmunoResearch Laboratories, Inc.). For F-actin staining, the cells were incubating with TRITC-labeled phalloidin (Sigma, 1:200). At the end, the cells were mounted by mounting medium with DAPI (dianova, SCR-038448) on a glass slides. Image acquisition was carried out with laser-confocal microscopy (SP5, Leica) using a 63x oil-immersion objective. The z-series were obtained and then visualized as single optical scans with concurrent orthogonal view.

Drug Treatment

Drugs were applied after cells attachment on PL/IK patterns and cell behavior was followed for 24 h. The following concentrations were used: 0.1% DMSO (control), Y27632 (Y27; 50 µM), Blebbistatin (Blebb; 50 µM), Latruculin B (LB; 2 µM), Paclitaxel (PTX; 1 µM) and Cytochalsin D (Cyto-D; 100nM).

Imaging and data Analysis

The acquired fluorescent images and phase contrast time series were processed and analyzed with Fiji (distribution of ImageJ). For the quantification of the thick of neurite,

z-stacks at a slice distance of 0.5 µm were acquired of fixed samples stained for neurofilament marker (SMI) or neuron marker (DCX). To assess the thick of neurite, a line scan perpendicular the neurite was performed and the plot profile of fluorescence was measured to get the FWHM value considered as neurite thickness. The yz optical section of z-stacks was generated by orthogonal view of Fiji.

For the analysis the influence of different ECM component on cells, the following parameters were quantified. i) The number of attached cells per mm^2 as a measure of adhesiveness of the coated protein, ii) the morphology of the cells attached on background (rounded, multipolar, bipolar, single process) [152] after 12 hours culture, iii) the length of the longest neurite attached on background after 12 hours culture as indicators of polarized or exploratory status of the cells, and iv) the percentage of cells undergoing neural somal translocation towards the PL lines during 24 hours as indicator of the efficiency of the ST process. Briefly, a phase contrast time series (708 ×531 μm^2) in a period of 24 hours was used to calculate (**Fig. 19**). The number of cell adhesion is the number of cells which attach to the substrate at the beginning of Time-lapse (0h). The cell migration efficiency (Efficiency), the cells which migrate to line protein (M) after 24 hours, and all the cells which located between lines (background) at the beginning of time-lapse (A) defined as:

$$\text{Efficiency} = M/A$$

The time of Phase 2 (T_2) corresponded to the spreading time of GC. The speed of the ST corresponds to the ratio between the length of leading process at the beginning of somal translocation (d_1), and the time of phase 3(T_3):

$$\text{Speed} = d_1/T_3$$

Cell trajectories were recorded with the Fiji MTrackJ plug-in. Every slide of the position of cell body or GC was marked by manually clicking on the cell. The migration efficiency related to the GC morphology is defined as the percentage of cells (M-S) that display spreading GC and migrate to line pattern divided by all cells that found the line pattern by spreading GC (A-S).

Efficiency =M-S/A-S

Or the percentage of cells (M-B) that form branching GC and migrate to line pattern divided by all cells that found the line pattern by branching GC (A-B).

Efficiency =M-B/A-B

For circle pattern, the migration efficiency (Efficiency-Circ) is defined as the percentage of cells (M-Circ) that migrate to PL circles divided by all cells that found the PL circles by neurites (A-Circ):

Efficiency-Circ =M-Circ/A-Circ

In the PL circle experiment, the morphology of cell was measured by the percentage of cells that showed one process, bipolar, or multipolar morphology after the neurites attached to PL circles. For migrating cells, the morphology was defined when the soma started to migrate. For non-migrating cell, the shape of cell was chosen at the end of time-lapse (24h).

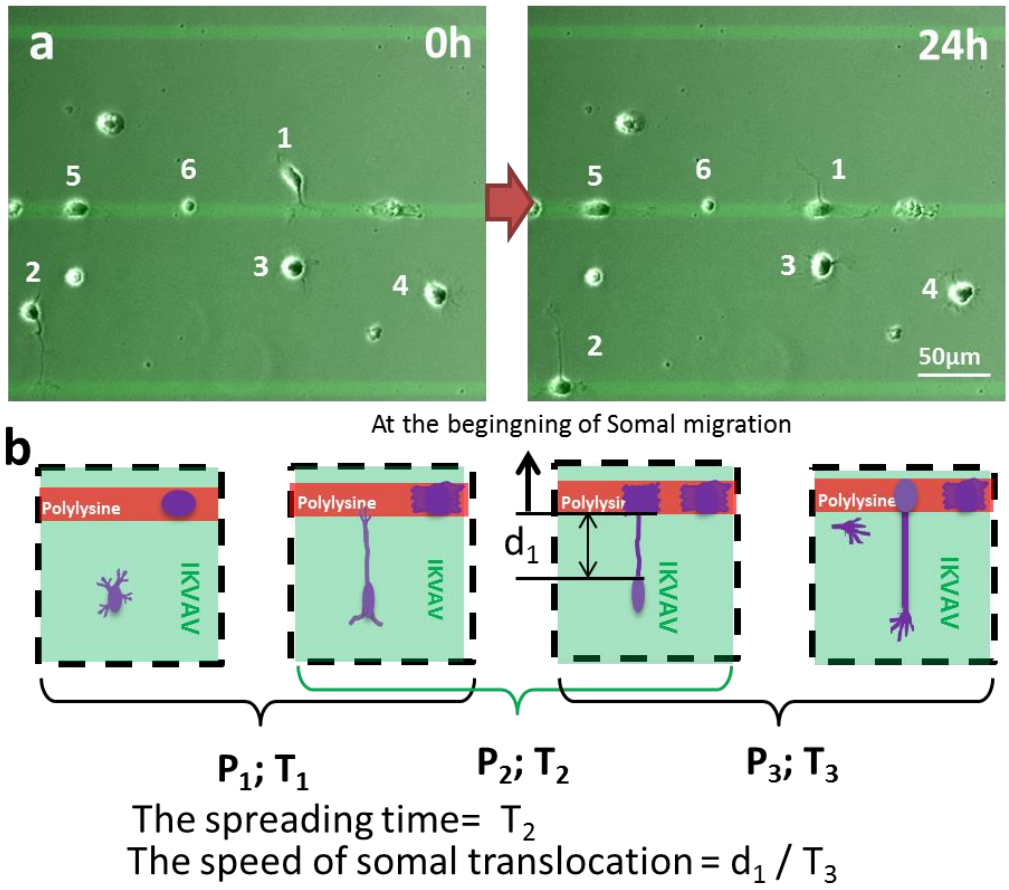

Figure 19: Representation of different variables used for quantification and data analysis.

(a) Microscopy pictures showing migration of attached cells from the background to the line pattern. In order to demonstrate clearly, here I use an example with small area cropped from a 708 ×531 µm2 image. As shown, there are 6 cells (except dead cells) on the area at 0 hour, so the number of cell adhesion is 6. And there are 4 cells located between lines, where two of them (number 1 and 2 cells) migrate to line protein after 24 hours. So the migration efficiency is 50 %. The morphology and length of longest neurite of cells located between lines and without touching lines were calculated by the image of 12 hours from time series. (b) Schematic depicting the calculation of spreading time and somal translocation.

Statistical analysis

For each condition a minimum of three independent experiments were performed. Data were expressed as mean ± standard deviation. Box plots represent the middle 50% of data between the 1st to the 3th quartile (interquartile range IQR); the whiskers indicate variability outside the upper and lower quartiles. One-way ANOVA was used to determine significance between groups followed by a post-hoc Tukey contrast (GraphPad Software). For non-parametric data, I performed Kruskal-Wallis analysis followed by Dunn's post-hoc multiple comparisons. All the cases a value of $p < 0.05$ was used for statistical significance.

Chapter 3

3. Guided neurite extension by light

Note: Parts of this chapter have been published in: Photoactivatable Adhesive Ligands for Light-guided Neuronal Growth, Aleeza Farrukh, Wenqiang Fan, Shifang Zhao, Marcelo Salierno, Julieta I. Paez, Aránzazu del Campo, ChemBioChem, 2018. doi: 10.1002/cbic.201800118

Parts of this chapter are submitted as a manuscript: In-situ Light-guided axon growth with photoactivatable Laminin peptidomimetics, Aleeza Farrukh, Shifang Zhao, Julieta I. Paez, Adolfo Cavalié, Aránzazu del Campo, 2018.

The spatial guidance of neurite growth is necessary for functional regeneration of neural tissue. In this chapter, a light-based approach for directional neurite growth is presented. It exploits photoactivatable cell adhesive peptides to control the interaction between adhesive receptors (integrin) at the neuronal cell membrane and the supportive biomaterial. Using a scanning laser, in situ and directional control of axon growth is demonstrated by regulating the availability and spatial localization of the adhesive motifs. Photo-activatable derivatives of the IKVAV peptide, a peptidomimetic of laminin 111, in combination with soft hydrogels supported neurite outgrowth and allowed site-selective guidance of neurites extension by light. Neurites

outgrowth in a predicted pathways and connection between two selected neurons to build a neural circuit are demonstrated.

3.1 Introduction

Guidance in neurite growth plays a vital role in nerve repair and is a desirable ability to construct neuronal networks. Different approaches for guided neuronal extension have been reviewed in Chapter 1 in this Thesis. Among them, the use of light to guide directional neurite growth in situ is of particular relevance for this chapter. Recently, weak optical forces have been shown to guide the direction of a growth cone of a nerve cell [100]. A near-IR laser (800 nm) spot placed in front of a nerve's leading edge enhances the growth of the dendrites following the beam focus. Likewise, it has been shown that an IR laser (1455 nm) triggers the growth of dendrites and axons by as much as 10 μm in 1 min [101]. Although the mechanism by which neurons follow light stimulus is not very clear, it is generally accepted that cells respond to gradient forces or temperature caused by illumination. A different strategy that could be used to guide neurite outgrowth with light is to use biomaterials functionalized with photo-activatable adhesive ligands This strategy has been used to spatially define the attachment and migration of other cell types.[131, 132, 153-156] A photoremovable protecting group is covalently attached to the adhesive peptidomimetic at a relevant binding site. In this way, the bioactivity of the peptide is temporally inhibited. The illumination at appropriate wavelength and doses releases the chromophore and activates cell binding. Surfaces functionalized with the photoactivatable peptidomimetic become cell-adhesive upon illumination. Masked or scanned exposure can generate active sites and be used to site-selectively attach or

guide cellular attachment. This strategy could be also extended to neuronal cells, provided that an effective adhesive ligand for these cells can be identified.

High expression of β1 integrin in cells and the presence of laminin in the ECM are two factors that promote cell chain migration and also involve the neurites extension[157]. Laminin is an abundant protein in the neural niche fundamental for neuronal migration, differentiation and neurite outgrowth.[158, 159] Laminin mimetic peptides YIGSR, RKRLQVQLSIRT, CASIKVAVSADR and the shorter version IKVAV have been used as simplified mimics of laminin to functionalize biomaterials to support adhesion of neural cells and neurite out-growth[160]. The IKVAV sequence is present at the globular region of the α-chain in Laminin-1 protein and interacts with integrin receptors α3β1, α4β1 and α6β1[161]. When immobilized on the culture plate, IKVAV-containing peptides have been shown to stimulate neurite growth, branching and maturation of neurons.[162-167] In del Campo's Lab, photoactivatable variants of IKVAV-containing peptidomimetics have been developed (synthesis work done by Dr. Aleeza Farrukh). These molecules contain a photocleavable group 2,2'-((3'-(1-hydroxypropan-2-yl)-4'-nitro-[1,1'-biphenyl]-4-yl)azanediyl)bis(ethan-1-ol) (HANBP) at the lysine amino acids of the IKVAV sequence, since this position has been demonstrated to be crucial for integrin recognition and cell attachment.[168] The photo-triggerable variants are the 12-mer CASIK(HANBP)VAVSADR (IK-12 (HANBP)) and the 5-mer IK(HANBP)VAV (**Figure 1**).[156] Previous experiments by Dr. Farrukh demonstrated the light-regulated bioactivity of these peptides. As follow-up work, I have used these molecules to light-guide the outgrowth of neurites on biomaterials in light-defined directions.

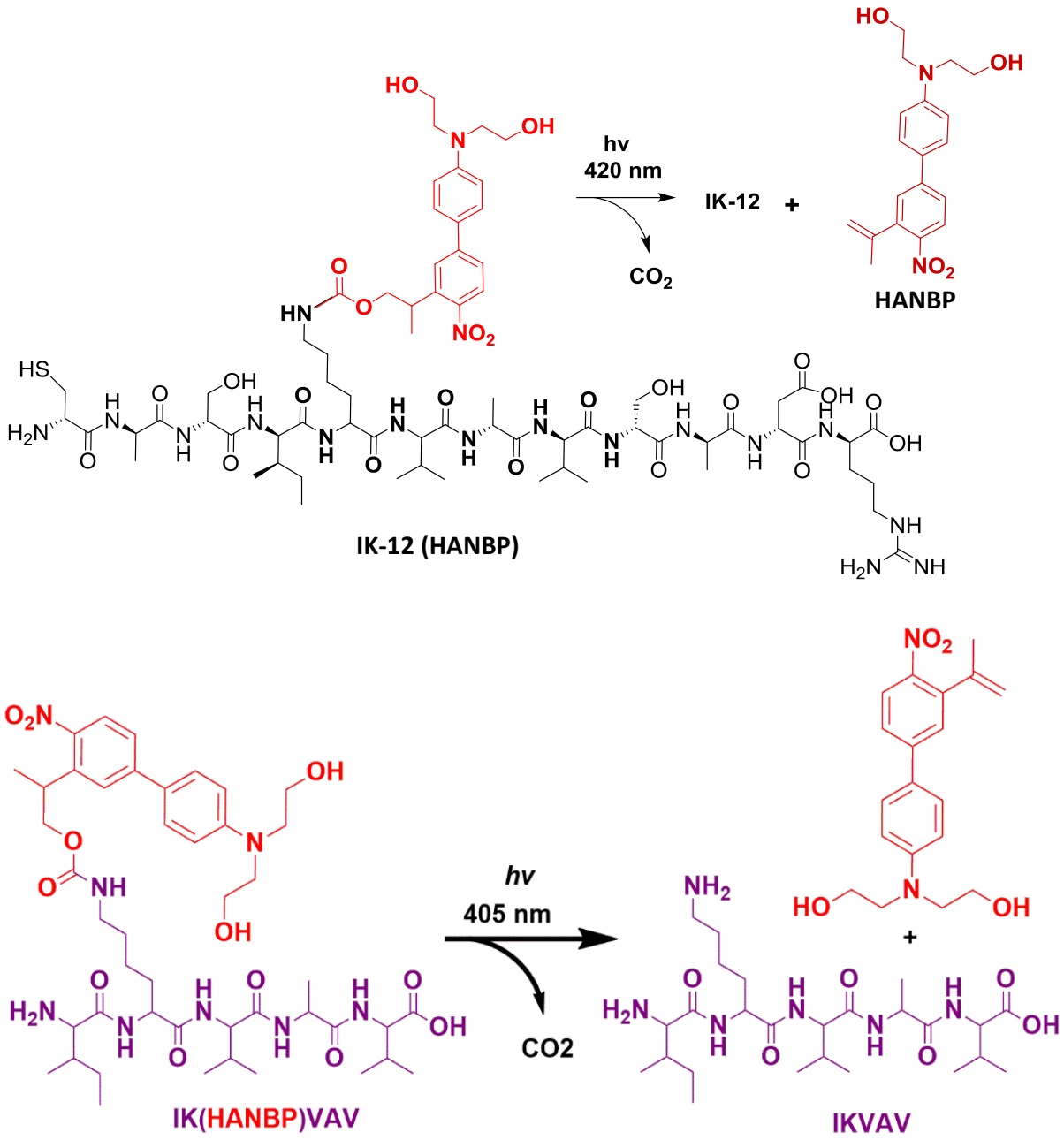

Fig. 1: Structure of IK-12 (HANBP) and its photochemical activation reaction (upper part). In the lower part, structure of IK (HANBP)VAV and its photochemical activation reaction were presented.

3.2 Result and discussion

3.2.1 Preparation of substrates for guided neuronal attachment

Poly(acrylamide-co-acrylic acid) P(AAm-AA) gels have been recently reported as valuable platforms for study of neuron differentiation and maturation.[169] These gels do not allow protein absorption and are cell repellent. Through the COOH group of the AA units (5% molar concentration in monomer mixture), specific biofunctionalities can be incorporated. For the studies in this chapter, the photoactivatable peptidomimetic IK (HANBP) VAV and IK-12 (HANBP) were used to modify the gels. According to previous experience, gels of 2-kPa stiffness were prepared for the neuronal cultures and modified with the peptides.[170] Conditions for photoactivation were taken from previous results in the group (Dr. Aleeza Farrukh).

3.2.2 Directional guidance of neuronal attachment and differentiation on photo-activated IK-12 (HANBP) patterns.

Neuronal Stem Cells (NSCs) are the self-renewing, multipotent cells that differentiate into the main phenotypes of the nervous system: neurons, astrocytes, and oligodendrocytes. These cells are frequently used to study the influence of biomaterials on differentiation of neuronal cell.[22] In in vitro cultures NSCs keep their undifferentiated status in the presence of growth factors (EGF, FGF), and undergo differentiation when growth factors are removed from the culture medium. Neural stem cells (NSCs) dissociated from neurospheres were used for the experiments in this section. The neurospheres were isolated from mouse embryos (E14.5 days) following standard protocol (see experimental section).

The NSCs were seeded on the hydrogels functionalized with CASIK(HANBP)VAVSADR (IK-12 (HANBP)) in the absence of growth factors. Using a mask and a LED lamp, a micropattern with active (exposed) and non-active IK-

12(HANBP) regions was generated on the hydrogel surface (**Figure 2**). Attachment of neurons and extension of neurites were found selectively on the irradiated regions. Cells followed the irradiated pattern exclusively, spatially aligned and differentiated to neuron on the irradiated area demonstrating the specificity of the interactions between cells and active IK-12. Further, cells differentiated into neurons, as established by DCX staining (**Figure 2**). These results proved that the possibility of spatial distribution of neuronal attachment, differentiation through light exposure. The neuronal patterns could be maintained for at least 4 days, demonstrating that the photoactivatable peptide is stable in cell culture conditions.

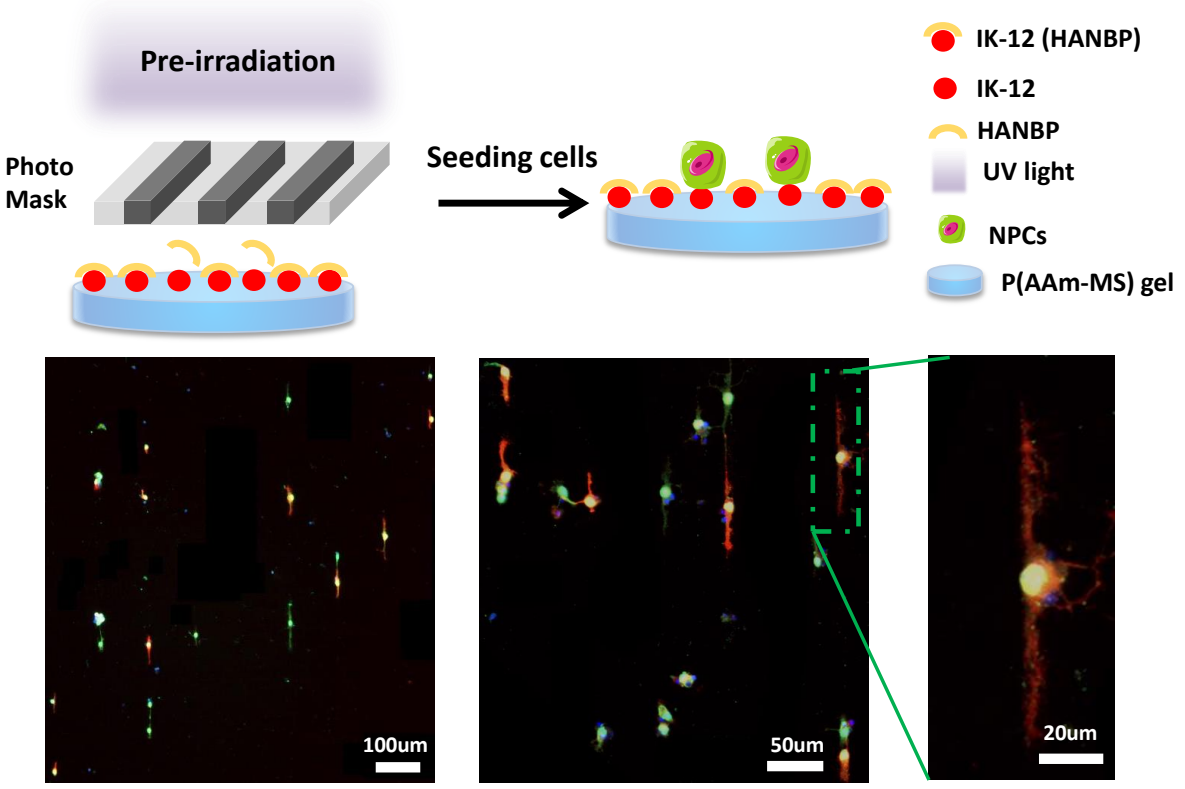

Figure 2 Micropatterned IK-12 substrates were prepared by a mask-illumination of hydrogels functionalized with IK-12(HANBP). The mask had 10 μm chrome stripes separated by 100 μm gaps. After pre-irradiation, NSCs from dissociated neurospheres (Passage 3) seeded on the substrate attached and followed the IK-12

pattern. After 24 h cultures, the cells were fixed and stained. Blue=DAPI, red=DCX, Green=neurofilament marker, SMI.

3.2.3 In-situ guidance of neurites growth and neuronal migration by light activation of IK(HANBP)VAV

For the study of neuronal behavior (e.g. migration and neurites extension) in response to the presence of IK (HANBP) VAV, I used the Embryonic Neural progenitor cells (eNPCs). The eNPCs can differentiate to neuron in short time and extend long processes compared to NSCs.

First the attachment of eNPCs isolated from cortex of mouse embryo (E 14.5) were tested on P(AAm-co-AA) gels modified with the IK(HANBP)VAV peptide before and after exposure. Cells did not attach on IK(HANBP)VAV modified substrates and formed clusters after 24h culture (**Figure 3**). In contrast, eNPCs spread and extended neurites on IK (HANBP) VAV modified gels that were preirradiated in order to activate the peptide. These results indicated the bioactivity of the photoactivated IK(HANBP)VAV modified hydrogels.

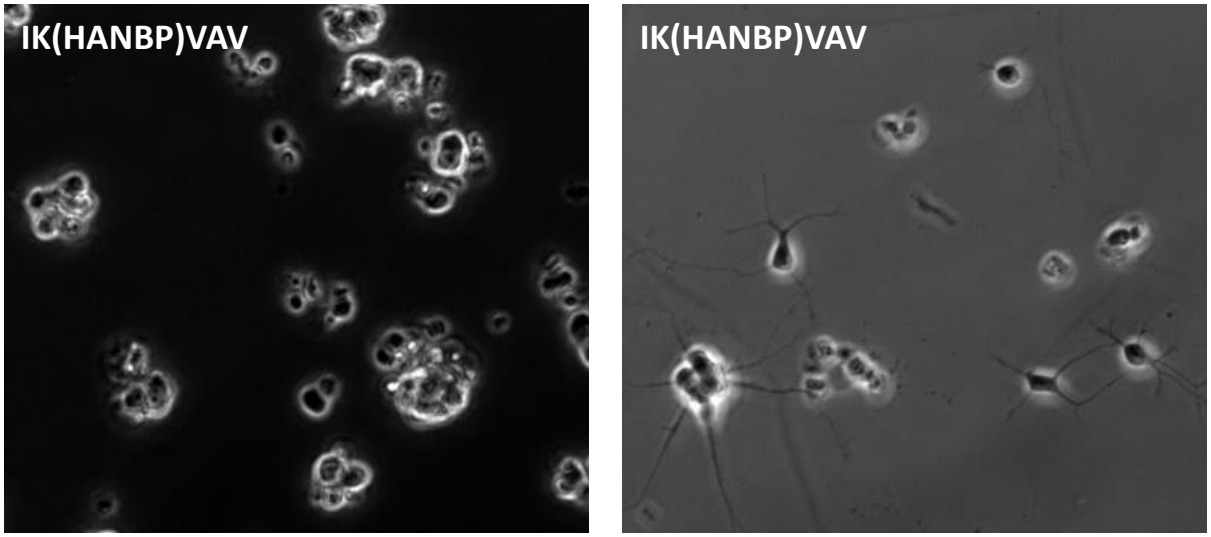

Figure 3 Embryonic Neural progenitor cells (eNPCs) seeded on hydrogels functionalized with IK(HANBP)VAV peptide before and after irradiation. Images were taken after 24 h culture.

In order to guide the growth of neurites in situ, a time lapse experiment was used to follow the cell behavior before and after irradiation. IK(HANBP)VAV modified hydrogels were put into 24 well plate and cells were seeded in parallel for time lapse experiments at multiple conditions. In order to avoid displacement of the substrates within the wells during movement of the microscopy stage for time lapse imaging, a stainless steel ring was used to fix the position of the IK(HANBP)VAV modified substrates within the 24well plates (**Figure 4.**). This experimental design allowed automatized imaging of multiple samples during the same experiment by time lapse microscope.

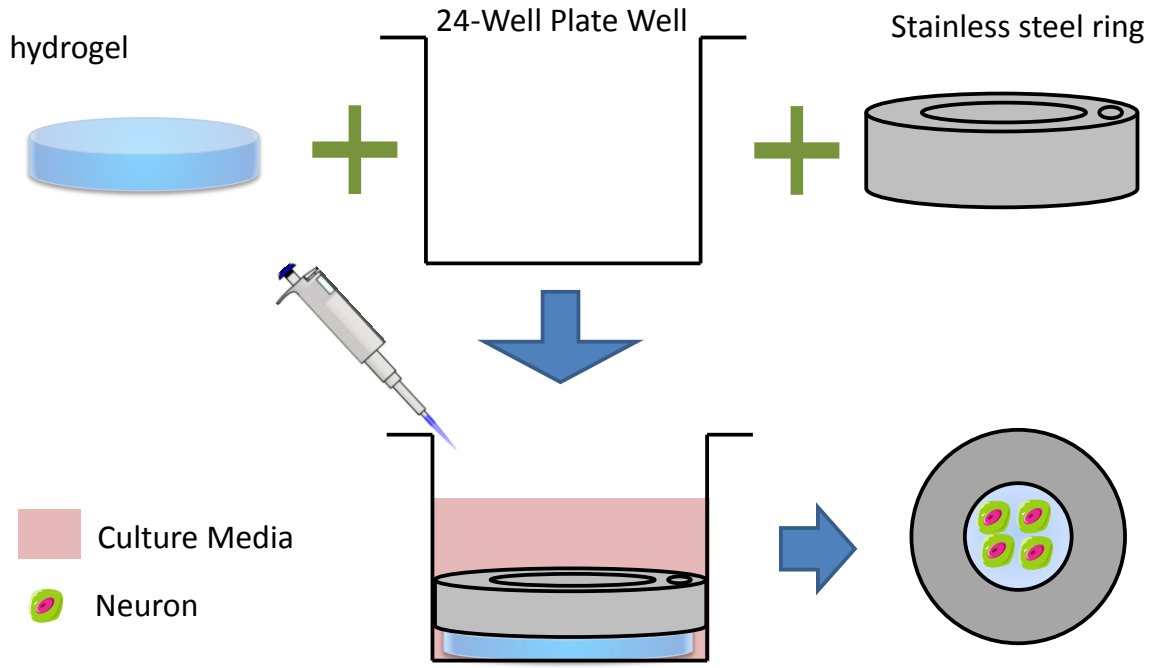

Figure 4 The scheme represents the time lapse experimental design with multiple substrates.

After cell seeding on the substrate, rectangular areas of 10x 100µm dimensions were irradiated close to selected cells using a scanning laser. In order to display the irradiated area, a photoactivatable fluorescein molecule was also introduced at the hydrogel surface. This molecule contains a bis-(5-carboxymethoxy-2-nitrobenzyl) ether (CMNB) chromophore that can be photo-removed to become fluorescent, at similar wavelength as HANBP chromophore. The fluorescence (green) pattern revealed the activated sites (**Figure 5).** Before irradiation, the cells extended and retraced neurites to explore the environment, and moved across the non-adhesive substrate. After irradiation, the neurite closed to the exposure area, extended in length and followed the irradiation line persistently (**Figure 5 lower part**). When the neurite reached the edge of irradiation area, it stopped extension and kept attached during at least 48 hours cell culture.

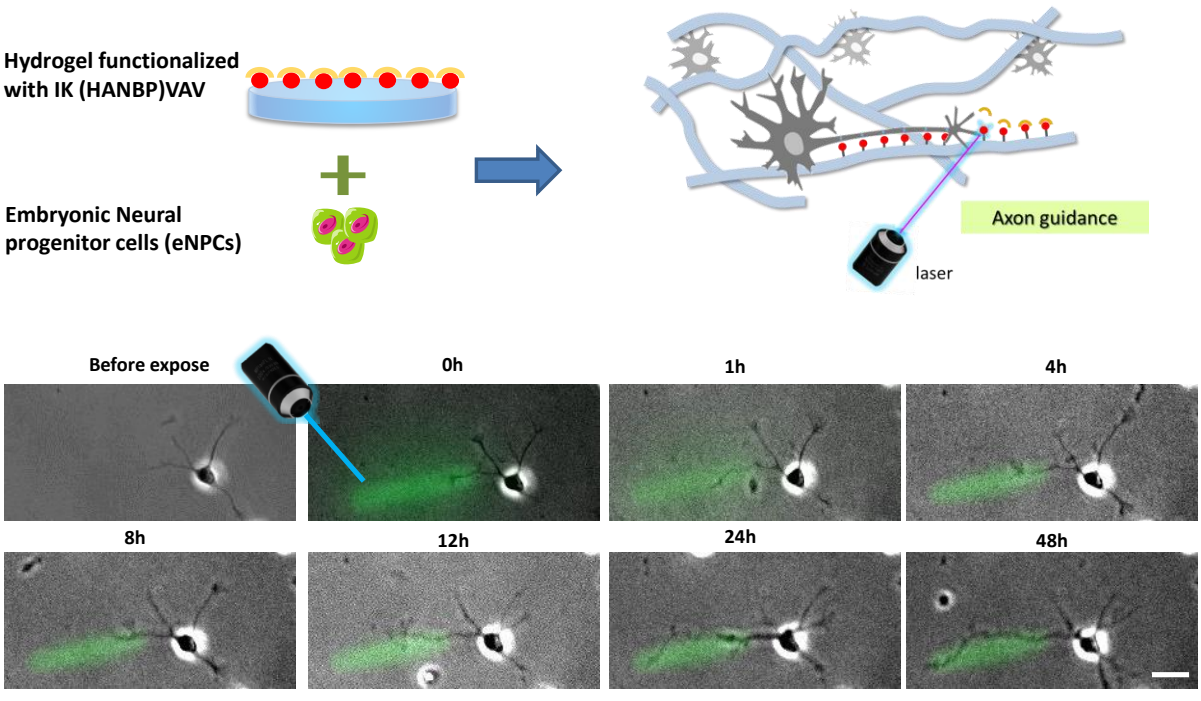

Figure 5 The scheme represents the in situ guiding neurite extension by irradiated IK-(HANBP) modified hydrogels in the presence of cells. Bellow, the microscopy images are snap-shots of a time lapse experiment showing the behavior of a eNPCs after in-situ irradiation to activate IK (HANBP) VAV on the surface during 24 hours. The green line is the expose area indicated by the photoactivation of fluorescein derivative. Scale bar is 20 µm.

Apart from in situ, directional neurite extension in light-activated directions (**Figure 5**), also directional migration and directional connection of two neurons was achieved (**Figure 6**). After in-situ irradiation, the neurite extended and follow the expose area, as shown in **Figure 5 and Figure 6** left part. Normally, when the neuron showed no process, one process or multipolar morphology, only the neurites follow the irradiation area and the cell body keep static. However, when the cells displayed bipolar morphology before irradiation, the neurite found and extended further on the expose area. Subsequently, the soma preferred to follow the neurite and migrated to exposed area (**Figure 6 middle part**). It was also possible to connect neurites of two neighboring neurons by irradiating a line between two cells (**Figure 6 right part**). These results indicate that IK(HANBP)VAV peptide can be applied to directional growth of neurites with temporal resolution, selection of neurite connection and can be extended to create customized neuronal circuit.

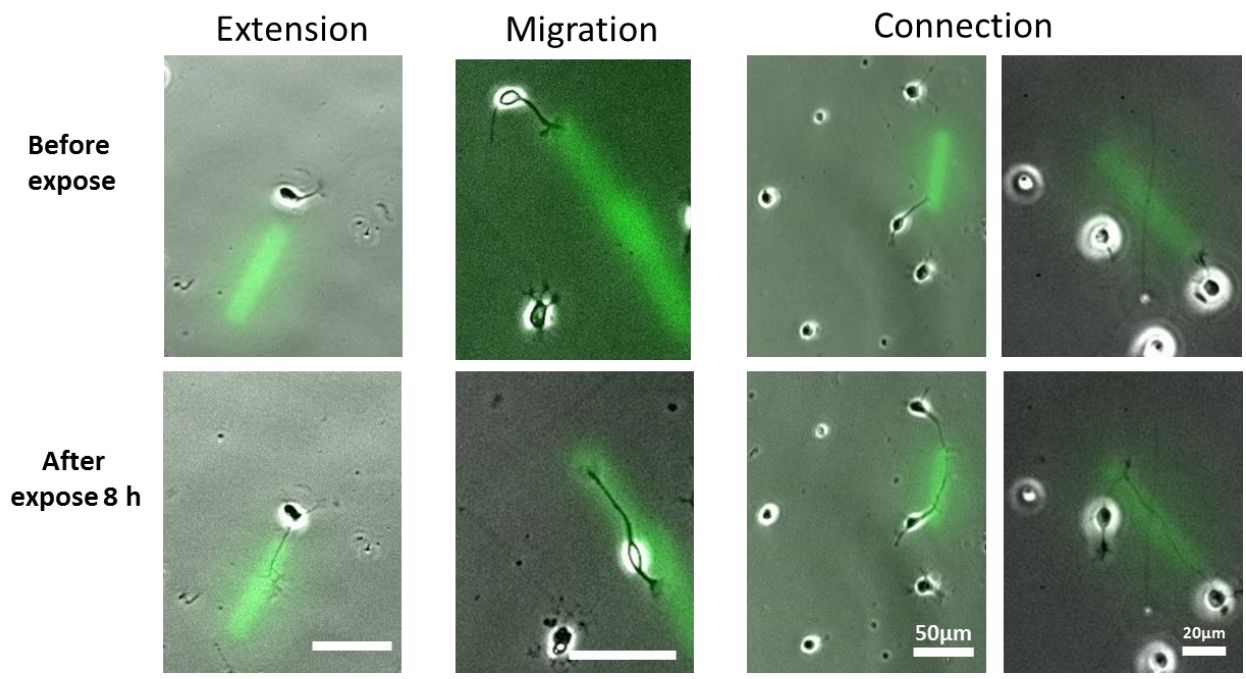

Figure 6 In situ control direction of neurite extension, migration and connection by light. Representative images of neurite extension, migration and connection between two neurons after in-situ irradiation. The green line is the expose area indicated by activation of immobilized photoactivatable fluorescein on the substrates.

3.3 Conclusion

The spatiotemporally controlled neuronal attachment, migration, differentiation and neurites extension on substrates modified with photoactivatable laminin mimetic peptides IK12(HANBP) and IK(HANBP)VAV peptide are demonstrated. The HANBP modified peptides did not support cells attachment and cells formed clusters on the substrates. Irradiation activated the IKVAV sequence the substrates and they supported cell attachment, neurites extension and formation of cells pattern in pre-designed geometries. Further, gels functionalized with IK(HANBP)VAV and photoactivatable fluorescein allowed visualization of the irradiation area and guided

neurite extension *in situ*. The in-*situ* activation of photoresponsive Laminin peptidomimetic by using scanning lasers provided spatiotemporal guidance to neuron migration, neurite extension and connection.

3.4 Materials and methods

Materials

All chemicals were purchased from commercial sources (Sigma Aldrich, Acros, or Novabiochem Merck) and used without purification. 6 well or 24 well cell culture plates were purchase from BD falcon and Hank's Balanced Salt Solution (HBSS) purchase from Thermo Fisher.

Cell culture experiments

Isolation of Cerebral cortex from embryonic mouse

1. Sacrifice a pregnant female (E14.5 days) according to the Policies on the Use of Animals approved by the Saarland University. Open abdominal cavity and remove uterus, containing embryos. Place in 10 cm dish containing ice-cold HBSS solution.

2. Carefully remove placenta using two forceps with gentle opposite pulling motions. Then remove embryo from remaining sac and place in ice-cold HBSS solution.

3. Decapitate embryo with clean sterile scalpel and place in 3 cm dish containing ice-cold HBSS solution.

4. Under dissecting microscope, use two Dumont forceps and carefully remove thin skin layer by pinching skin at center and peeling away. To remove forming skull

pieces, anchor head by piercing orbital cavities with forceps and place the second set of forceps at an angle to grab the skull flap. Pull gently to remove soft bone fragments and use a forceps, angle beneath the brain, lift and remove brain from skull.

5. Separate two hemispheres from the midbrain. Using one forceps, anchor tissue in the midbrain and use knife to gently separate the two hemispheres. Then cut the midbrain from each of the two hemispheres.

6. With the outer surface of the hemisphere facing upwards, remove meninges. Use one forceps to anchor tissue and forceps to carefully peel away meninges from the outer surface. 7. Proceed to isolate cortex from remaining inner midbrain region for each hemisphere. Using one forceps as an anchor, carefully remove the midbrain from the inner side of the cortex with short cuts using the other forceps.

8. Collect the cortices from multiple brains, and put into ice-cold HBSS.

Embryonic Neural progenitor cells

Finally, we get the cortex (Crescent shape) and put into HBSS. Remove HBSS, and add 0.5% trypsin EDTA (GIBCO) for 15 min at 37 C. Then trypsin was inactivated by the plating DMEM medium (GIBCO) and 10% FBS (Hyclone) and gently triturated with a 5-ml disposable pipette to get single cells. Centrifugation at 1000 rpm was performed for 5 min, cell pellets were re-suspended in 1 ml differentiating medium DMEM/F12 (GIBCO) and 2% B27(Invitrogen) and cell density was counted. Substrates functionalized with different ligands were sterilized with ethanol, washed with PBS and placed in 24-well cell culture plate. $5x10^4$ cells were seeded in each well and cell growth was followed by regular intervals and cells were fixed after 24-48 hours.

Neurospheres Culture

The cells isolated from cerebral cortex of embryonic mouse (E14.5) obtained from C57BL/6 mice as described above, were centrifuged at 1000 rpm for 5 min and cell pellet was re-suspended in DMEM/F12 media containing 1% N2 (Invitrogen), 0.1% Heparin, 20 ng/ml basic fibroblast growth factors (bFGF, Invitrogen), 20 ng/ml epidermal growth factors (EGF, Invitrogen) and penicillin-streptomycin (N2 complete medium).[171, 172] Dissociated cells were seeded in 6-well plate and maintained as undifferentiated neurospheres. The neurospheres were gathered and dissociate mechanically with 1ml pipette. Then medium was changed from N2 complete media to differentiation media (DMEM-F12/glutamax, 2% B27, penicillin-streptomycin). At the end, dissociated cells were seeded (50,000 cells per well in 24-well plate) on peptide modified hydrogel and maintained for 2-4 days. The absence of growth factors and addition of differentiation medium (B27) support neuronal cells survival in comparison to glial cells. All animal procedures were carried out in accordance with the Policies on the Use of Animals approved by the Saarland University.

Immunostaining

Cells were fixed with 4% PFA solution (paraformaldehyde) for 10 min and washed 3 times with PBS pH 7.4 followed by blocking and permeabilization by incubating for 45 min with bovine serum albumin BSA 2% and Triton 0.2% in PBS at room temperature. Cells were incubated for 2 hours at room temperature with (1:500 DCX (guinea pig, Dianova) to stain cell body and 1:800 SMI-312 (Anti mouse, Biolegend) to stain axon. Cells were washed 3 times with PBS followed by incubation for 2 hours at room temperature with (1:500 Cy3 (anti-guinea pig) and 1:800 (alexa 488 antimouse). The samples were mounted with immune select Antifading Mounting Medium (Dianova)

containing DAPI for nucleus staining by using following standard protocols. Images were taken with Zeiss Axio Observer microscope at 0.42 µm per px.

Time-Lapse microscopy

Video microscopy of neurons was performed with a Cell Observer microscope (Zeiss) at 37°C and 5% CO_2. Phase contrast images were acquired every 6 minutes during 2 days using a 20x phase contrast objective (Zeiss) and an AxioCamHRm camera with Zen blue software. Single-cell tracking and movies assembling were performed using ImageJ 1.42q (National Institute of Health, MD, USA) software.

Time-Lapse experiment

The thin film hydrogel supported by coverslips were put into 24 well plates. Subsequently, the stainless steel rings (**Figure 7**) were put into the 24 well plates. Before cell culture, the hydrogels and stainless steel rings were sterilized by 70% ethanol for 3 min. During time lapse, when the stage move to different positions, the stainless steel rings can help the hydrogels to keep the same position in every circle. It means that we could do time lapse with several samples at the same time, which significantly increase the efficiency of experiment and save lots of time.

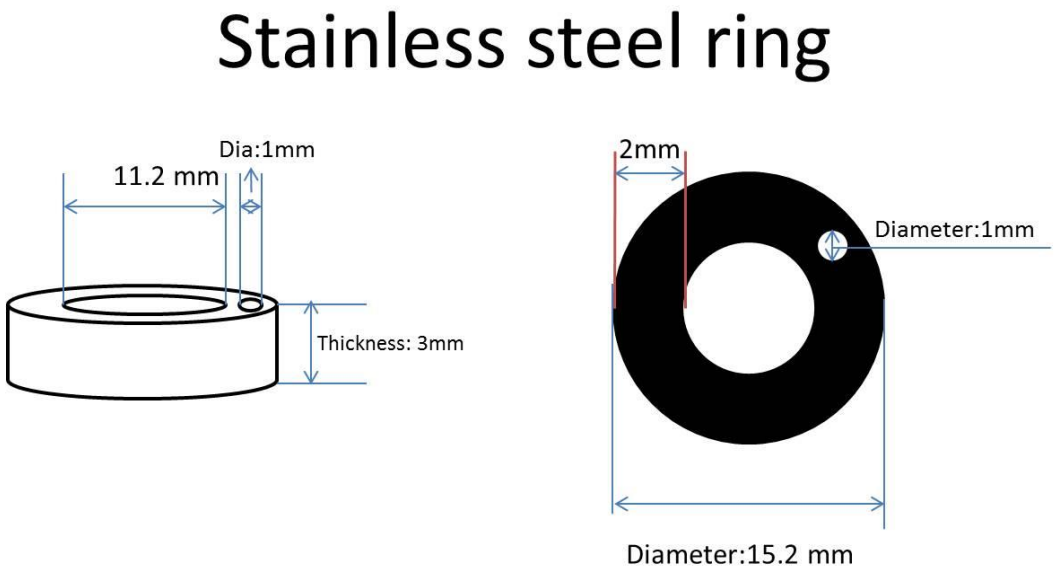

Figure 7 The stainless ring was design for time lapse experiment to help the hydrogel to keep the position. The out diameter is a little bit smaller than the diameter of 24 wells plates, which make ring stuck in the bottom of 24 well plates. The inner diameter will allow most part of samples could be observed. And the small hole (diameter is 1mm) was design for the tweezers, which allow me to place or take out the ring easily by tweezers.

***In-situ* photo-activation experiment**

The samples were placed in 24-well cell culture plate and $1.2x10^4$ cells were seeded in each well. Cells were allowed to attach/sediment for 2 h at 37C, 5% CO_2. The samples were placed in Zeiss Axio Observer microscope equipped with RAPP irradiation source with 405 nm laser source. The laser power was kept at 90% and irradiation time was adjust from 30 sec to 60 sec depend on the different geometries drawled with RAPP software. The samples were followed by time-lapse microscope for 24 h.

Chapter 4

4. Regulation of cytoskeletal actin by light

Note: Part of this chapter has been submitted as a manuscript: Spatiotemporal regulation of actin dynamics with Photoactivatable Cytochalasin D, Roshna V. Nair, Shifang Zhao, Emmanuel Terriac, Franziska Lautenschläger, Aránzazu del Campo, Chemical Engineering, 2017.

Roshna V. Nair and Shifang Zhao contribute equally to this work. Roshna V. Nair focused on the synthesis of Photoactivatable Cytochalasin D, whereas Shifang Zhao focused on the cell experiment part. Emmanuel Terriac contributed with the experiments done on Retinal Pigment Epithelial cells and data quantification. Franziska Lautenschläger and Aránzazu del Campo contributed to the design of the experiments and helped with writing of the manuscript.

The development of functional neural tissue (e.g. cortex) relies on the correct positioning of neurons (achieved by directed migration) and polarization of neurons (formation of a single axon and multiple dendrites). Both migration and polarization of neurons depend on coordinated rearrangements of the cellular actin cytoskeleton[107, 152]. In order to study the role of the actin cytoskeleton in cellular processes, tools to specifically interfere with actin dynamics in-situ (i.e. in living cells) with spatiotemporal control are required. For this purpose, a phototriggerable derivative of the potent actin disruptor Cytochalasin D (CytoD) was developed in del

Campo's lab (Nvoc-CytoD synthesized by Dr. Roshna V. Nair at INM-Leibniz Institute for New Materials). This chapter describes the demonstration of the applicability of this molecule to disturb actin dynamics and study related cellular processes. Firstly, the toxicity of the compound was tested. Secondly, it was demonstrated that light-dosed delivery of CytoD in living cells can be realized at seconds time scale and with subcellular resolution using conventional light sources of microscopy setups. Further, the transient character (minutes time scale) of the actin disruption effect of Nvoc-CytoD disruption was demonstrated, and thereby the possibility to perform repeated experiments in the same culture without changing medium. These results demonstrate how Nvoc-CytoD might be used in cell biology experimentation, and identifies the advantages and limits of this approach.

4.1 Introduction

The cellular cytoskeleton is a dynamic network of different protein superstructures with relevant functions in cellular motility. The external regulation of the dynamics of cytoskeletal elements - in particular actin – enables interference with cellular processes involving the generation or transmission of forces, as in cellular attachment, migration or polarization.[173] The study of the actin-related cellular processes requires tools to specifically interfere with actin dynamics in-situ and with spatiotemporal control. An established strategy to control actin dynamics is by using small molecule inhibitors that selectively interact with actin components. For example, cytochalasins are widely used in cell biology and biophysics to externally interfere with the actin network and investigate cytoskeleton dynamics and related cellular processes. CytoD shows good cell permeability and high binding affinity to

the growing end of the actin microfilaments (F-actin), preventing their elongation.[174-178]. However, the fundamental role of actin in many cellular pathways makes treatment with Cytochalasins D often non-practicable due to systemic side-effects, and useless to tackle delicate actin dynamics related questions in mechanobiology.

A strategy to precisely regulate the activity of a drug with temporal and spatial control is by using photoactivatable drug derivatives.[179] In this approach the drug is derivarized with a photocleavable group at a relevant position for its bioactivity. In this way, the drug becomes temporally inactive, but can restore its function upon light exposure. Light exposure cleaves the chromophore and restores activity of the drug only at the exposed position and at a defined time point without causing side effects. Two examples of photoactivatable drugs to control the dynamics of microtubules have been reported. A photoactivatable derivative of CMPD1, a tubulin polymerization inhibitor, was obtained by attaching the photoremovable protecting group 4,5-dimethoxy-2-nitrobenzyl (DMNB) to the drug to temporally inhibit its activity. [180] A similar strategy was used to locally deliver paclitaxel (PTX), a drug that inhibits depolymerization of microtubules.[181] The study of the dynamics of other cytoskeletal components, like actin, would also benefit from the availability of photoactivatable drugs. However, such compounds have not yet been developed. In this context, a photoactivatable variant of the actin inhibitor Cytochalasin D (CytoD) was synthesized by Dr. R. V. Nair at del Campo's Lab. The CytoD molecule modified with a nitroveratryloxycarbonyl (Nvoc) photoremovable group to obtain a non-active, "latent" drug (**Figure 1**). Taking into account the interactions between CytoD and monomeric actin in the reported crystal structure[182] and the chemical reactive groups of CytoD, the Nvoc photoremovable group was introduced at the secondary

hydroxyl group at C7. The obtained Nvoc-CytoD molecule was readily soluble in DMSO. It was stable in PBS (pH = 7.4) and 10% DMSO for at least 24 hours. Light exposure of Nvoc-CytoD lead to photolysis of the Nvoc and effective release of CytoD following the expected photocleavage pathway (**Figure 1**).

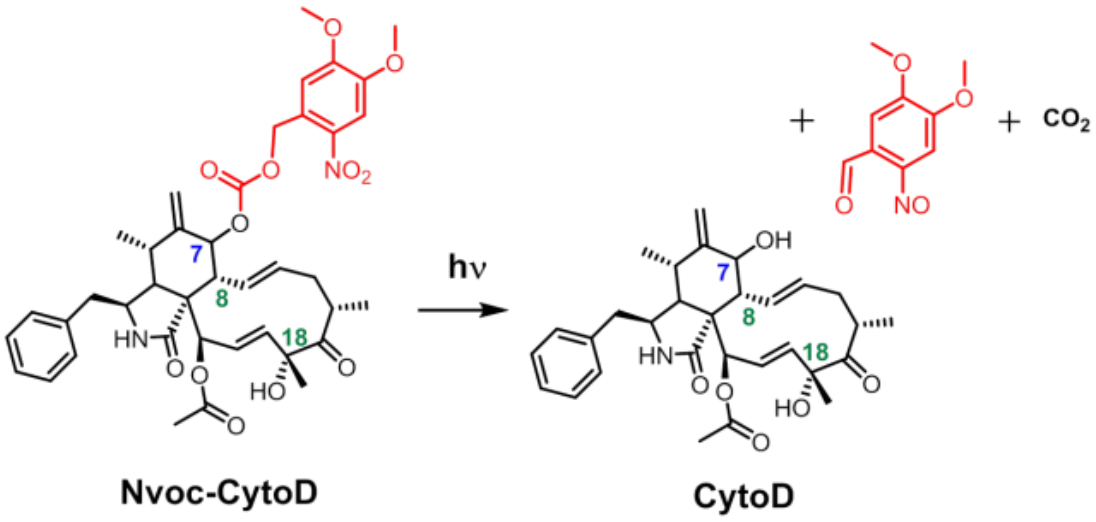

Figure. 1: Structure of Nvoc-CytoD and its photochemical activation reaction.

In this chapter, the effect of the photoactivatable drug Nvoc-CytoD in cells was studied. First its toxicity was tested at different concentrations and time scale. Secondly, the cell permeability of Nvoc-CytoD and the light-mediated local delivery of the CytoD were tested in different cell types (Mouse fibroblast L929, WT eGFP-Vinculin mouse embryonic fibroblast lines (MEFs) and Retinal Pigment Epithelial cells (h-tert RPE1)). Finally, site-directed disruption of F-actin and shrinkage of cell area was demonstrated, and the changes in the focal adhesion size by the local delivery of Cyto-D were quantified.

4.2 Results and Discussion

4.2.1 Toxicity tests

L929 cells were incubated with CytoD and Nvoc-CytoD solutions at concentrations between 0.01 µM and 100 µM (the concentration range span from no cytotoxicity to cytotoxicity) in order to test and compare cytotoxicity[183]. L929 cells incubated for 24 hours with CytoD showed a drop in viability at concentration of 1 µM (**Fig. 2a**); while a concentration of 10 µM was necessary to see cytotoxic effects with Nvoc-CytoD in the same time scale. These results confirm the activity inhibition caused by the presence of the chromophore. Typical cell experiments with cytoskeletal drugs are performed within 1-2 hours after addition of the drug and, therefore, the toxicity of the compounds at short culture times was also examined in live imaging experiments of the actin cytoskeleton using Sir-actin marker. L929 cells were first incubated overnight with Sir-actin for F-actin labeling. Upon addition of 0.1 µM CytoD, the F-actin was immediately disrupted and cells could not spread properly (**Fig. 3**).

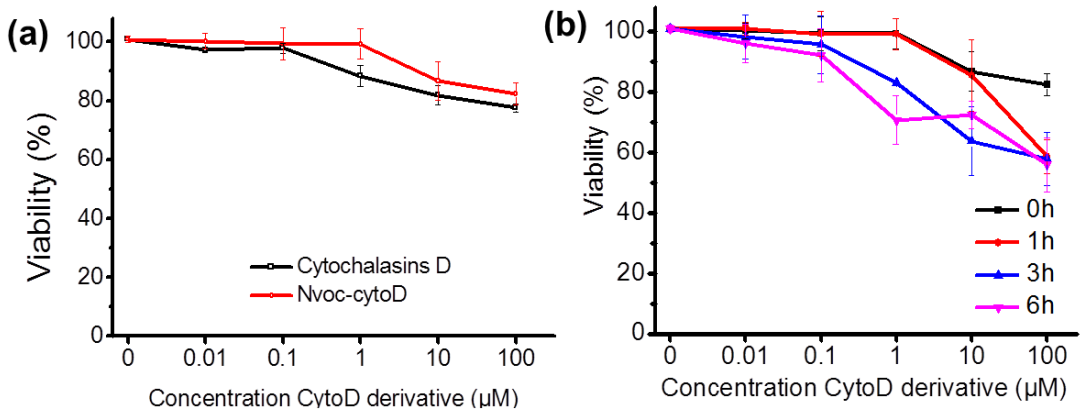

Figure 2 Toxicity assays. (a) Viability of L929 cells after exposure to varying concentrations of CytoD or Nvoc-CytoD for 24 h. (b) The viability of cells incubated

with pre-irradiated solution of Nvoc -CytoD for 24 h. Each result represents the mean viability ± standard deviation (SD) of three independent experiments and each of these was performed in biological triplicates. Cell viability was calculated as percentage of viable cells compared to untreated control cells.

In contrast, cells exposed to 0.1 µM Nvoc-CytoD did not show any disrupted cytoskeleton. Moreover, a further increase of Nvoc-CytoD to 50µM did not change the cell morphology or actin cytoskeleton after 6 hours cell culture times (**Fig. 4**). In summary, single cell imaging and population vitality results demonstrated that the introduction of the Nvoc chromophore at the C7 position significantly inhibits the ability of CytoD to bind to F-actin.

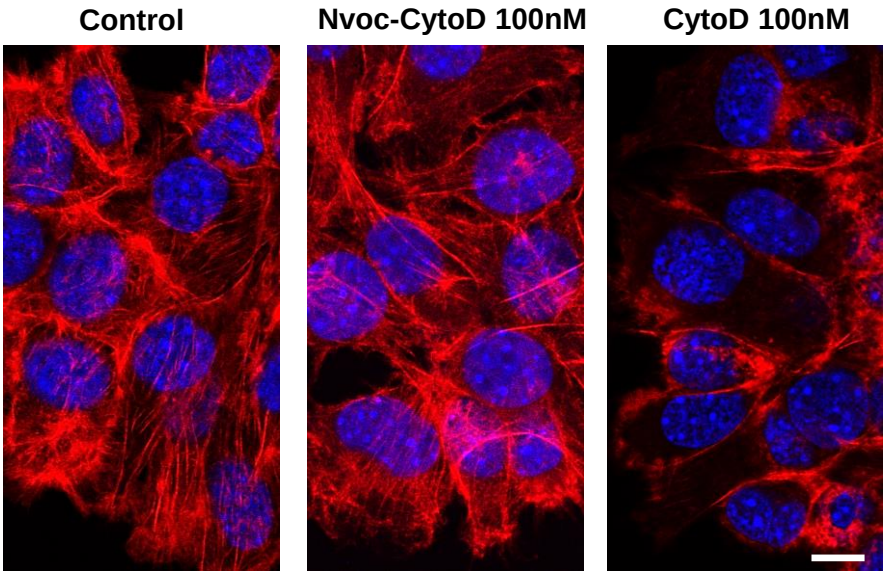

Figure 3 Mouse fibroblast L929 after 3 hours of treatment with CytoD and Nvoc-CytoD. Stress fibers were hampered only on cell treated with CytoD. Scale bar is 10µm. Blue = DAPI; Red = F-actin.

The vitality of L929 cells treated with defined concentrations of pre-irradiated solutions of Nvoc-CytoD was also measured (**Fig. 2b**). The irradiated solutions contained a mixture of Nvoc-CytoD and free CytoD at different ratios. A significant

reduction in vitality with increasing exposure time was visible, indicating light-triggered release of CytoD. The Nvoc-CytoD concentration at which cell vitality was compromised decreased with increasing exposure time. This result confirms that Nvoc-CytoD can liberate active CytoD upon light exposure in a dose-dependent way.

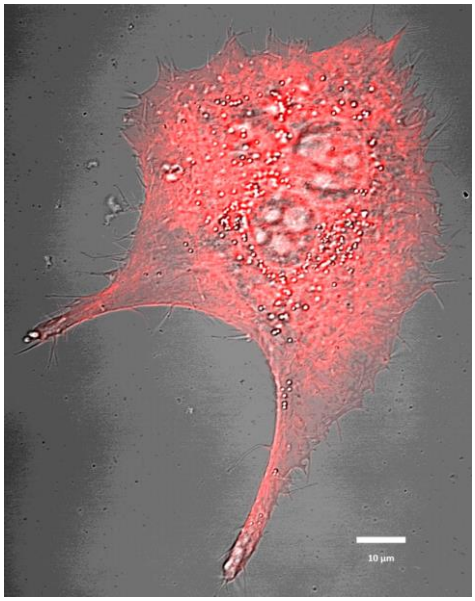

Figure 4 The morphology of L929 cells incubated with 50 µM Cage-CytoD for 6 hours. The red is F-actin and scale bar is 10 µm.

4.2.2 Local Photoactivation of Nvoc-CytoD

The possibility to use Nvoc-CytoD as a photoactivatable drug to locally and temporally interfere with the actin cytoskeleton upon light exposure in cell cultures was tested with different cell types: L929, MEFs and RPE1 cells. L929 cells exposed to 50 µM Nvoc-CytoD retained their spread status and the actin cytoskeleton did not show any morphological changes or differences to control samples.

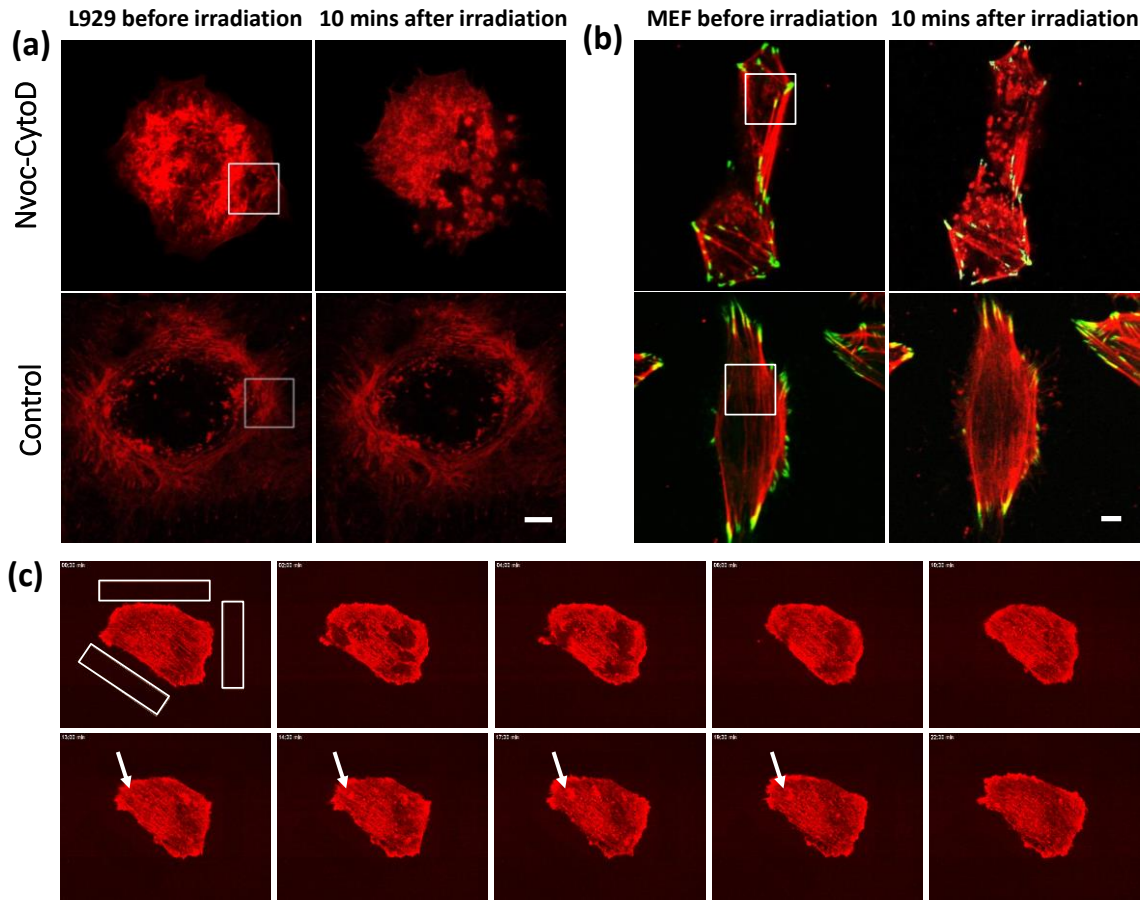

Figure 5 (a, b) Actin reorganization after photoactivation of Nvoc-CytoD. Representative fluorescence images of (a) L929 cells and (b) MEFs cells incubated with 0.1% DMSO (control) or with 50 µM Nvoc-CytoD in DMSO. Images correspond to cells immediately before exposure and 10 min after exposure (irradiation time was 45 s). F-actin disruption was observed in the Nvoc-CytoD group and not in the control group. (c) Disruption of actin fibers and increase of short actin fragments upon light exposure close to the cell membrane. Selected panels of a time-lapse movie (time frame of 30 s, the full movie can be found in SI) of a RPE1 cell stably expressing LifeAct-mcherry. The first panel shows the activation frame, with white rectangles depicting the region of illumination. During reconstruction of the actin network, actin waves (white arrows) can be detected.

A 180 µm2 area of a spread L929 cell containing visible stress fibers was irradiated for 45 sec (**Fig. 5a**). A fast fluorescence loss was observed within the irradiated area. The same fluorescence loss was also observed in the control experiments, indicating bleaching of the F-actin fluorophore at the exposure conditions. Fluorescence recovered in 10 min in the control experiments to show similar F-actin structures as before exposure. In contrast, cells treated with Nvoc-CytoD showed a fully distorted actin cytoskeleton. Clusters of actin and actin-free areas became visible in the irradiated cell (**Fig.5a**). Similar morphological changes were observed in MEFs (**Fig. 5b**). These results indicate that free CytoD was delivered inside the cell during light exposure and the free drug interfered with the F-actin cytoskeleton of the irradiated cells.

We then tested if localized delivery of CytoD could also be realized by irradiating a region outside of the cell and close to the cell membrane. This strategy reduces possible photodamage effects during the exposure step and avoids bleaching of the labeled molecules during irradiation. Such an experiment is represented in **Fig. 5c.** RPE 1 cells expressing LifeAct were imaged before and after irradiating the area around the cell. About 1 minute after activation, rupture of the dense actin fiber network occurred. In parallel, strong actin dynamics was observed in form of formation of actin waves (white arrows in **Fig. 5c**).

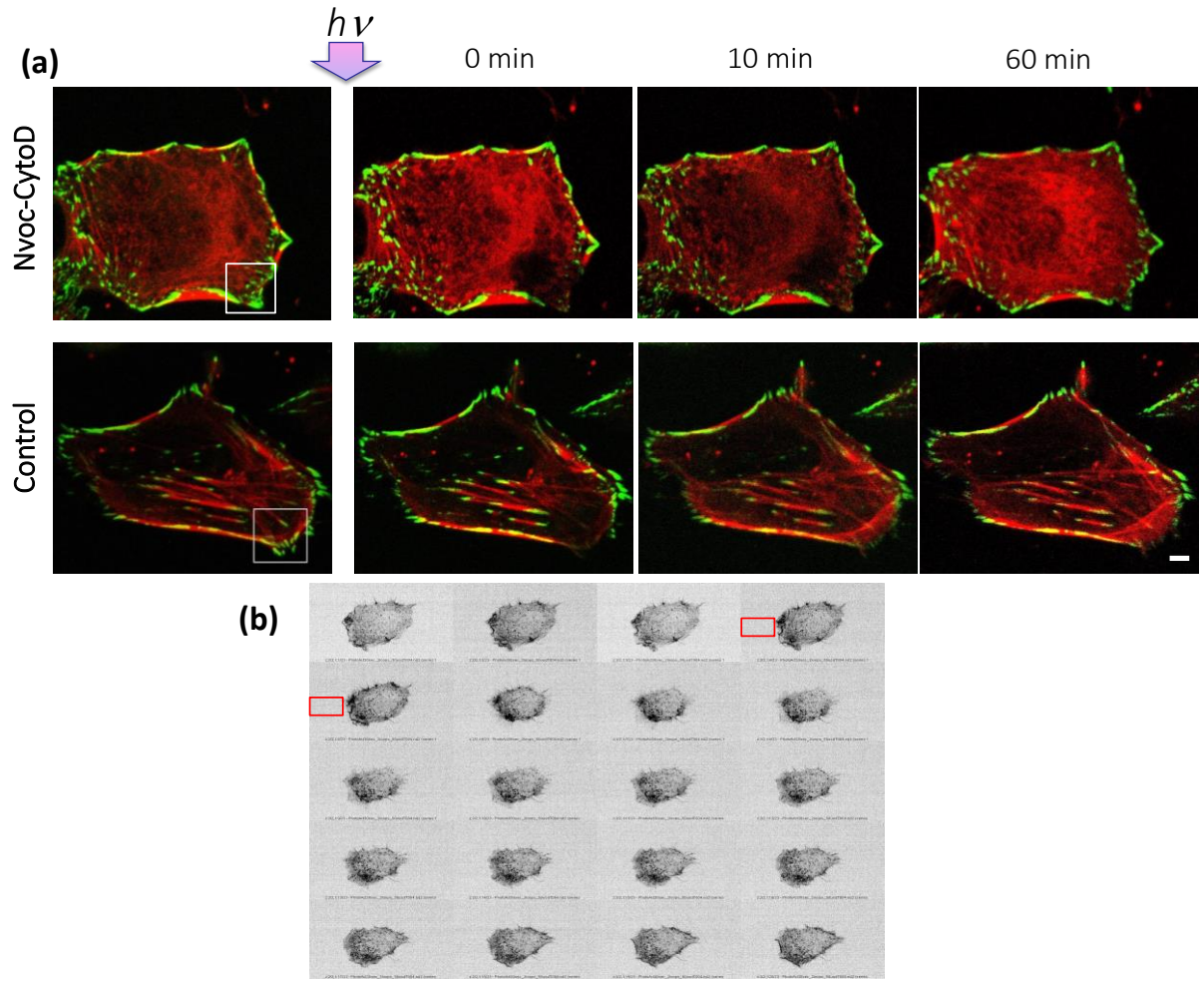

Figure 6 Reversibility of the effect of local photoactivation of Nvoc-CytoD. (a) Fluorescence images from a time lapse experiment with MEFs incubated with 50 µM Nvoc-CytoD or 0.1% DMSO. After exposure (45 s) fluorescence signal in the irradiated area (white square) was bleached. Fluorescence recovered after ca. 10 minutes in control group. In contrast, a locally distorted actin cytoskeleton was observed in Nvoc-CytoD treated cells, as a consequence of the photo-liberated CytoD. In 1 h cells reorganized their actin cytoskeleton to normal status. The scale bar corresponds to 5 µm. Red is F-actin and green is vinculin. (b) The montage of microscopy images shows the evolution of the actin cytoskeleton. Light exposure occurred in close vicinity (white square) of the RPE1 cell expressing mcherry-lifeAct between frame 4 and 5 of the montage. Frames were taken every 30 seconds.

A similar phenomenon has been reported upon cell treatment with Latrunculin A.[184] The generated actin waves were explained by the sudden increase of G-Actin concentration upon drug treatment. These experiments demonstrate the possibility to light-activate CytoD outside of the cell to interfere with actin dynamics within the cell.

4.2.3 Cell recovery after photodelivery of CytoD

The effects observed in actin cytoskeleton as a consequence of light activation of CytoD were temporal and reversible. Reorganization of the actin cytoskeleton to normal status after exposure was observed within 1 hour after exposure in the previously described experiment with MEFs. This is a consequence of the drop in the local concentration of the drug due to the dilution of the liberated CytoD in the medium (**Fig. 6a**). In other words, the release of CytoD by photoactivation can be regarded as a short impulse which creates a time- and site-defined and reversible effect on actin structure (**Fig. 6b**). The cells became smaller and rounder after photoactivation of Nvoc-CytoD and disruption of the actin stress fibers. This effect was reversed in about 5 min after exposure, when cells recovered their original dimensions and actin morphology. We also tested if repetitive experiments could be performed on the same cell. Cells exposed to light in two consecutive steps underwent similar changes and recovery to original status after each exposure (**Fig. 7**). In addition, when the exposed area was smaller, a lower concentration of free CytoD was available and only the subarea closest to the irradiated area or the cytoskeleton was disrupted (**Fig. 8**).

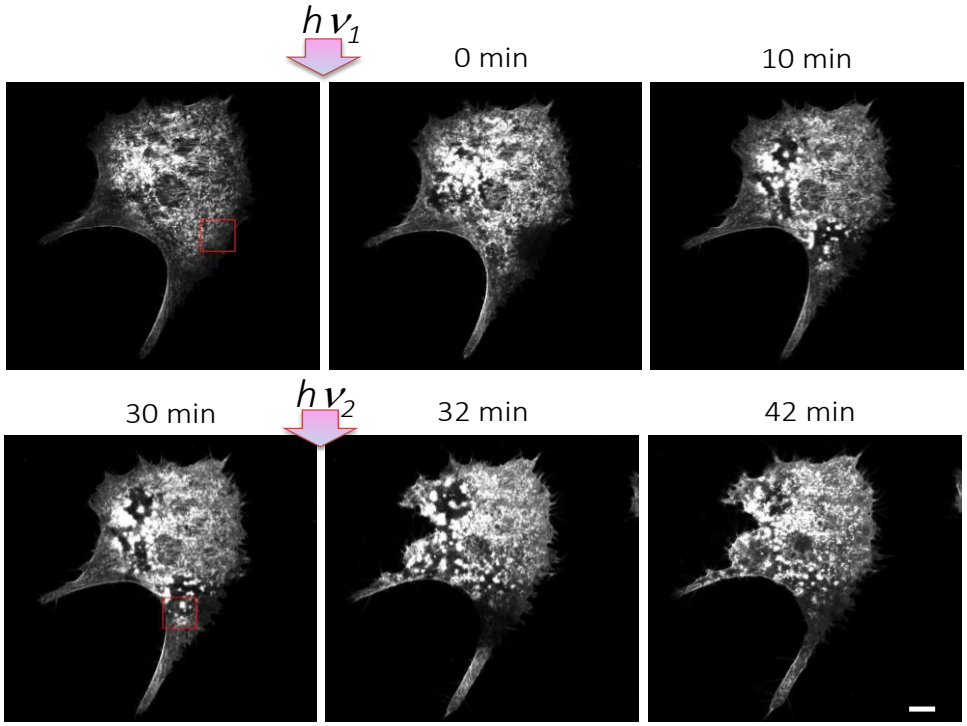

Figure 7 Photoactivation and recovery of Nvoc-CytoD in two sequential steps on the same cell. Scale bar is 10µm. Fluorescence signal in the irradiated area disappears during exposure. Fluorescence recovered after ca. 10 mins to show a distorted actin cytoskeleton locally. Cells could recover and reorganize their actin cytoskeleton. White is F-actin and scale bar represents 10 µm.

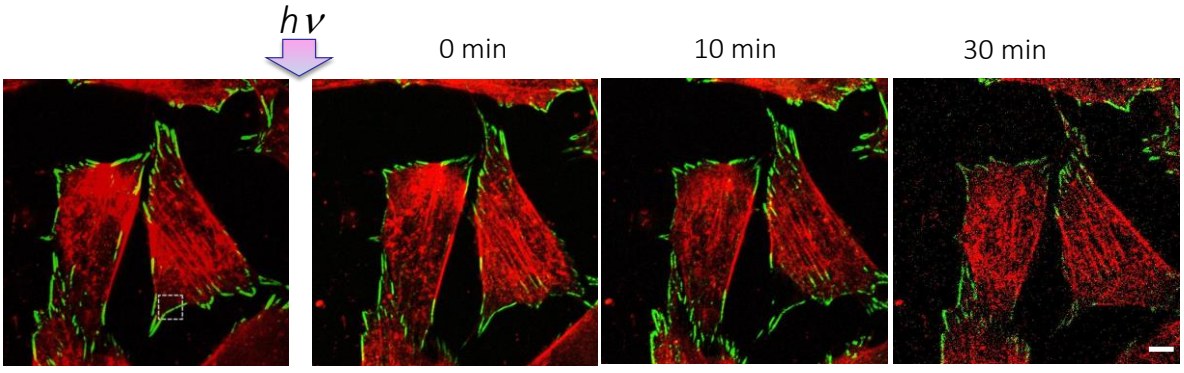

Figure 8 Reduced release of CytoD by irradiation of a small cell area. Disruption of the cytoskeleton only occurred in part of the cytosol and recovered in 30 mins. Red is F-actin, green is Vinculin and scale bar is 10 µm.

In summary, the described experiments demonstrate the possibility to interfere with actin dynamics locally and temporally using Nvoc-CytoD and a light source. Activation and disruption occur within tens of seconds and allows comfortable experimentation. The effect is reversible within a time frame spanning from 5 min to 1 hour depending on the concentration of Nvoc-CytoD used for the experiment, the exposure dose and cell types. After that time the actin cytoskeleton reorganizes back to its normal state. While a regular illumination should allow maintenance of a constant drug local concentration over time, single pulses allow observing repetitive disturbance and recovery events in an individual cell or in different cells of the same dish, without the need of changing the cell medium.

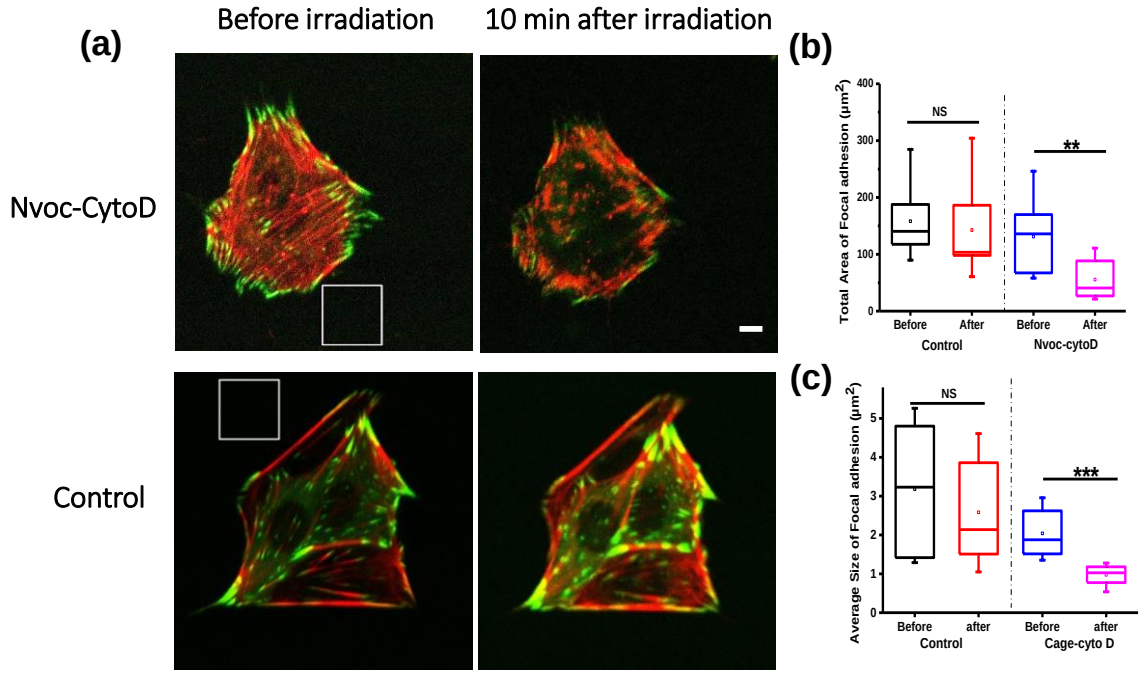

Figure 9 Focal adhesion reorganization after uncaging of Nvoc-CytoD. (a) Representative images of MEFs incubated with Nvoc-CytoD before and after light exposure and controls. (b) The total area of Focal adhesions and (c) the average size of Focal adhesion before and after light irradiation. The irradiation area is labeled by

a white square box. Red is F-actin, and green is Vinculin. Scale bar is 5 µm. *** p <0.001, ** p <0.01, NS = not significance. See experimental section for detailed explanation of quantification protocol.

4.2.4 Nvoc-CytoD induced changes in focal adhesions

We further looked at the possibility to affect other cellular phenomena dependent on the actin network. Upon integrin activation, cells create local adhesion points that maturate into focal adhesions depending on the building of stress fibers. The maintenance of tension in the fibers is essential to the stability of the focal adhesion.[185] We looked therefore at the changes in the focal adhesions of MEFs labeled with GFP-vinculin upon local activation of Nvoc-CytoD. Irradiation of a 180 µm2 area outside of the MEF cell lead to changes in the actin cytoskeleton close to the irradiated area and formation of actin clusters in the following 10 min (**Fig. 9a**). Quantification of the total area and average size of the focal adhesions 10 min after exposure showed that both parameters significantly decreased after exposure (**Fig. 9b,c**), whereas no significant changes were observed in the control experiments. These changes corroborate that the controlled interference in the dynamics of actin cytoskeleton caused by light-activated CytoD can be used to regulate and study actin-related phenomena like maturation of focal adhesions.

4.3 Conclusions

Nvoc-CytoD is a photoactivatable derivative of CytoD able to penetrate the cell membrane and to allow light-mediated local delivery of the CytoD drug. Nvoc-CytoD can be applied to temporarily disturb the actin cytoskeleton in a living cell without causing photodamage. Using photoactivable Nvoc-CytoD the time point at which

actin is disturbed can be precisely controlled. Nvoc-CytoD treated and control cells can be analyzed in the same dish - even in the same field of view – due to site-resolution of the drug release process when using a focused laser. Nvoc-Cyto D can be applied to temporally disturb the F-actin cytoskeleton and study cytoskeletal dynamics and related cellular structures and processes. Here we demonstrated site-directed disruption of F-actin and shrinkage of cell area and focal adhesion size by locally delivering Cyto-D by light exposure inside or outside of different kinds of cells. The experiments can be performed using a normal confocal microscope equipped with a 405 nm laser (without photo-manipulation unit). Exposure times in the tens of seconds time scale were used and the F-actin changes were observed in time scales of 10 min. The changes were reversible and cells survived repetitive exposures.

Nvoc-CytoD can be easily added to the cell culture medium for experimentation, in contrast to other reported approaches using photoactivatable actin-binding proteins that required microinjection (photoactivatable Thymosin β4 applied to photocontrol actin dynamics and the direction of migration of keratocytes[186] and photoactivatable Cofilin tested with MTLn3 cells[187]). It does not require optogenetic engineering of the cell of interest[188, 189] and can be widely applied to any cell type.

4.4 Materials and methods

Reagents and Materials

4 compartments-CELLview™ Cell Culture Dishes were purchased from Greiner bio-one (627870). Live Cell Fluorogenic F actin Labeling Probe (SiR-actin, SC001) was purchased from Tebu-bio. All other reagents were purchased from Sigma-Aldrich unless otherwise specified.

Cell culture and sample preparation

Mouse Fibroblasts L929 (NCTC clone, ATCC) were cultured in RPMI 1640 medium (GIBCO) supplemented with 10% fetal calf serum (FCS; GIBCO). WT eGFP-Vinculin mouse embryonic fibroblast lines (MEFs) were cultured in DMEM with 10% fetal bovine serum, 1% Nonessential Amino Acids, 1% Sodium Pyruvate and 4 mM L-Glutamine (all of them purchase from GIBCO).[190] L929 and MEFs expressing Vinculin-GFP were cultured in a humidified incubator at 37 C/5%CO2.

SiR-actin was used for actin imaging. After cell attachment, cell culture medium was replaced by fresh medium containing SiR-actin (100nM). After 12h incubation F-actin was labeled by Sir-actin. Then Nvoc-CytoD in DMSO was added to the medium to a final concentration of 50 µM Nvoc-CytoD or 0.1% DMSO. DMSO was used for the control group.

For sample preparation for microscopy, 0.5 ml of cell suspension (30.000 cells/ml) was filled into each of the 4 compartments of cell culture dish CELLview™.

Live-Cell Imaging

Time-lapse recordings were acquired with 20x, 63x objectives using either a Cell Observer inverted microscope (Zeiss Axio Observer Z1) controlled by ZEN blue software or a confocal microscope (Zeiss LSM 880) controlled by ZEN black software. All microscopes were equipped with an incubation chamber which maintained the temperature at 37°C and CO_2 concentration at 5%.

In situ photolysis of Nvoc-CytoD

A selected position in the cell culture was scanned using a Zeiss LSM 880 with a 405 nm laser (laser power 0.234 mW) for 45 seconds. Briefly, the selected position was zoomed in full field of view, then took a picture by 405 nm laser (108.7µs per pixel, image area is 179.99 µm2). The irradiation area was labeled with square by ZEN black software. For inside cell irradiation, the 15% laser power was used, while 100% laser power was used for outside cell irradiation. Images of the cells were recorded shortly before and 10 min after irradiation. For time lapse movies, images were acquired every 30 seconds during 10 min using a 63x oil objective after irradiation.

Cell viability assays

Viability tests were performed using WST-1 staining (Sigma) following manufactures protocol. Briefly, L929 cells (20,000cells/well) were seeded in 96 well-plates (Greiner bio-one). After 24 hours, culture medium was replaced by CytoD or Nvoc-CytoD (0.001 - 1µM) supplemented medium, or by medium with 0.1% DMSO as control. After 24 h, cells were stained with 10 µl WST-1 reagent per well. Metabolically active cells cleaved the stable tetrazolium salt WST-1 to a soluble formazan. After 2h incubation, the 96 well plates were measured at wavelengths 450 and 690 with a plate reader (infinite M200; Techan, Durham, NC, USA).

Imaging and data Analysis

The acquired fluorescent images and DIC time series were processed and analyzed with Fiji (distribution of ImageJ), or ZEN blue software, or homemade routines under Fiji (Macros). For the quantification of the size of focal adhesion, the images of MEFs before and 10 min after expose were acquired. To assess the size of focal adhesion, an automatic particle analysis (homemade macros) was performed and the number,

area and total area of particle were measured to get the number, size and total area of focal adhesion.

Statistical analysis

For each condition a minimum of three independent experiments were performed. Data were expressed as mean ± standard deviation. Box plots represent the middle 50% of data between the 1st to the 3th quartile (interquartile range IQR); the whiskers indicate variability outside the upper and lower quartiles. One-way ANOVA was used to determine significance between groups followed by a post-hoc Tukey contrast (GraphPad Software). For non-parametric data we performed Kruskal-Wallis analysis followed by Dunn's post-hoc multiple comparisons. All the cases a value of $p < 0.05$ was used for statistical significance.

Chapter 5

5. The interaction between mammalian cell and a bacterial biomaterial regulated by light

Note: The content of this chapter is part of the submitted manuscript: Towards Optogenetically-Regulated Living Biomaterials, Shrikrishnan Sankaran, Shifang Zhao, Christina Muth, Julieta Paez, Aránzazu del Campo, 2018. Shrikrishnan Sankaran and I contribute equally to this work. I performed the experiments with mammalian cells in this work and contributed to manuscript writing.

The properties of the natural extracellular microenvironment are dynamic, i.e. they change over the life time of a cell or a tissue. In order to introduce dynamic properties in synthetic materials, Dr. Shrikrishnan Sankaran in del Campo's Lab has modified biomaterials with genetically engineered bacteria to express cell adhesive proteins upon light exposure. These materials were used in this chapter to mediate cell-materials interactions. The following sections describe the biological demonstration of the dynamic interaction between mammalian cells and bacterial biointerfaces regulated by light-tunable surface display of cell adhesive receptors at the bacteria surface. The secretion of the fluorescent protein from the bacteria and the uptake by the mammalian is also described, indicating the potential of such a bacterial material to deliver complex cargo to cells in a targeted manner.

5.1 Introduction

The regulation of the dynamics of extracellular microenvironment enables interference with cellular processes such as cellular attachment, migration or differentiation. The study of the ECM-regulated dynamic cellular processes requires biomaterials to specifically interfere with cells in-situ and with spatiotemporal control. The development of biomaterials able to regulate cellular process is an active area of research with potential for industrial and medical translation.[191] Research efforts nowadays are particularly dedicated towards creating dynamic biomaterials enabling active regulation of signaling molecules (adhesive ligands or growth factors) or matrix mechanics upon application of external stimuli.[192] Light has emerged as an advantageous stimulus in this context. It allows non-invasive, spatiotemporally resolved activation, tunable regulation by varying exposure dose, and multiplexing by using different wavelengths. Light-regulated ligand availability,[104, 105] material stiffness,[193, 194] topography,[132, 195] and degradation[194, 196] have been achieved in biomaterials through the introduction of synthetic chromophores either in the material or the ligand structure. However, most of these approaches are irreversible, cannot be re-activated, and require specific chemical design and extensive synthesis for each individual ligand or polymeric chain.[192] We do not have strategies to study the interaction between the cells and biomaterials in a truly dynamic manner and involving complex molecules, as it happens in living tissues.[197]

A new strategy to circumvent these limitations is by using living biomaterials that could dynamically interact with cells. M Salmeron-Sanchez and coworkers have pioneered the concept of bacterial biointerfaces, based on *L. lactis*.[198-200] Poly

(ethyl acrylate) substrates coated with *L. lactis* displayed a fibronectin fragment on their outer surfaces and were used to guide stem cell differentiation. This fascinating approach opened a new window for dynamic biomaterials design. Dr. S. Sankaran in del Campo's Lab has followed up on Salmerón's work and optogenetically engineered *E. coli* to surface display cell adhesive proteins upon light exposure. In this chapter, I present the experiments that demonstrate how cellular attachment to a biomaterial can be tuned using these bacteria as intermediate dynamic biofunctional layer and light.

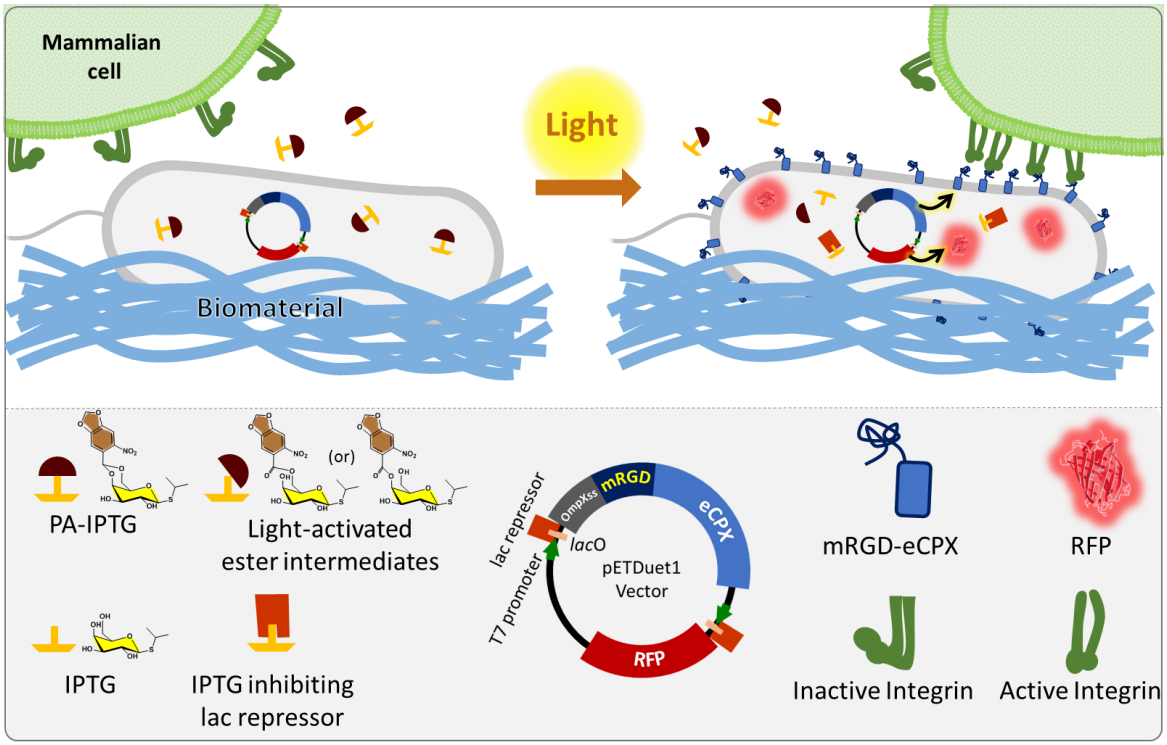

Figure 1. Molecular design of the light-inducible *E. coli*-biomaterial system. PA-IPTG used along with an IPTG-inducible dual expression vector enables light-controlled protein expression.[201] Upon light irradiation, PA-IPTG gets converts to an ester intermediate that is enzymatically hydrolyzed into active IPTG within *E. coli*. The free IPTG inhibits the lac repressor and starts production of the genetically encoded proteins, mRGD-eCPX and RFP. The transmembrane carrier protein eCPX allows

surface display of the mRGD at the bacterial membrane. RFP acts as a reporter to identify the activated bacterial cells. Integrins at the surface of mammalian cells interact with mRGD displayed on the bacterial surface and mediate cellular attachment to the bacterial biomaterial. The scheme was provided by Dr. Shrikrishnan Sankaran.

The molecular design of the light-inducible *E. coli*-biomaterial system developed by Dr. S. Sankaran is described in **Figure 1**. He combined a commercially available genetically engineered endotoxin-free strain named ClearColi® with a photoactivatable version of the chemical inducer isopropyl β-d-1-thiogalactopyranoside (IPTG), named PA-IPTG.[202, 203] The E*. coli* strain was engineered to display an RGD-containing miniprotein (mRGD) on its surface[204] along with the red fluorescent protein, TagRFP (RFP), as a reporter to visualize activation of protein expression in the bacterial cells (**Figure 1**). The expression of both genes was simultaneously induced in the presence of IPTG. A negative control strain was also engineered in which mRGD was replaced by the scrambled version, mRDG.[204] The bacterial strain expressing mRGD-eCPX will be referred to as *E. coli*+, and the one expressing the scrambled mRDG-eCPX as *E. coli*- in the following sections. Bacteria immobilized on Poly-D-lysine (PDL) coated Nexterion coverslips and induced with IPTG were able to express the proteins on their surface, as indicated by the red fluorescence in the microscopy images (**Figure 2**). Control experiments without IPTG solution and with a PA-IPTG solution without irradiation at equivalent concentrations were also performed and there is no red fluorescence observed even 24 hours culture (**Figure 2**). This system was used for regulating cell adhesion to the material in the next sections.

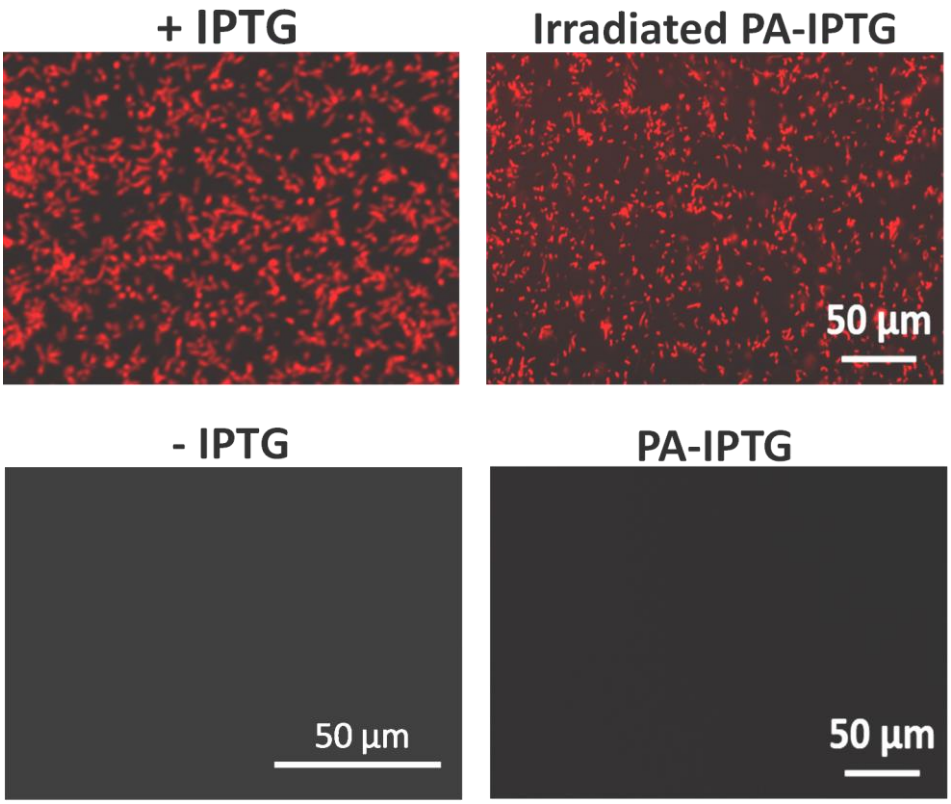

Figure 2. RFP expression of *E. coli*+ cells immobilized on PDL-coated surfaces. Expression was induced with IPTG or PA-IPTG and images were made 2 hours after induction. In the absence of IPTG or PA-IPTG without irradiation, red fluorescence is not observed in the bacteria after 24 hours culture.

5.2 Result and discussion

The possibility to light-control mammalian cell response on the bacterial biointerface was tested using mouse embryonic fibroblasts expressing vinculin-GFP (MEF-vincGFP). Vinculin is one of the proteins that localizes at focal adhesions and therefore these cells were expected to allow visualization of the formation of focal adhesions in response to the light-induced display of mRGD adhesive miniprotein on the surface of the bacteria. After cell seeding and addition of PA-IPTG, the substrate

was irradiated at one corner in order to prevent photodamage on the MEFs. Initially, MEF-vincGFP cells did not show interaction with the bacterial biomaterial. Cells remained predominantly round and migrated very little (**Figure 3a**). Approximately 3 hours after irradiation, bacteria started exhibiting red fluorescence. Shortly before that, the MEF-vincGFP cells started to spread, extending protrusions and pulling on the bacteria around them. This observation indicates that the mRGD displayed at the bacterial surface was recognized by integrin at MEFs membrane effectively, at protein expression levels below the fluorescence detection limit on the microscope. As time progressed, the cells recognized and rapidly pulled the *E. coli*+ bacteria off the surface. This seemed to happen in all directions around the MEF-vincGFP cells and resulted in the cells migrating over the surface and accumulating *E. coli*+ cells around under them (**Figure 3a,b**). The accumulation of bacteria is a consequence of the traction forces applied by cells at the adhesion points, which seem to be larger than the adhesion force of the bacteria with the underlying substrate. It is important to note that previous studies had shown that *E. coli* can strongly adhere to poly-L-lysine surfaces with rupture forces around 5 nN.[205]

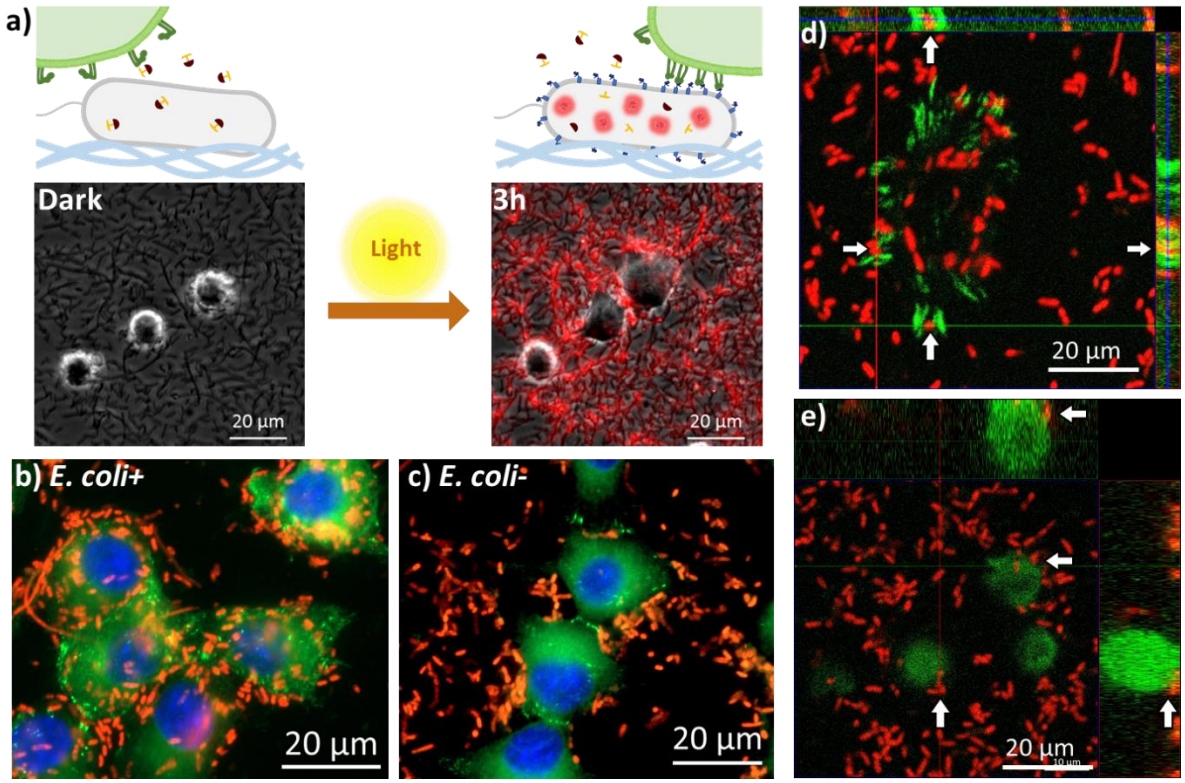

Figure 3. Optoregulated interactions between cells and bacterial material. **a)** Microscopy images (Merged phase contrast and red fluorescence channels) of *E.coli*+ surfaces seeded with MEF-vincGFP cells in the presence of PA-IPTG in the dark (left) and 3h (right) after light exposure. **b,c)** Epifluorescence images of MEF-vincGFP cells on *E. coli*+ (b) and *E. coli*- (c) surfaces at 7 h after light activation. Images were taken after fixation**. d,e)** Laser scanning confocal Z-stack orthogonal projection images of focal adhesions wrapped around *E. coli*+ (d) and not around *E. coli*- (e). Images correspond to living cell 10 h after IPTG induction. Red: bacteria, Green: vincGFP in MEF-vincGFP cells, Blue: DAPI. The white arrows indicate particular bacterial cells in both the XY plane image and the XZ and YZ orthogonal projections on the top and right respectively. Arrows pointing in the same direction correspond to the same bacterial cell.

MEF-vincGFP cells seeded on control surfaces coated with *E. coli*- did not interact with the bacteria (**Figure 3c**). Similar results were observed when the bacterial surfaces were chemically induced by adding IPTG to the medium. MEF-vincGFP cells migrated across the substrate and bacteria were accumulated around and under them (**Figure 4**). Z-stack confocal imaging revealed that focal adhesions formed around *E. coli*+ bacterial cells (**Figure 3d**), and not around *E. coli*- (**Figure 3e**). Z-stack images of MEF-vincGFP cells on *E. coli*+ surfaces, show focal adhesions completely enveloping the bacteria, indicating that the cells used some sort of gripping mechanism to pull the bacteria off the surface (**Figure 3d**), while no such interaction was seen with *E. coli*- (**Figure 3e**).

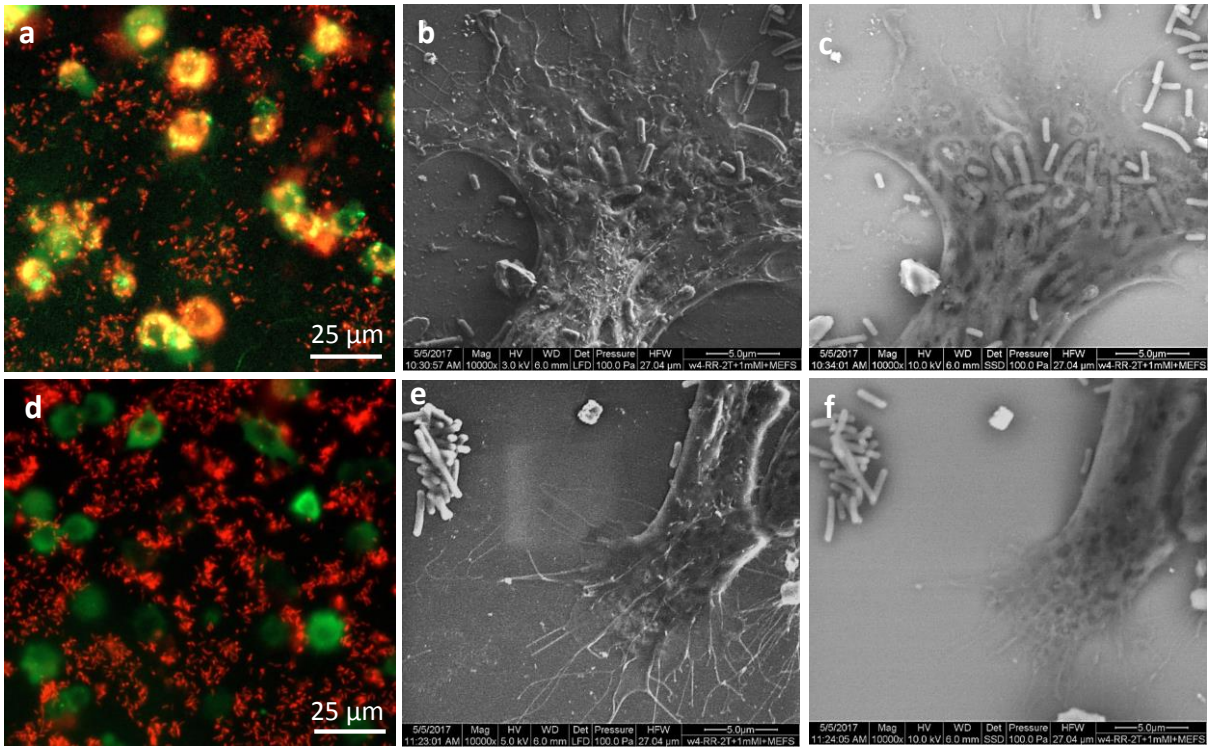

Figure 4. Epifluorescence images of MEF-vincGFP cells colocalized with bacterial cells in the case of (a) *E. coli*+ and completely separated in the case of (d) *E. coli*-. Red: bacteria, Green: vincGFP in MEF-vincGFP cells. SEM images of a cellular protrusion interacting with *E. coli*+ obtained using (b) Secondary electron and (d) backscattered electron detection methods or with *E. coli*- obtained by (e) secondary

electron detection and (f) backscattered electron detection. All images are of samples fixed 10 h after IPTG induction was performed.

Scanning Electron Microscopy (SEM) imaging of MEF-vincGFP with IPTG induced *E. coli*+ revealed close contact between the mammalian and bacterial cells, with cell protrusions completely covering the bacteria (**Figure 4**). SEM images further revealed MEF cell completely engulfing the light-activated *E. coli*+ (**Figure 5**). The bacteria were seen both below and above the cell extensions and some even emerging from underneath through pores. And there is no interaction observed between activated *E. coli*- and MEF cells. These results demonstrate the possibility to *in situ* regulate cell-materials interactions using light exposure and optogenetically engineered bacteria as active components of the artificial microenvironment.

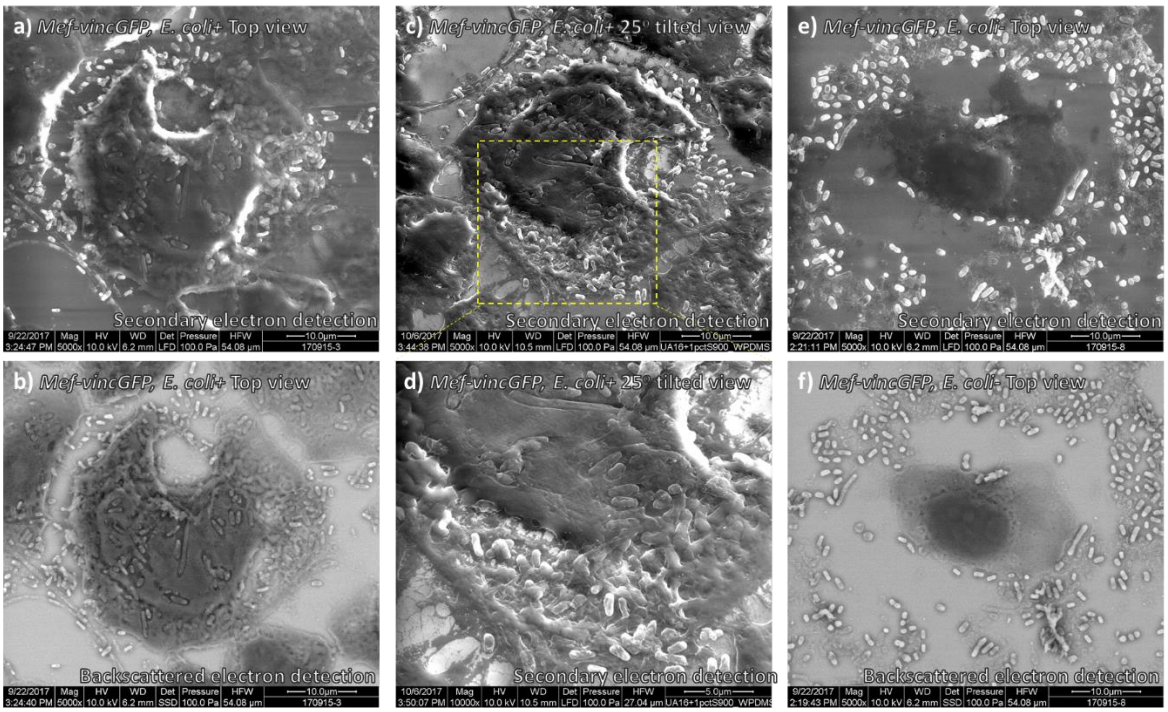

Figure 5. SEM images of mammalian cells interacting with light-activated E. coli. SEM images of MEF-vincGFP with *E. coli*+ obtained by (a) secondary electron detection and (b) backscattered electron detection. (c) The same cell was imaged at

an angle of 25º and (d) with higher magnification showing bacterial cells above and below a cell protrusion. MEF-vincGFP with *E. coli*- obtained by (e) secondary electron detection and (f) backscattered electron detection. Scale bar is 10 µm.

After 3 hours of interaction between MEF-vincGFP cells and induced *E. coli*+ bacteria, faint red fluorescence was also observed in the intracellular space (**Figure 6**). Such red fluorescence was not observed in cells on the *E. coli*- bacterial surface, even after 20 hours (**Figure 6**). No indication of bacterial lysis or endocytosis was observed by phase contrast, epifluorescence and SEM imaging of the surface. Based on the recent discovery that *E. coli* can secrete negatively-charged β-barrel-shaped fluorescent proteins,[206] it was hypothesized that the RFP used as a protein-expression indicator was secreted from the bacteria.

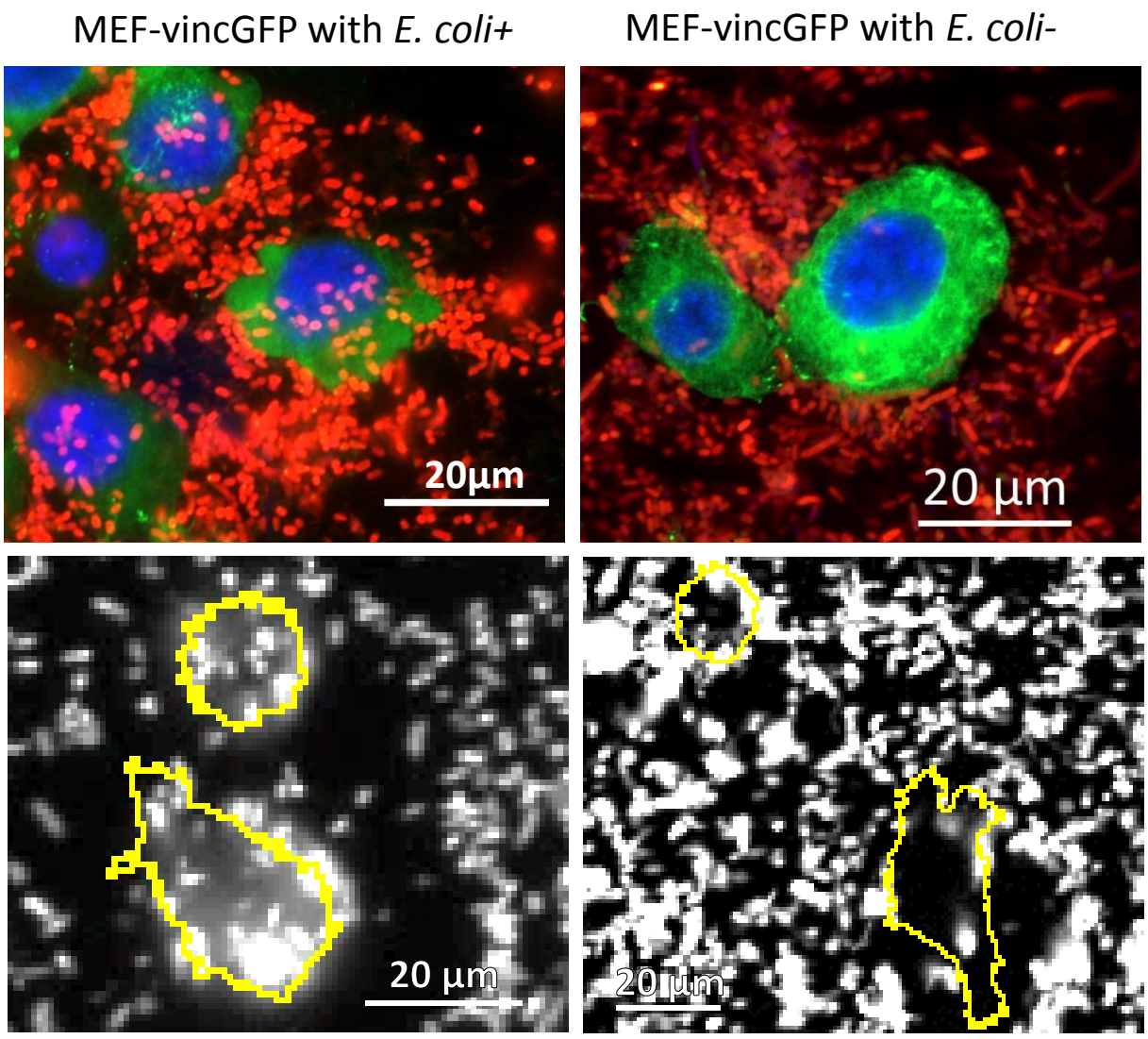

Figure 6 Microscopy images of MEF-vincGFP cells on *E. coli*+ and *E. coli*- surfaces. Fluorescent haze visible within the boundaries of MEF-vincGFP cells (approximate outlines in yellow) in the case of *E. coli*+ and not visible with *E. coli*- cells.

To test this theory, labeling live L929 cell membrane with green fluorescent (WGA-488) was used to reveal the location of RFP (Figure 7). Z-stack confocal imaging revealed that RFP localized inside or around L929 cell membrane with *E. coli*+ bacterial (**Figure 7, left**), and not inside L929 cell with *E. coli*- (**Figure7, right**). Z-stack orthogonal projection images of L929 cells on *E. coli*+ surfaces, show red fluorescence distributed completely inside the L929 membrane, even there is no bacterial adhesive on cell membrane. While no such red fluorescence was seen with

E. coli- (**Figure 7**). Similar results were observed when a line scan cross the cell membrane (white dash line) was performed and the fluorescence intensity was measured to display that there is red fluorescence (RFP) between green fluorescence (membranes) with *E. coli*+. This observation, even if it was unintended in our study, opens interesting possibilities for using bacterial biomaterials for light-controlled targeted delivery of proteins from *E. coli* to mammalian cells.

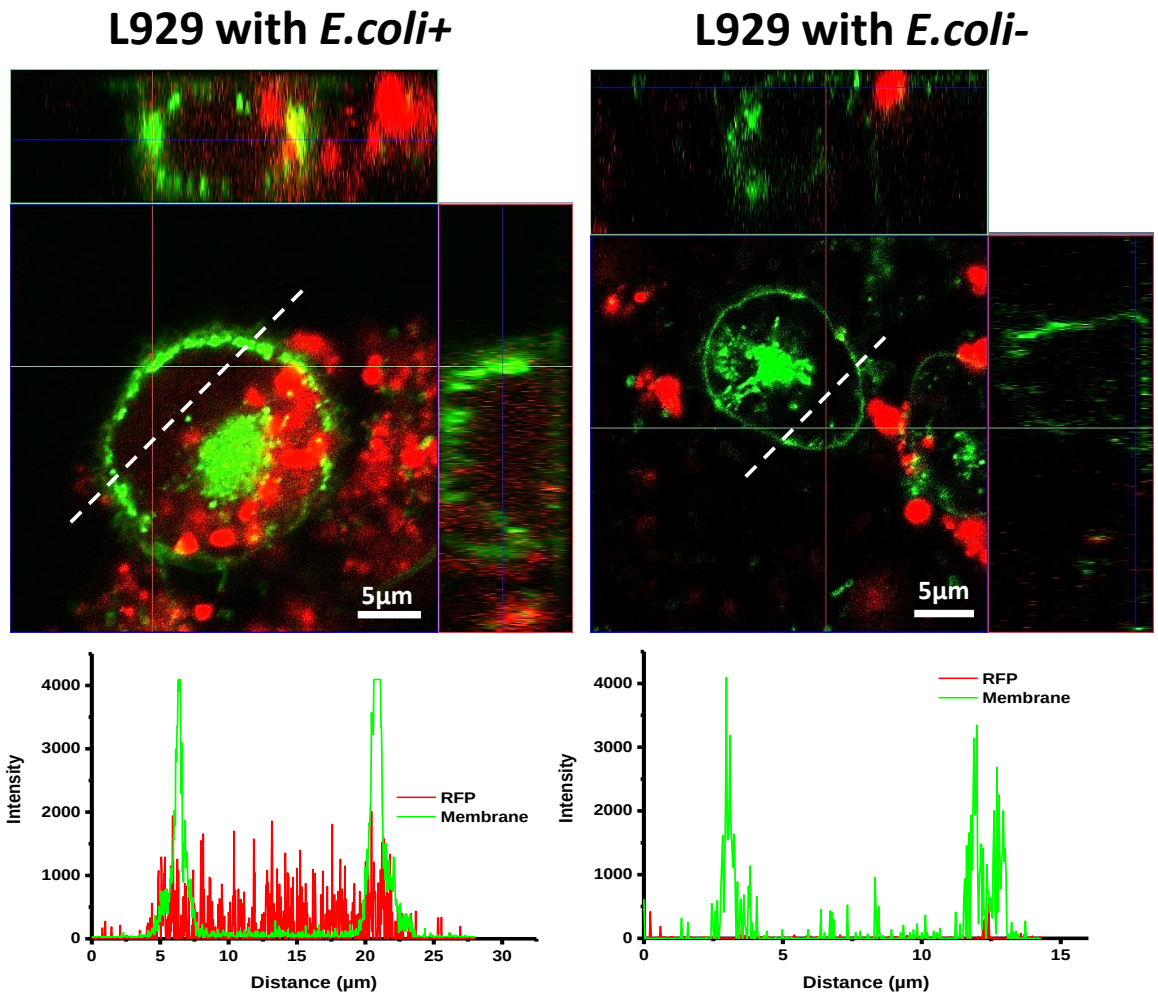

Figure 7. Characterization of fluorescent protein delivery by *E. coli*+ into mammalian cells. Laser scanning confocal Z-stack orthogonal projection images of the location of RFP inside *E. coli*+ and outside *E. coli*- . Images correspond to fixed samples 12h after IPTG induction. Red: bacteria, Green: WGA-488 for membrane staining in L929

cells. A line scan cross the cell membrane (white dash line) was performed and the plot profile of fluorescence intensity was measured for better illustration of RFP location.

5.3 Conclusion

The results in this chapter show that the interaction between mammalian cells and an engineered endotoxin-free *E. coli* based biomaterial can be temporally regulated by light. Specific adhesive interactions between integrin at the cell membrane and immobilized bacteria were observed through mRGD displayed on the bacterial surface. Due to the traction forces applied by cells, bacteria were pulled across the surface and accumulated around cells as they migrated. Finally, the unexpected observation that mammalian cells on *E. coli*+ containing surfaces developed red fluorescence within their intracellular space provides an indication that this method can be extended to deliver other soluble factors from bacterial materials to cells.

5.4 Materials and methods

Reagents and Materials

N-hydroxysuccinimide (NHS) functionalized Nexterion coverslip H (Schott, Material code: 1098523), silicon gasket (ibidi GmbH, Material code: 81201), Poly-D-lysine (SERVA Electrophoresis GmbH), were purchase from specified companies. Sterile Dubelcco's Phophate-Buffered Saline (PBS) was purchased from ThermoFisher Scientific. All water used in the work was ultrapure water with a resistivity of 18 MΩ.cm.

Bacterial surface preparation and Cell culture

The Nexterion coverslip was divided in 12 wells (0.56 cm^2 per well) by placing a silicone gasket on the top. 50 µL Poly-D-lysine solutions (2 mg/ml in PBS) were incubated in the wells for 60 min, allowing covalent immobilization of the molecules by reaction of their amine groups with the activated carboxylic acids at the Nexterion surface. Substrates were blocked by immersing in 50mM ethanolamine in PBS for 60 min and rinsed with water 3 times. Before the cell experiment, the substrates were sterilized by incubating in 70% ethanol for 5 min and rinsed with sterile PBS 3 times.

To immobilize bacteria on these surfaces, bacteria were inoculated from glycerol stocks in 5 mL LB broth containing 50 µg/mL ampicillin and grown overnight at 30^{o}C, 250 rpm. The bacterial densities typically reached ~0.5 $O.D._{600nm}$ by the morning. The cultures were then spun down at 4000 rpm for 10 mins and the pellets were resuspended in in sterile PBS with $O.D._{600nm}$ 1.0. 100 µL of these bacterial solutions

were incubated for 30 min in each well. These surfaces were then washed 3 times with sterile PBS by vigorous pipetting.

WT eGFP-Vinculin mouse embryonic fibroblast lines (MEF-vincGFP) were cultured in DMEM with 10% fetal bovine serum, 1% Nonessential Amino Acids, 1% Sodium Pyruvate and 4 mM L-Glutamine (all of them purchase from GIBCO) in a humidified incubator at 37^{o}C/5%CO_2. For every experiment, the cells were trypsinized and the cell density was determined a TC20™ Automated Cell Counter (Bio-Rad). The cells were directly seeded in the wells at a density of 2.5 x 10^4 cells / well. For all experiments with bacteria, the cell-culture medium was supplemented with 50 µg/mL ampicillin.

Image acquisition and Time lapse experiment

Microscopy images and time-lapse recordings were acquired with 20x and 63x objectives using either a Cell Observer inverted microscope (Zeiss Axio Observer Z1) controlled by ZEN blue software, a confocal microscope (Zeiss LSM 880) controlled by ZEN black software or an inverted Nikon Ti-Eclipse microscope controlled by NIS Elements software. All microscopes were equipped with an incubation chamber which maintained the temperature at 37°C and CO_2 concentration at 5%. Image processing and analyses were performed using Fiji edition of ImageJ.

Induction of protein expression

Three strategies were used to induce protein expression in the surface-immobilized bacteria using PA-IPTG and IPTG. PA-IPTG stock solution was prepared in DMSO at a concentration of 500 mM and IPTG stock solution was prepared in water at a concentration of 100 mM.

(i) PA-IPTG was diluted in the appropriate medium at a final concentration of 500 µM and this solution was exposed to 360 nm irradiation using a Lumos 43 illuminator (Atlas photonics) for 1 min. This medium was then added on the bacterial surfaces.

(ii) PA-IPTG was diluted in the appropriate medium at a final concentration of 500 µM and added on the bacterial surfaces in the dark. When required, 360 nm light was irradiated from the Zeiss Axio Observer Z1 microscope using a Colibri 2/365 nm LED module light source at 50% intensity and an EC-Plan NeoFluar 20x objective for 2 min. When only bacteria were present, the objective was scanned over the whole well and when MEF-vincGFP cells were also present, irradiation was done only in one corner of the well.

(iii) IPTG was added to the medium at a final concentration of 100 µM

Sample fixation and staining

For high magnification and confocal imaging, samples were fixed by washing 3 times with sterile PBS then incubating for 15 min with 4% paraformaldehyde (PFA) solution in PBS then washing again 3 times with sterile PBS. The cell nuclei were stained using DAPI and mounted using standard protocols.

Sample Preparation for Scanning Electron Microscopy and Image acquisition

The samples were washed with PBS, fixed for 30 min with 2 wt% glutaraldehyde in 0.1 M Cacodylat (214 g/mol), and then washed 3 times with sterile PBS. In order to dehydrate, the samples were immersed into ethanol with increasing concentrations, 30% for 10 min, 50% for 10 min, 70% for 10 min, 80% for 10 min, 90% for 10 min, 96% for 10 min, 100% for 2x15 min. Subsequently, the sample was incubated in 100% ethanol mixed at a 1:1 volume ratio with hexamethyldisilazan (HMDS) for 15 min. After that, samples were immersed into pure HMDS for 15 min twice. At the end, the samples were dried in an exhaust fume hood. The surface of the cell membrane was observed using the scanning electron microscope (SEM) (JSM-7500F; JEOL).

Sample Preparation for Membrane Labeling and Image acquisition

After L929 fibroblast cells seeding on the E. coli+ or E. Coli- bacterial surface, the IPTG (100nM) was add to the medium to continue culture overnight to allow the bacterial express enough flourescent protein. After that, the samples were washed with Hank's balanced salt solution (HBSS). The wheat germ agglutinin conjugates Oregon Green® 488 (WGA, invitrogen) was diluted to 5 µg /ml by HBSS to get the work concentration. The labeling solution was added to cover cells and incubate for 10 minutes at 37°C. When labeling is complete, remove the labeling solution, and wash cells twice in HBSS buffer. Then samples were mounted in pre-warmed HBSS buffer for imaging.

The fluorescent of the L929 cell membrane and RFP was observed using a confocal microscope (Zeiss LSM 880) controlled by ZEN black software. For the quantification and comparison of the fluorescent intensity, all the z-stacks images were acquired in the same condition.To assess the fluorescent intensity, a line scan cross the cell

membrane was performed and the plot profile of fluorescence was measured. The xy, xz and yz optical section of z-stacks was generated by orthogonal view of ZEN black software.

Chapter 6

6. Conclusions and Outlook

In this thesis, I have developed and tested artificial biomaterials that mimic the minimal features of the natural microenvironment of neurons that support migration, neurite extension and eventually differentiation. I have demonstrated that somal translocation can be triggered by neuronal cells when their exploratory growth cone crosses to regions of different adhesiveness on a substrate. I have used photoactivatable peptidomimetics of laminin to guide neuronal outgrowth by light. I have demonstrated spatiotemporal control of the actin cytoskeleton of a cell by light-dosed release of a photoactivatable variant of the actin drug Cytochalasin D at seconds time scale and at subcellular resolution using conventional microscopy setups. Finally, I have experimentally demonstrated how fibroblasts can interact with bacterial interfaces and respond to light-activated surface display of adhesive ligands.

The following are the major conclusions and outlook of this work:

- Uniquely, I have developed a simple biomaterial platform to in vitro trigger and study the characteristic phenomenon of terminal somal translocation (ST) during cortical layering. This works on the basis of a generic design with

micropatterns with contrasting adhesiveness. These findings indicate that the adhesive properties of the environment may serve as key determinant of neuronal ST and neuronal organization during corticogenesis, challenging the view of specific membrane receptor-ligand interactions as triggers for ST. This is an ideal in vitro model to study environmental cues stimulating directional neuronal migration.

- Using a photoactivatable IK(HANBP)VAV, I have demonstrated light-guided neurite outgrowth in a predicted pathways, and light-based establishment of connections between selected neurons. The possibilities of this approach to build neural circuits will be explored in the future. Furthers studies can be extend this system in 3D cell culture by taking advantage of the two-photon efficiency of the photosensitive molecule.
- The phototriggerable Nvoc-CytoD can be applied to disturb the actin cytoskeleton in a living cell at seconds time scale, with subcellular resolution and in a reversible manner. Further, this thesis demonstrated the possibility to perform repeated experiments in the same cell after cell recovery, and the possibility to perform control experiments in the same dish. The Nvoc-CytoD approach can be applied to study cellular processes where actin dynamics plays a major role. This work can be further extended in the future to 3D cell culture system by redesigning a photoactivatable CytoD molecule with effective two-photon sensitivity.
- This Thesis demonstrated that optogenetically regulated E. coli-based bacterial biointerfaces can be used to dynamically interact with mammalian cells. Although this Thesis only demonstrates RGD-mediated adhesive interactions, this principle could be extended to a variety of cellular processes by engineering other ligands on the bacterial surface. The possibility to deliver

proteins from the E. coli+ to the intracellular space of mammalian cells when they are interacting was unexpectedly found. This finding might also be extended to deliver soluble factors from bacterial biomaterials to mammalian cells. Moreover, the 2D approach used in this Thesis could be expanded to 3D scaffolds by encapsulating bacteria in polymeric nanofibers by electrospinning or bioprinting.

List of Scientific Contributions

Articles

1. **S. Zhao**, W. Fan, X. Guo, L. Xue, B. Berninger, M.J. Salierno, A. del Campo, Microenvironments to study migration and somal translocation in cortical neurons, Biomaterials, 2018. 156: p. 238-247.

2. J. Feng, X.A. Ton, **S. Zhao**, J.I. Paez, A. del Campo, Mechanically Reinforced Catechol-Containing Hydrogels with Improved Tissue Gluing Performance. Biomimetics 2017, 2(4), 23; doi:10.3390/biomimetics2040023

3. A, Farrukh, W. Fan, **S. Zhao**, M. Salierno, J.I. Paez, A. del Campo, M.J. Salierno, Photoactivatable Adhesive Ligands for Light-guided Neuronal Growth, ChemBioChem, 2018. https://doi.org/10.1002/cbic.201800118

4. Shrikrishnan Sankaran, **Shifang Zhao**, Christina Muth, Julieta Paez, Rebecca Ludwig, Aránzazu del Campo Bécares. Toward Light-Regulated Living Biomaterials. Advanced Science 2018: 1800383**, co-first author.**

5. Roshna V. Nair, **Shifang Zhao**, Emmanuel Terriac, Franziska Lautenschläger, Aránzazu del Campo, Spatiotemporal regulation of actin dynamics with Photoactivatable Cytochalasin D, 2017. **Submitted, co-first author.**

6. A. Farrukh, **S. Zhao**, A. del Campo, Biomaterials designed to support growth and function of neuronal cells. Frontiers in Materials, section Biomaterials, 2018. **Submitted.**

7. A. Farrukh, **S. Zhao**, J. Paez, M. Salierno, A. del Campo, In situ light-guided axon growth with photoactivatable laminin peptidomimetics. **Manuscript in preparation**.

Poster Presentations

1. **S. Zhao**, W. Fan, B. Berninger, M.J. Salierno, A. del Campo. In vitro recapitulation of neuronal somal translocation. 3D Cell Culture 2016-How close to 'in vivo' can we get? Models, applications & translation, 19 – 21 April 2016, Konzerthaus Freiburg.
2. **S. Zhao**, W. Fan, B. Berninger, M.J. Salierno, A. del Campo. In vitro recapitulation of neuronal somal translocation. The 3 rd Eurogenesis Meeting in Bordeaux, 2016, Bordeaux, France.
3. **S. Zhao**, W. Fan, B. Berninger, M.J. Salierno, A. del Campo. Differential adherence triggers somal translocation of cortical neurons. WE-Heraeus-Seminar (622) on Neural Mechanics, August 2016, Bad Honnef, Germany.
4. **S. Zhao**, W. Fan, B. Berninger, M.J. Salierno, A. del Campo. In vitro recapitulation of neuronal somal translocation and mechanism of external triggers. Cell Physics 2016, 22.-24.6.2016, Saarbrücken, Germany.
5. **S. Zhao**, W. Fan, B. Berninger, M.J. Salierno, A. del Campo. I n vitro recapitulation of neuronal somal translocation and mechanism of external triggers Leibniz PhD Workshop on Health Technologies, September 2016,

Berlin, Germany.

Participation in exercises

1. “Histology practical Course”, at institute of Molecular Biology gGmbH (IMB), July 2016, Mainz, Germany.
2. “Moderne laser-Mikroskopie in der Zellbiologie (2 SWS, 3ECTS-CP)”, at University of Saarlands, 2016, Saarbrücken, Germany.
3. “Federation of Europen Laboratory Animal Science Associations course(FELASA, category B) ”, at Humboldt University of Berlin, 2016, Berlin, Germany.

Curriculum Vitae

Name: Shifang Zhao

Sex: Male

Date of Birth: 12 September 1986

Nationality: P. R. China

Tel +49 (0)6131 379264

E-mail: ShifangZhao@Hotmail.com

Address: Leibniz for New materials

Campus D2 2, 66128, Saarbrücken

Germany

EDUCATION

PhD 2013-2018

- Doctorate studies at the Max Planck Institute for Polymer Research (Mainz), Leibniz Institute for New Materials and Saarland University, Saarbrücken, Germany
- Tentative title of the Thesis: Microenvironments to regulate cellular behavior for neural development and Regeneration
- Supervisor: Prof. Dr. A. del Campo
- 11/2015 – 08/2018 Doctorate Research at Leibniz Institute for New Materials, Saarbrucken
- 07/2014 – 10/2015 Doctorate Research at the Max Planck Institute for Polymer Research, Mainz

Master of Science -Donghua University

- Duration:2010-2013
- Major: Biochemistry and molecular biology

Bachelor of Engineering-The North University of China

- Duration:2005-2009
- Major: Bioengineering

HONORS

- The outstanding master's thesis of shanghai, 2014
- The scholarship of China Scholarship Council, 2013-2017
- Donghua University “Zhou Huasheng” Scholarship, 2011-2012
- “Outstanding Poster” in 2012 International Forum on Biomaterial Textile Materials
- Donghua University First-class Scholarship, 2010-2011
- Merit award of Mathematical Modeling, 2008

INTERESTS

Music, basketball, playing the guitar, badminton, running, acting

WORK STYLE

- Willing to perform basic tasks and move on to solve complex problems
- Able to learn new knowledge and adapt to new environments quickly

References

1. Liu, K., et al., *Neuronal intrinsic mechanisms of axon regeneration.* Annual review of neuroscience, 2011. **34**: p. 131-152.
2. Lee, W., C.W. Frank, and J. Park, *Directed Axonal Outgrowth Using a Propagating Gradient of IGF‐1.* Adv. Mater., 2014.
3. Lunn, J.S., et al., *Stem cell technology for neurodegenerative diseases.* Annals of neurology, 2011. **70**(3): p. 353-361.
4. Casarosa, S., Y. Bozzi, and L. Conti, *Neural stem cells: ready for therapeutic applications?* Molecular and cellular therapies, 2014. **2**(1): p. 31.
5. Gage, F.H. and S. Temple, *Neural stem cells: generating and regenerating the brain.* Neuron, 2013. **80**(3): p. 588-601.
6. Roach, P., et al., *Surface strategies for control of neuronal cell adhesion: a review.* Surface Science Reports, 2010. **65**(6): p. 145-173.
7. Higuchi, A., et al., *Biomimetic Cell Culture Proteins as Extracellular Matrices for Stem Cell Differentiation.* Chemical Reviews, 2012. **112**(8): p. 4507-4540.
8. Albritton, J.L. and J.S. Miller, *3D bioprinting: improving in vitro models of metastasis with heterogeneous tumor microenvironments.* Disease Models & Mechanisms, 2017. **10**(1): p. 3-14.
9. Calof, A.L. and A.D. Lander, *Relationship between neuronal migration and cell-substratum adhesion: laminin and merosin promote olfactory neuronal migration but are anti-adhesive.* The Journal of cell biology, 1991. **115**(3): p. 779-794.
10. Joo, S., et al., *Effects of ECM protein micropatterns on the migration and differentiation of adult neural stem cells.* Scientific reports, 2015. **5**.
11. Joo, S., K. Kang, and Y. Nam, *In vitro neurite guidance effects induced by polylysine pinstripe micropatterns with polylysine background.* Journal of Biomedical Materials Research Part A, 2015. **103**(8): p. 2731-2739.
12. Fujioka, T., et al., *β1 integrin signaling promotes neuronal migration along vascular scaffolds in the post-stroke brain.* EBioMedicine, 2017. **16**(Supplement C): p. 195-203.
13. Jeon, N.L., et al., *Neutrophil chemotaxis in linear and complex gradients of interleukin-8 formed in a microfabricated device.* Nature biotechnology, 2002. **20**(8): p. 826-830.
14. Mason, H.A., S. Ito, and G. Corfas, *Extracellular signals that regulate the tangential migration of olfactory bulb neuronal precursors: inducers, inhibitors, and repellents.* Journal of Neuroscience, 2001. **21**(19): p. 7654-7663.
15. Wood, M.D. and S.E. Sakiyama‐Elbert, *Release rate controls biological activity of nerve growth factor released from fibrin matrices containing affinity‐based delivery systems.* Journal of Biomedical Materials Research Part A, 2008. **84**(2): p. 300-312.
16. Pakulska, M.M., B.G. Ballios, and M.S. Shoichet, *Injectable hydrogels for central nervous system therapy.* Biomed Mater, 2012. **7**(2): p. 024101.
17. Kolb, B., et al., *Growth factor-stimulated generation of new cortical tissue and functional recovery after stroke damage to the motor cortex of rats.* Journal of cerebral blood flow & metabolism, 2007. **27**(5): p. 983-997.
18. Valiente, M. and O. Marín, *Neuronal migration mechanisms in development and disease.* Current opinion in neurobiology, 2010. **20**(1): p. 68-78.

19. Schmid, R.S. and P.F. Maness, *L1 and NCAM adhesion molecules as signaling coreceptors in neuronal migration and process outgrowth.* Current opinion in neurobiology, 2008. **18**(3): p. 245-250.
20. Wiencken-Barger, A., et al., *The role of L1 in axon pathfinding and fasciculation.* Cerebral Cortex, 2004. **14**(2): p. 121-131.
21. Struzyna, L.A., K. Katiyar, and D.K. Cullen, *Living scaffolds for neuroregeneration.* Current Opinion in Solid State and Materials Science, 2014. **18**(6): p. 308-318.
22. Franze, K., *Atomic force microscopy and its contribution to understanding the development of the nervous system.* Current opinion in genetics & development, 2011. **21**(5): p. 530-537.
23. Engler, A., et al., *Substrate compliance versus ligand density in cell on gel responses.* Biophysical journal, 2004. **86**(1): p. 617-628.
24. Deroanne, C.F., C.M. Lapiere, and B.V. Nusgens, *In vitro tubulogenesis of endothelial cells by relaxation of the coupling extracellular matrix-cytoskeleton.* Cardiovascular research, 2001. **49**(3): p. 647-658.
25. Discher, D.E., P. Janmey, and Y.L. Wang, *Tissue cells feel and respond to the stiffness of their substrate.* Science, 2005. **310**(5751): p. 1139-1143.
26. Lo, C.-M., et al., *Cell movement is guided by the rigidity of the substrate.* Biophysical journal, 2000. **79**(1): p. 144-152.
27. Franze, K., P.A. Janmey, and J. Guck, *Mechanics in Neuronal Development and Repair.* Annual Review of Biomedical Engineering, 2013. **15**(1): p. 227-251.
28. Bray, D., *Axonal growth in response to experimentally applied mechanical tension.* Developmental biology, 1984. **102**(2): p. 379-389.
29. Hanein, Y., et al., *Neuronal soma migration is determined by neurite tension.* Neuroscience, 2011. **172**: p. 572-579.
30. Koser, D.E., et al., *Mechanosensing is critical for axon growth in the developing brain.* Nature Neuroscience, 2016. **19**: p. 1592.
31. Rosso, G., P. Young, and V. Shahin, *Mechanosensitivity of Embryonic Neurites Promotes Their Directional Extension and Schwann Cells Progenitors Migration.* Cell Physiol Biochem, 2017. **44**(4): p. 1263-1270.
32. Wrobel, M.R. and H.G. Sundararaghavan, *Directed migration in neural tissue engineering.* Tissue Engineering Part B: Reviews, 2013. **20**(2): p. 93-105.
33. Malatesta, P., I. Appolloni, and F. Calzolari, *Radial glia and neural stem cells.* Cell and tissue research, 2008. **331**(1): p. 165-178.
34. Gumera, C., B. Rauck, and Y. Wang, *Materials for central nervous system regeneration: bioactive cues.* Journal of Materials Chemistry, 2011. **21**(20): p. 7033-7051.
35. Hoffman-Kim, D., J.A. Mitchel, and R.V. Bellamkonda, *Topography, cell response, and nerve regeneration.* Annual review of biomedical engineering, 2010. **12**: p. 203-231.
36. Webb, A., et al., *Guidance of oligodendrocytes and their progenitors by substratum topography.* Journal of cell science, 1995. **108**(8): p. 2747-2760.
37. Gomez, N., S. Chen, and C.E. Schmidt, *Polarization of hippocampal neurons with competitive surface stimuli: contact guidance cues are preferred over chemical ligands.* Journal of The Royal Society Interface, 2007. **4**(13): p. 223-233.
38. Nikkhah, M., et al., *Engineering microscale topographies to control the cell-substrate interface.* Biomaterials, 2012. **33**(21): p. 5230-46.
39. Sarig-Nadir, O., et al., *Laser photoablation of guidance microchannels into hydrogels directs cell growth in three dimensions.* Biophys J, 2009. **96**(11): p. 4743-52.

40. Shin, H., S. Jo, and A.G. Mikos, *Biomimetic materials for tissue engineering.* Biomaterials, 2003. **24**(24): p. 4353-4364.
41. Schmidt, C.E. and J.B. Leach, *Neural tissue engineering: Strategies for repair and regeneration.* Annual Review of Biomedical Engineering, 2003. **5**: p. 293-347.
42. Schense, J.C., et al., *Enzymatic incorporation of bioactive peptides into fibrin matrices enhances neurite extension.* Nature biotechnology, 2000. **18**(4): p. 415-419.
43. Tashiro, K., et al., *A synthetic peptide containing the IKVAV sequence from the A chain of laminin mediates cell attachment, migration, and neurite outgrowth.* Journal of Biological Chemistry, 1989. **264**(27): p. 16174-16182.
44. Iwamoto, Y., et al., *YIGSR, a synthetic laminin pentapeptide, inhibits experimental metastasis formation.* Science, 1987. **238**(4830): p. 1132-1134.
45. Ranieri, J.P., et al., *Neuronal cell attachment to fluorinated ethylene propylene films with covalently immobilized laminin oligopeptides YIGSR and IKVAV. II.* Journal of Biomedical Materials Research Part A, 1995. **29**(6): p. 779-785.
46. Kam, L., et al., *Selective adhesion of astrocytes to surfaces modified with immobilized peptides.* Biomaterials, 2002. **23**(2): p. 511-515.
47. Rønn, L.C.B., et al., *Neurite Outgrowth Induced by a Synthetic Peptide Ligand of Neural Cell Adhesion Molecule Requires Fibroblast Growth Factor Receptor Activation.* Journal of Neurochemistry, 2000. **75**(2): p. 665-671.
48. Zou, Z.W., et al., *Biocompatibility of functionalized designer self-assembling nanofiber scaffolds containing FRM motif for neural stem cells.* Journal of Biomedical Materials Research Part A, 2014. **102**(5): p. 1286-1293.
49. Guimard, N.K., N. Gomez, and C.E. Schmidt, *Conducting polymers in biomedical engineering.* Progress in Polymer Science, 2007. **32**(8): p. 876-921.
50. Holmes, T.C., et al., *Extensive neurite outgrowth and active synapse formation on self-assembling peptide scaffolds.* Proceedings of the National Academy of Sciences, 2000. **97**(12): p. 6728-6733.
51. Stukel, J.M. and R.K. Willits, *Mechanotransduction of Neural Cells Through Cell–Substrate Interactions.* Tissue Engineering Part B: Reviews, 2016. **22**(3): p. 173-182.
52. Zhang, Z., et al., *Neurite outgrowth on well-characterized surfaces: preparation and characterization of chemically and spatially controlled fibronectin and RGD substrates with good bioactivity.* Biomaterials, 2005. **26**(1): p. 47-61.
53. Straley, K.S., C.W. Foo, and S.C. Heilshorn, *Biomaterial design strategies for the treatment of spinal cord injuries.* J Neurotrauma, 2010. **27**(1): p. 1-19.
54. A. Farrukh, S.Z., J. Paez, M. Salierno, A. del Campo., *In situ light-guided axon growth with photoactivatable laminin peptidomimetics.*
55. Borkenhagen, M., et al., *Three‐dimensional extracellular matrix engineering in the nervous system.* Journal of Biomedical Materials Research Part A, 1998. **40**(3): p. 392-400.
56. Dodla, M.C. and R.V. Bellamkonda, *Differences between the effect of anisotropic and isotropic laminin and nerve growth factor presenting scaffolds on nerve regeneration across long peripheral nerve gaps.* Biomaterials, 2008. **29**(1): p. 33-46.
57. Moore, K., M. Macsween, and M. Shoichet, *Immobilized concentration gradients of neurotrophic factors guide neurite outgrowth of primary neurons in macroporous scaffolds.* Tissue engineering, 2006. **12**(2): p. 267-278.
58. Göpferich, A., *Mechanisms of polymer degradation and erosion.* Biomaterials, 1996. **17**(2): p. 103-114.

59. Chiono, V., C. Tonda‐Turo, and G. Ciardelli, *Chapter 9 Artificial Scaffolds for Peripheral Nerve Reconstruction*, in *International Review of Neurobiology*. 2009, Academic Press. p. 173-198.
60. Pfister, L.A., et al., *Nerve conduits and growth factor delivery in peripheral nerve repair.* Journal of the Peripheral Nervous System, 2007. **12**(2): p. 65-82.
61. Weber, R.A., et al., *A randomized prospective study of polyglycolic acid conduits for digital nerve reconstruction in humans.* Plastic and reconstructive surgery, 2000. **106**(5): p. 1036-1045.
62. He, L., et al., *Manufacture of PLGA multiple-channel conduits with precise hierarchical pore architectures and in vitro/vivo evaluation for spinal cord injury.* Tissue Engineering Part C: Methods, 2009. **15**(2): p. 243-255.
63. Chiono, V. and C. Tonda-Turo, *Trends in the design of nerve guidance channels in peripheral nerve tissue engineering.* Progress in Neurobiology, 2015. **131**: p. 87-104.
64. De Ruiter, G.C., et al., *Accuracy of motor axon regeneration across autograft, single-lumen, and multichannel poly(lactic-co-glycolic acid) nerve tubes.* Neurosurgery, 2008. **63**(1): p. 144-153.
65. Gu, X.S., et al., *Construction of tissue engineered nerve grafts and their application in peripheral nerve regeneration.* Progress in Neurobiology, 2011. **93**(2): p. 204-230.
66. Lundborg, G., et al., *A new type of "bioartificial" nerve graft for bridging extended defects in nerves.* The Journal of Hand Surgery: British & European Volume, 1997. **22**(3): p. 299-303.
67. Daly, W., et al., *A biomaterials approach to peripheral nerve regeneration: bridging the peripheral nerve gap and enhancing functional recovery.* Journal of The Royal Society Interface, 2012. **9**(67): p. 202-221.
68. Fawcett, J.W., *Spinal cord repair: from experimental models to human application.* Spinal cord, 1998. **36**(12).
69. Fawcett, J., *Repair of spinal cord injuries: where are we, where are we going?* Spinal cord, 2002. **40**(12): p. 615.
70. Li, W., et al., *Large-scale Topographical Screen for Investigation of Physical Neural-Guidance Cues.* Scientific Reports, 2015. **5**.
71. Chua, J.S., et al., *Extending neurites sense the depth of the underlying topography during neuronal differentiation and contact guidance.* Biomaterials, 2014. **35**(27): p. 7750-7761.
72. Tsai, E.C., et al., *Synthetic hydrogel guidance channels facilitate regeneration of adult rat brainstem motor axons after complete spinal cord transection.* Journal of neurotrauma, 2004. **21**(6): p. 789-804.
73. Lietz, M., et al., *Neuro tissue engineering of glial nerve guides and the impact of different cell types.* Biomaterials, 2006. **27**(8): p. 1425-1436.
74. Schnell, E., et al., *Guidance of glial cell migration and axonal growth on electrospun nanofibers of poly-ε-caprolactone and a collagen/poly-ε-caprolactone blend.* Biomaterials, 2007. **28**(19): p. 3012-3025.
75. Sell, S., et al., *Extracellular matrix regenerated: tissue engineering via electrospun biomimetic nanofibers.* Polymer International, 2007. **56**(11): p. 1349-1360.
76. Corey, J.M., et al., *Aligned electrospun nanofibers specify the direction of dorsal root ganglia neurite growth.* Journal of Biomedical Materials Research Part A, 2007. **83**(3): p. 636-645.

77. Yang, F., et al., *Electrospinning of nano/micro scale poly(l-lactic acid) aligned fibers and their potential in neural tissue engineering.* Biomaterials, 2005. **26**(15): p. 2603-2610.
78. Smeal, R.M., et al., *Substrate curvature influences the direction of nerve outgrowth.* Annals of Biomedical Engineering, 2005. **33**(3): p. 376-382.
79. Smeal, R.M. and P.A. Tresco, *The influence of substrate curvature on neurite outgrowth is cell type dependent.* Experimental neurology, 2008. **213**(2): p. 281-292.
80. Xie, J., et al., *Neurite outgrowth on electrospun nanofibers with uniaxial alignment: the effects of fiber density, surface coating, and supporting substrate.* ACS nano, 2014. **8**(2): p. 1878-1885.
81. Kim, Y.-t., et al., *The role of aligned polymer fiber-based constructs in the bridging of long peripheral nerve gaps.* Biomaterials, 2008. **29**(21): p. 3117-3127.
82. Xie, J., et al., *Electrospun nanofibers for neural tissue engineering.* Nanoscale, 2010. **2**(1): p. 35-44.
83. Newman, K., et al., *Bioactive hydrogel-filament scaffolds for nerve repair and regeneration.* The International journal of artificial organs, 2006. **29**(11): p. 1082-1091.
84. Novikova, L.N., et al., *Biodegradable poly-β-hydroxybutyrate scaffold seeded with Schwann cells to promote spinal cord repair.* Biomaterials, 2008. **29**(9): p. 1198-1206.
85. Ceballos, D., et al., *Magnetically aligned collagen gel filling a collagen nerve guide improves peripheral nerve regeneration.* Experimental neurology, 1999. **158**(2): p. 290-300.
86. Dubey, N., P. Letourneau, and R. Tranquillo, *Guided neurite elongation and Schwann cell invasion into magnetically aligned collagen in simulated peripheral nerve regeneration.* Experimental neurology, 1999. **158**(2): p. 338-350.
87. Yao, S.L., et al., *Co-effects of matrix low elasticity and aligned topography on stem cell neurogenic differentiation and rapid neurite outgrowth.* Nanoscale, 2016. **8**(19): p. 10252-10265.
88. Rose, J.C., et al., *Nerve Cells Decide to Orient inside an Injectable Hydrogel with Minimal Structural Guidance.* Nano Letters, 2017. **17**(6): p. 3782-3791.
89. Johnson, B.N., et al., *3D printed anatomical nerve regeneration pathways.* Advanced functional materials, 2015. **25**(39): p. 6205-6217.
90. Silva, G.A., et al., *Selective Differentiation of Neural Progenitor Cells by High-Epitope Density Nanofibers.* Science, 2004. **303**(5662): p. 1352-1355.
91. Tuft, B.W., et al., *Material stiffness effects on neurite alignment to photopolymerized micropatterns.* Biomacromolecules, 2014. **15**(10): p. 3717-27.
92. Tarus, D., et al., *Design of Hyaluronic Acid Hydrogels to Promote Neurite Outgrowth in Three Dimensions.* ACS Appl Mater Interfaces, 2016. **8**(38): p. 25051-9.
93. Lampe, K.J., A.L. Antaris, and S.C. Heilshorn, *Design of three-dimensional engineered protein hydrogels for tailored control of neurite growth.* Acta Biomaterialia, 2013. **9**(3): p. 5590-5599.
94. Winter, C.C., et al., *Transplantable living scaffolds comprised of micro-tissue engineered aligned astrocyte networks to facilitate central nervous system regeneration.* Acta Biomaterialia, 2016. **38**: p. 44-58.
95. East, E., et al., *Alignment of astrocytes increases neuronal growth in three-dimensional collagen gels and is maintained following plastic compression to form a spinal cord repair conduit.* Tissue engineering Part A, 2010. **16**(10): p. 3173-3184.

96. Miller, C., S. Jeftinija, and S. Mallapragada, *Micropatterned Schwann cell–seeded biodegradable polymer substrates significantly enhance neurite alignment and outgrowth.* Tissue engineering, 2001. **7**(6): p. 705-715.
97. Schmalenberg, K.E. and K.E. Uhrich, *Micropatterned polymer substrates control alignment of proliferating Schwann cells to direct neuronal regeneration.* Biomaterials, 2005. **26**(12): p. 1423-1430.
98. Thompson, D.M. and H.M. Buettner, *Oriented Schwann cell monolayers for directed neurite outgrowth.* Annals of biomedical engineering, 2004. **32**(8): p. 1121-1131.
99. Iwata, A., et al., *Long-term survival and outgrowth of mechanically engineered nervous tissue constructs implanted into spinal cord lesions.* Tissue engineering, 2006. **12**(1): p. 101-110.
100. Ehrlicher, A., et al., *Guiding neuronal growth with light.* Proceedings of the National Academy of Sciences, 2002. **99**(25): p. 16024-16028.
101. Oyama, K., et al., *Triggering of high-speed neurite outgrowth using an optical microheater.* Scientific reports, 2015. **5**.
102. Mohanty, S.K., et al., *Controlled induction, enhancement, and guidance of neuronal growth cones by use of line optical tweezers.* Optics letters, 2005. **30**(19): p. 2596-2598.
103. Stevenson, D., et al., *Optically guided neuronal growth at near infrared wavelengths.* Optics express, 2006. **14**(21): p. 9786-9793.
104. Brown, T.E. and K.S. Anseth, *Spatiotemporal hydrogel biomaterials for regenerative medicine.* Chemical Society Reviews, 2017. **46**(21): p. 6532-6552.
105. Lee, T.T., et al., *Light-triggered in vivo activation of adhesive peptides regulates cell adhesion, inflammation and vascularization of biomaterials.* Nature materials, 2015. **14**(3): p. 352.
106. Sekine, K., K.-i. Kubo, and K. Nakajima, *How does Reelin control neuronal migration and layer formation in the developing mammalian neocortex?* Neuroscience Research, 2014. **86**: p. 50-58.
107. Ayala, R., T. Shu, and L.-H. Tsai, *Trekking across the Brain: The Journey of Neuronal Migration.* Cell, 2007. **128**(1): p. 29-43.
108. Gupta, A., L.-H. Tsai, and A. Wynshaw-Boris, *Life is a journey: a genetic look at neocortical development.* Nat Rev Genet, 2002. **3**(5): p. 342-355.
109. Nadarajah, B. and J.G. Parnavelas, *Modes of neuronal migration in the developing cerebral cortex.* Nature Reviews Neuroscience, 2002. **3**(6): p. 423-432.
110. Nadarajah, B., et al., *Two modes of radial migration in early development of the cerebral cortex.* Nature neuroscience, 2001. **4**(2): p. 143-150.
111. Rakic, P., *Mode of cell migration to the superficial layers of fetal monkey neocortex.* Journal of Comparative Neurology, 1972. **145**(1): p. 61-83.
112. Sekine, K., et al., *The Outermost Region of the Developing Cortical Plate Is Crucial for Both the Switch of the Radial Migration Mode and the Dab1-Dependent "Inside-Out" Lamination in the Neocortex.* The Journal of Neuroscience, 2011. **31**(25): p. 9426-9439.
113. Marín, O., et al., *Guiding neuronal cell migrations.* Cold Spring Harbor perspectives in biology, 2010. **2**(2): p. a001834.
114. Cooper, J.A., *Mechanisms of cell migration in the nervous system.* The Journal of Cell Biology, 2013. **202**(5): p. 725-734.
115. Wu, W., et al., *Directional guidance of neuronal migration in the olfactory system by the protein Slit.* Nature, 1999. **400**(6742): p. 331-336.

116. Hatten, M.E., *New Directions in Neuronal Migration.* Science, 2002. **297**(5587): p. 1660-1663.
117. Marín, O., et al., *Sorting of Striatal and Cortical Interneurons Regulated by Semaphorin-Neuropilin Interactions.* Science, 2001. **293**(5531): p. 872-875.
118. Trommsdorff, M., et al., *Reeler/Disabled-like Disruption of Neuronal Migration in Knockout Mice Lacking the VLDL Receptor and ApoE Receptor 2.* Cell, 1999. **97**(6): p. 689-701.
119. Tissir, F. and A.M. Goffinet, *Reelin and brain development.* Nat Rev Neurosci, 2003. **4**(6): p. 496-505.
120. Sekine, K., et al., *Reelin controls neuronal positioning by promoting cell-matrix adhesion via inside-out activation of integrin α5β1.* Neuron, 2012. **76**(2): p. 353-369.
121. D'Arcangelo, G., *Reelin in the Years: Controlling Neuronal Migration and Maturation in the Mammalian Brain.* Advances in Neuroscience, 2014. **2014**: p. 19.
122. Chai, X., et al., *Reelin Induces Branching of Neurons and Radial Glial Cells during Corticogenesis.* Cerebral Cortex, 2015. **25**(10): p. 3640-3653.
123. Chai, X., et al., *Reelin stabilizes the actin cytoskeleton of neuronal processes by inducing n-cofilin phosphorylation at serine3.* The Journal of Neuroscience, 2009. **29**(1): p. 288-299.
124. Frotscher, M., *Role for Reelin in stabilizing cortical architecture.* Trends in Neurosciences, 2010. **33**(9): p. 407-414.
125. Cooper, J.A., *A mechanism for inside-out lamination in the neocortex.* Trends in Neurosciences, 2008. **31**(3): p. 113-119.
126. Ishii, K., K.-i. Kubo, and K. Nakajima, *Reelin and Neuropsychiatric Disorders.* Frontiers in Cellular Neuroscience, 2016. **10**(229).
127. Jossin, Y. and J.A. Cooper, *Reelin, Rap1 and N-cadherin orient the migration of multipolar neurons in the developing neocortex.* Nature neuroscience, 2011. **14**(6): p. 697-703.
128. Franco, S.J., et al., *Reelin Regulates Cadherin Function via Dab1/Rap1 to Control Neuronal Migration and Lamination in the Neocortex.* Neuron, 2011. **69**(3): p. 482-497.
129. Dulabon, L., et al., *Reelin Binds α3β1 Integrin and Inhibits Neuronal Migration.* Neuron, 2000. **27**(1): p. 33-44.
130. Sanada, K., A. Gupta, and L.-H. Tsai, *Disabled-1-Regulated Adhesion of Migrating Neurons to Radial Glial Fiber Contributes to Neuronal Positioning during Early Corticogenesis.* Neuron, 2004. **42**(2): p. 197-211.
131. Salierno, M.J., A.J. García, and A. del Campo, *Photo‐activatable surfaces for cell migration assays.* Advanced Functional Materials, 2013. **23**(48): p. 5974-5980.
132. Salierno, M.J., et al., *Phototriggered fibril-like environments arbitrate cell escapes and migration from endothelial monolayers.* Biomaterials, 2016. **82**: p. 113-123.
133. Elias, L.A.B., D.D. Wang, and A.R. Kriegstein, *Gap junction adhesion is necessary for radial migration in the neocortex.* Nature, 2007. **448**(7156): p. 901-907.
134. Arnold, M., et al., *Induction of Cell Polarization and Migration by a Gradient of Nanoscale Variations in Adhesive Ligand Spacing.* Nano Letters, 2008. **8**(7): p. 2063-2069.
135. He, M., et al., *Leading tip drives soma translocation via forward F-actin flow during neuronal migration.* The Journal of Neuroscience, 2010. **30**(32): p. 10885-10898.
136. Jiang, J., et al., *Spatiotemporal dynamics of traction forces show three contraction centers in migratory neurons.* The Journal of Cell Biology, 2015. **209**(5): p. 759-774.

137. Corey, J., B. Wheeler, and G. Brewer, *Compliance of hippocampal neurons to patterned substrate networks.* Journal of neuroscience research, 1991. **30**(2): p. 300-307.
138. Flanagan, L.A., et al., *Regulation of human neural precursor cells by laminin and integrins.* Journal of Neuroscience Research, 2006. **83**(5): p. 845-856.
139. Mazia, D., G. Schatten, and W. Sale, *Adhesion of cells to surfaces coated with polylysine. Applications to electron microscopy.* The Journal of cell biology, 1975. **66**(1): p. 198-200.
140. Ruiz, A., et al., *Micro-stamped surfaces for the patterned growth of neural stem cells.* Biomaterials, 2008. **29**(36): p. 4766-4774.
141. Hall, P.E., et al., *Laminin enhances the growth of human neural stem cells in defined culture media.* BMC Neuroscience, 2008. **9**(1): p. 71.
142. Manthorpe, M., et al., *Laminin promotes neuritic regeneration from cultured peripheral and central neurons.* The Journal of Cell Biology, 1983. **97**(6): p. 1882-1890.
143. Adams, D.N., et al., *Growth cones turn and migrate up an immobilized gradient of the laminin IKVAV peptide.* Journal of neurobiology, 2005. **62**(1): p. 134-147.
144. Pankov, R. and K.M. Yamada, *Fibronectin at a glance.* Journal of Cell Science, 2002. **115**(20): p. 3861-3863.
145. Gertz, C.C. and A.R. Kriegstein, *Neuronal Migration Dynamics in the Developing Ferret Cortex.* The Journal of Neuroscience, 2015. **35**(42): p. 14307-14315.
146. Fernández, V., C. Llinares‐Benadero, and V. Borrell, *Cerebral cortex expansion and folding: what have we learned?* The EMBO Journal, 2016.
147. Parsons, J.T., A.R. Horwitz, and M.A. Schwartz, *Cell adhesion: integrating cytoskeletal dynamics and cellular tension.* Nat Rev Mol Cell Biol, 2010. **11**(9): p. 633-43.
148. Small, J.V., et al., *The lamellipodium: where motility begins.* Trends in Cell Biology, 2002. **12**(3): p. 112-120.
149. Xia, Y. and G.M. Whitesides, *Soft Lithography.* Angewandte Chemie International Edition, 1998. **37**(5): p. 550-575.
150. Campo, A.d. and C. Greiner, *SU-8: a photoresist for high-aspect-ratio and 3D submicron lithography.* Journal of Micromechanics and Microengineering, 2007. **17**(6): p. R81.
151. Greiner, C., A. del Campo, and E. Arzt, *Adhesion of Bioinspired Micropatterned Surfaces: Effects of Pillar Radius, Aspect Ratio, and Preload.* Langmuir, 2007. **23**(7): p. 3495-3502.
152. Tahirovic, S. and F. Bradke, *Neuronal polarity.* Cold Spring Harbor perspectives in biology, 2009. **1**(3): p. a001644.
153. Petersen, S., et al., *Phototriggering of cell adhesion by caged cyclic RGD peptides.* Angew Chem Int Ed Engl, 2008. **47**(17): p. 3192-5.
154. Wang, G., et al., *The effect of topology of chitosan biomaterials on the differentiation and proliferation of neural stem cells.* Acta biomaterialia, 2010. **6**(9): p. 3630-3639.
155. Piant, S., F. Bolze, and A. Specht, *Two-photon uncaging, from neuroscience to materials.* Optical Materials Express, 2016. **6**(5): p. 1679-1691.
156. Farrukh, A., et al., *Photoactivatable Adhesive Ligands for Light-guided Neuronal Growth.* Chembiochem, 2018.
157. Cao, L., et al., *Physiological electrical signals promote chain migration of neuroblasts by up-regulating P2Y1 purinergic receptors and enhancing cell adhesion.* Stem Cell Reviews and Reports, 2015. **11**(1): p. 75-86.

158. Lee, W., C.W. Frank, and J. Park, *Directed Axonal Outgrowth Using a Propagating Gradient of IGF‐1.* Advanced Materials, 2014. **26**(29): p. 4936-4940.
159. Lei, W.-L., et al., *Laminin/β1 integrin signal triggers axon formation by promoting microtubule assembly and stabilization.* Cell research, 2012. **22**(6): p. 954-972.
160. Potter, W., R.E. Kalil, and W.J. Kao, *Biomimetic material systems for neural progenitor cell-based therapy.* Front Biosci, 2008. **13**: p. 806-21.
161. Frith, J.E., et al., *Tailored integrin–extracellular matrix interactions to direct human mesenchymal stem cell differentiation.* Stem cells and development, 2012. **21**(13): p. 2442-2456.
162. Kibbey, M.C., et al., *beta-Amyloid precursor protein binds to the neurite-promoting IKVAV site of laminin.* Proceedings of the National Academy of Sciences, 1993. **90**(21): p. 10150-10153.
163. Agius, E., et al., *Antibodies directed against the β1-integrin subunit and peptides containing the IKVAV sequence of laminin perturb neurite outgrowth of peripheral neurons on immature spinal cord substrata.* Neuroscience, 1996. **71**(3): p. 773-786.
164. Hosseinkhani, H., et al., *Engineering three-dimensional collagen-IKVAV matrix to mimic neural microenvironment.* ACS chemical neuroscience, 2013. **4**(8): p. 1229-1235.
165. Sun, W., et al., *Viability and neuronal differentiation of neural stem cells encapsulated in silk fibroin hydrogel functionalized with an IKVAV peptide.* Journal of tissue engineering and regenerative medicine, 2017. **11**(5): p. 1532-1541.
166. Kleinman, H., et al., *Laminin receptors for neurite formation.* Proceedings of the National Academy of Sciences, 1988. **85**(4): p. 1282-1286.
167. Nomizu, M., et al., *Identification of cell binding sites in the laminin α1 chain carboxyl-terminal globular domain by systematic screening of synthetic peptides.* Journal of Biological Chemistry, 1995. **270**(35): p. 20583-20590.
168. Yamada, M., et al., *Ile‐Lys‐Val‐Ala‐Val (IKVAV)‐containing laminin α1 chain peptides form amyloid‐like fibrils.* FEBS letters, 2002. **530**(1-3): p. 48-52.
169. Farrukh, A., et al., *Bifunctional poly (acrylamide) hydrogels through orthogonal coupling chemistries.* Biomacromolecules, 2017. **18**(3): p. 906-913.
170. Hopkins, A.M., et al., *Silk hydrogels as soft substrates for neural tissue engineering.* Advanced Functional Materials, 2013. **23**(41): p. 5140-5149.
171. Costa, M.R., R. Jagasia, and B. Berninger, *Directed neuronal differentiation of embryonic and adult-derived neurosphere cells.* Protocols for Neural Cell Culture: Fourth Edition, 2010: p. 29-49.
172. Azari, H., et al., *Establishing embryonic mouse neural stem cell culture using the neurosphere assay.* JoVE (Journal of Visualized Experiments), 2011(47): p. e2457-e2457.
173. Blanchoin, L., et al., *Actin dynamics, architecture, and mechanics in cell motility.* Physiol. Rev., 2014. **94**(1): p. 235-63.
174. Schliwa, M., *Action of cytochalasin D on cytoskeletal networks.* J. Cell Biol., 1982. **92**(1): p. 79-91.
175. Brenner, S.L. and E.D. Korn, *Substoichiometric concentrations of cytochalasin D inhibit actin polymerization. Additional evidence for an F-actin treadmill.* J. Biol. Chem., 1979. **254**(20): p. 9982-5.
176. Casella, J.F., M.D. Flanagan, and S. Lin, *Cytochalasin D inhibits actin polymerization and induces depolymerization of actin filaments formed during platelet shape change.* Nature, 1981. **293**(5830): p. 302-305.

177. Mortensen, K. and L.I. Larsson, *Effects of cytochalasin D on the actin cytoskeleton: association of neoformed actin aggregates with proteins involved in signaling and endocytosis.* Cell Mol. Life Sci., 2003. **60**(5): p. 1007-12.
178. Cooper, J.A., *Effects of cytochalasin and phalloidin on actin.* J. Cell Biol., 1987. **105**(4): p. 1473-1478.
179. Borowiak, M., et al., *Photoswitchable Inhibitors of Microtubule Dynamics Optically Control Mitosis and Cell Death.* Cell, 2015. **162**(2): p. 403-11.
180. Dobber, A., et al., *Development and Biological Evaluation of a Photoactivatable Small Molecule Microtubule-Targeting Agent.* ACS Med. Chem. Lett., 2017. **8**(4): p. 395-400.
181. Gropeanu, R.A., et al., *Phototriggerable 2′,7-Caged Paclitaxel.* PLoS ONE, 2012. **7**(9): p. e43657.
182. Nair, U.B., et al., *Crystal structures of monomeric actin bound to cytochalasin D.* J. Mol. Biol., 2008. **384**(4): p. 848-64.
183. Shankar, J. and I.R. Nabi, *Actin cytoskeleton regulation of epithelial mesenchymal transition in metastatic cancer cells.* PloS one, 2015. **10**(3): p. e0119954.
184. Gerisch, G., et al., *Mobile actin clusters and traveling waves in cells recovering from actin depolymerization.* Biophys. J., 2004. **87**(5): p. 3493-503.
185. Geiger, B. and A. Bershadsky, *Exploring the neighborhood: adhesion-coupled cell mechanosensors.* Cell, 2002. **110**(2): p. 139-42.
186. Roy, P., et al., *Local Photorelease of Caged Thymosin β4 in Locomoting Keratocytes Causes Cell Turning.* J. Cell Biol., 2001. **153**(5): p. 1035-1048.
187. Ghosh, M., et al., *Cofilin Promotes Actin Polymerization and Defines the Direction of Cell Motility.* Science, 2004. **304**(5671): p. 743.
188. Wu, Y.I., et al., *A genetically encoded photoactivatable Rac controls the motility of living cells.* Nature, 2009. **461**(7260): p. 104-108.
189. Shimizu-Sato, S., et al., *A light-switchable gene promoter system.* Nat. Biotech., 2002. **20**(10): p. 1041-1044.
190. Dumbauld, D.W., et al., *How vinculin regulates force transmission.* Proc. Natl. Acad. Sc. USA, 2013. **110**(24): p. 9788-9793.
191. Green, J.J. and J.H. Elisseeff, *Mimicking biological functionality with polymers for biomedical applications.* Nature, 2016. **540**(7633): p. 386.
192. Leijten, J., et al., *Spatially and temporally controlled hydrogels for tissue engineering.* Materials Science and Engineering: R: Reports, 2017. **119**: p. 1-35.
193. Rosales, A.M., et al., *Hydrogels with reversible mechanics to probe dynamic cell microenvironments.* Angewandte Chemie, 2017. **129**(40): p. 12300-12304.
194. Ruskowitz, E.R. and C.A. DeForest, *Photoresponsive biomaterials for targeted drug delivery and 4D cell culture.* Nature Reviews Materials, 2018. **3**: p. 17087.
195. Koçer, G., et al., *Light‐Responsive Hierarchically Structured Liquid Crystal Polymer Networks for Harnessing Cell Adhesion and Migration.* Advanced materials, 2017. **29**(27).
196. Tamura, M., et al., *Click-crosslinkable and photodegradable gelatin hydrogels for cytocompatible optical cell manipulation in natural environment.* Scientific reports, 2015. **5**: p. 15060.
197. Brochu, A.B., S.L. Craig, and W.M. Reichert, *Self‐healing biomaterials.* Journal of Biomedical Materials Research Part A, 2011. **96**(2): p. 492-506.
198. Hay, J.J., et al., *Living biointerfaces based on non-pathogenic bacteria support stem cell differentiation.* Scientific reports, 2016. **6**: p. 21809.

199. Rodrigo-Navarro, A., et al., *Living biointerfaces based on non-pathogenic bacteria to direct cell differentiation.* Scientific Reports, 2014. **4**: p. 5849.
200. Saadeddin, A., et al., *Functional living biointerphases.* Advanced healthcare materials, 2013. **2**(9): p. 1213-1218.
201. Mamat, U., et al., *Detoxifying Escherichia coli for endotoxin-free production of recombinant proteins.* Microbial cell factories, 2015. **14**(1): p. 57.
202. Binder, D., et al., *Light-responsive control of bacterial gene expression: precise triggering of the lac promoter activity using photocaged IPTG.* Integrative biology, 2014. **6**(8): p. 755-765.
203. Young, D.D. and A. Deiters, *Photochemical activation of protein expression in bacterial cells.* Angewandte Chemie International Edition, 2007. **46**(23): p. 4290-4292.
204. Moore, S.J., et al., *Engineered knottin peptide enables noninvasive optical imaging of intracranial medulloblastoma.* Proceedings of the National Academy of Sciences, 2013. **110**(36): p. 14598-14603.
205. Potthoff, E., et al., *Bacterial adhesion force quantification by fluidic force microscopy.* Nanoscale, 2015. **7**(9): p. 4070-4079.
206. Zhang, Z., et al., *Non-peptide guided auto-secretion of recombinant proteins by super-folder green fluorescent protein in Escherichia coli.* Scientific reports, 2017. **7**(1): p. 6990.